ISTANBUL TECHNICAL UNIVERSITY ★ GRADUATE SCHOOL OF SCIENCE ENGINEERING AND TECHNOLOGY

CLOSED - LOOP CONTROL OF THE SATCOM ON THE MOVE ANTENNA USING JACOBIAN OPERATOR

M.Sc. THESIS

Oğuz Kaan HANCIOĞLU

Department of Mechatronics Engineering

Mechatronics Engineering Programme

OCTOBER 2019

ISTANBUL TECHNICAL UNIVERSITY ★ GRADUATE SCHOOL OF SCIENCE ENGINEERING AND TECHNOLOGY

CLOSED - LOOP CONTROL OF THE SATCOM ON THE MOVE ANTENNA USING JACOBIAN OPERATOR

M.Sc. THESIS

Oğuz Kaan HANCIOĞLU
(518161017)

Department of Mechatronics Engineering

Mechatronics Engineering Programme

Thesis Advisor: Prof. Dr. Ovsanna Seta Estrada

OCTOBER 2019

İSTANBUL TEKNİK ÜNİVERSİTESİ ★ FEN BİLİMLERİ ENSTİTÜSÜ

SATCOM ON THE MOVE ANTENİNİN JACOBIAN OPERATÖRÜ KULLANILARAK KAPALI - ÇEVRİM KONTROLÜ

YÜKSEK LİSANS TEZİ

Oğuz Kaan HANCIOĞLU
(518161017)

Mekatronik Mühendisliği Anabilim Dalı

Mekatronik Mühendisliği Programı

Tez Danışmanı: Prof. Dr. Ovsanna Seta Estrada

EKİM 2019

Oğuz Kaan HANCIOĞLU, a M.Sc. student of ITU Graduate School of Science Engineering and Technology 518161017 successfully defended the thesis entitled "CLOSED - LOOP CONTROL OF THE SATCOM ON THE MOVE ANTENNA USING JACOBIAN OPERATOR", which he/she prepared after fulfilling the requirements specified in the associated legislations, before the jury whose signatures are below.

Thesis Advisor :	**Prof. Dr. Ovsanna Seta Estrada** Istanbul Technical University	.....
Jury Members :	**Prof. Dr. Metin Gökaşan** Istanbul Technical University	.....
	Asst. Prof. Dr. Taner Arsan Kadir Has University	.....
		.....

Date of Submission : **23 September 2019**
Date of Defense : **11 October 2019**

To my Gökçil,

FOREWORD

Firstly, I would like to express my sincere gratitude to Prof. Dr. Seta Bogosyan and Prof. Dr. Metin Gökaşan at Istanbul Technical University, for their continued support, guidance, and encouragement in this research. I would also like to thank whole members of the Profen Communications Technologies & Services, Inc. for their technical help on the SOTM antennas. I am very grateful to Mustafa Çelik and Zafer Sali for both technical and personal help during the development of the thesis. I wish to extend my sincere thanks to Michal Bastl, Jan Najman and Prof. Robert Grepl from MECHLAB for valuable contributions to the development of this thesis. It has been a great pleasure for me to get an opportunity to work with all person who has a contribution to this thesis and complete the project successfully.

October 2019

Oğuz Kaan HANCIOĞLU
(Mechatronics Engineer)

TABLE OF CONTENTS

Page

ABBREVIATIONS

AHRS : Attitude Heading Reference System
ALSAT : All-Satellite License
APS : Antenna Positioning System
BLDC : Brushless DC Motors
CAD : Computer Aided Drawing
DC : Direct Current
DH : Denavit-Hartenberg
EL : Elevation
FCC : Federal Comminications Commission
GPS : Global Positioning System
IFOG : Interferomagnetic Fiber-Optic
ISP : Inertially Stabilized Platforms
LOS : Line of Sight
Mbps : Megabits
MEMS : Micro-electro-mechanical Sensor
NED : North-East-Down
PI : Proportional-Integral
PID : Proportional-Integral-Derivative
PMSM : Permanent Magnet Synchronous Motors
PWM : Pulse Width Modulation
RF : Radio Frequency
RLG : Ring Laser Gyro
SATCOM : Satellite Communication
SOTM : Satcom On The Move
XEL : Cross-Elevation

SYMBOLS

$\dot{\omega}$	: Angular acceleration
θ_i	: Axis angle of the i. link
J_w	: Angular Jacobian operator
ω	: Angular speed
ω_i	: Angular speed of i axis
${}^{i+1}n_{i+1}$	: Applied torque from link i+1 to link i
${}^{i+1}f_{i+1}$	: Applied force from link i+1 to link i
$\{x_i, y_i, z_i\}$	: Axis frame of the i. axis
τ	: Axis torque
l_i	: Dimention of the i. link
${}^{i}P_{i+1}$	: Distance matrix of between link i link i+1
T	: Dry friction
${}^{i}F_i$	: Generated force on the center of mass
${}^{i}N_i$	: Generated torque by rotation of link i
${}^{i}P_{C_i}$	: i axis center of mass
I	: Inertia
q	: Joints Angle
$\dot{\theta}_i$	: Relative angular speed of i axis
R^i_{i+1}	: Rotation matrix of between link i link i+1
β	: Tilt angle
T^i_{i+1}	: Transformation matrix of between link i link i+1
B	: Viscous friction

LIST OF TABLES

Page

LIST OF FIGURES

Page

CLOSED - LOOP CONTROL OF THE SATCOM ON THE MOVE ANTENNA USING JACOBIAN OPERATOR

SUMMARY

Nowadays, the internet has vital necessity in the terrestrial area and has become an important requirement on mobile platforms. In a commercial application, mostly they are used for sharing information about the application using satellite communication, in a military application they are used to make the autonomous system and data security. This requirement has resulted in development automatic antenna system which can find and track satellite on mobile platforms such as land, air, sea platforms. These systems are called Satcom on the Move (SOTM). They offer broadband satellite communication on land, air, and sea platforms. SOTM antennas consist of two main parts which are pedestal and antenna payload. The pedestal is the special robotic manipulator which has the gimbal structure. Generally, 2-axes azimuth-elevation pedestal is used in both commercial and military applications. Due to the gimbal lock problem of the 2-axes pedestal, the common solution which increases the number of the axis of the pedestal is applied in the industry. Antenna Positioning System (APS) manages and operates the whole antenna functions including the tracking controller and stabilization controller. According to the Federal Communications Commission (FCC) standards, the antenna must have the pointing error that is below than 0.2°.
In order to overcome this standard, a closed-loop pointing technique is used in the APS design. This thesis aims to develop the mathematical model and control system of the 3-axes pedestal which is designed as a shipborne antenna by Profen Communications Technologies & Services, Inc. The nominal APS does not include the closed-loop pointing technique and this resulted in the pointing error higher than standards during the scanning. This thesis develops an APS which includes stabilization controller, closed-loop controller, and scanning algorithms to achieve the pointing requirement.
The APS has both the stabilization controller algorithm that compensates the disturbance movement caused by the mobile platform and closed-loop control algorithm that finds and keeps the maximum signal level by measuring the RF signal feedback. The stabilization algorithm includes the gyroscope stabilization method using the Jacobian operator for kinematic transformation. The closed-loop control algorithm includes the position controller and scanning algorithm which finds the maximum signal level. The step-track and conical scan algorithms are implemented as the outer loop of the stabilization controller. The end effector stabilization performance and the pointing error is examined in the various test cases to determine a feasible closed-loop solution for the APS system.

SATCOM ON THE MOVE ANTENİNİN JACOBIAN OPERATÖRÜ KULLANILARAK KAPALI - ÇEVRİM KONTROLÜ

ÖZET

Günümüzde bir ihtiyaç haline gelen internet, mobil platformlarda da uydu haberleşmesinin artmasına neden olmaktadır. Ticari uygulamalarda internet hizmeti mobil platformdaki anlık veri paylaşımı ve müsterilerinin konforunu arttırmaya yönelik olup, askeri uygulamalarda ise mobil platformun uydu üzerinden kontrolü ve giziliği sağlamaya yöneliktir. Bu ihtiyaçlar otomatik uydu haberleşmesi yapabilen Satcom On the Move (SOTM) anten sistemlerinin gelişmesine neden olmaktadır.

SOTM antenlar kara, hava ve deniz platformlarında yaygın olarak uydu haberleşmesini sağlayan terminaller olarak kullanılmaktadır. Genelde SOTM antenleri azimut ve elevasyon eksenlerine sahip iki ekseni yapılardır. Bu iki eksenli yapı reflektör ve RF bileşenleri ile birlikte SOTM antenini oluşturmaktadır. İki eksenli yapının tasarımı, üretimi ve kontrolü kolay ve kompakt bir yapıya sahip olmasından dolayı tercih edilmektedir. Acnak elevasyon ekseninin 90° yaklaşırken, literatürde gimbal-lock olarak da bilinen tekil noktaya ulaşmaktadır. Bu tekillik anten sisteminin çalışma uzayını sınırlamaktadır. Tekillik problemini çözmek için üç eksenli bir gimbal yapısı kullanılmaktadır.

Bu tezde üç eksenili gimbal yapısına sahip deniz platformlarında çalışabilen SOTM anteni üzerinde yapılan çalışmalar anlatılmaktadır. SOTM anteni temel olarak iki ana parçadan oluşmaktadır. Bunlardan birincisi uydudan sinyalin alınıp ve gönderildiği reflektör ve RF bileşenleridir. İkincisi ise üç eksenli servomekanik gimbal yapıdır. Gimbal yapı aslında seri manipulatörlerden bir farkı bulunmamaktadır. Reflektör ve RF bileşenleri gimbal yapısına sahip seri robotun taşıdığı yüktür. SOTM anteninin tüm kontrolünü sağlayan yapıya da anten konumlama sistemi (APS) denilmektedir. SOTM antenleri mobil platformlarda çalışabilmektedir ancak her bir mobil platformunun gereksinimleri farklı olduğundan tasarımında değişik parametreler içermektedir. Bu tezde deniz platformları için APS geliştirilmesi anlatılacaktır.

Düşük maliyetli ve verimli bir APS tasarımı yapabilmek için öncelikle SOTM anteninin gereksinimlerinin çıkarılması gerekmektedir. Deniz platformunun hareketininden dolayı SOTM anteninin ana ekseninde en yüksek $15^\circ/s$ olacak şekilde sinüsoidal hareketler meydana gelmektedir. Bu da yapılması nispeten zor olmayan bir gereksinimdir. APS tasarımında en önemli gereksinim ise konumlama başarımının 0.2°'den az olması gerekmektedir. Bu gereksinim FCC standartlarına uyması için sağlanması gereken bir koşuldur. Tasarımda maliyet, verimlilik ve standartlara uygunluk amaçları ile birlikte en uygun APS sistemi tasarımı amaçlanmaktadır.

Geneksinimleri taşıyan APS sistemini tasarlamak için SOTM anteni matematiksel olarak modellenmesi gerekmektedir. SOTM anteni seri robotlara benzediğinden Denavit-Hartenberg yöntemi ile kinematik modeli oluşturulmaktadır. Kinematik model oluşturulurken GPS sensörü ile doğru şekilde çalışabilmesi için eksen ataması

yapılmıştır. SOTM anteninin dinamiği Newton-Euler yöntemi ile oluşturulmaktadır. Ancak manipulatörün gimbal yapısı ve kütle stabilizasyonu tasarımı sayesinde dinamik sadeleştirilebilmektedir. Kütle stabilizasyonu her bir eksenin kütle merkezinin eksenin dönme noktası ile çakıştırılması ile oluşan mekanik yapıdır. Bu iki özellik kullanarak SOTM dinamiği üç adet tek girişli tek çıkışlı sistem halinde ifade edilebilmektedir.

SOTM antenlerinde APS mobil platformun hareketi jiroskop sensörü yardımıyla sönümleyen stabilizasyon kontrol ve uyduyu bozucular altında sürekli olarak takip eden takip kontrol algoritmasını içermektedir. SOTM anteninin uç işlevci stabilizasyonu stabilizasyon kontrolcüsü ve kinematik dönüşümler olarak iki kısımdan oluşmaktadır. Kontrolcü olarak doğrusal PI kontrolcü tipi kullanılmış ve istenilen başarımlar sağlanmıştır. Kinmatik dönüşümler ise stabilizasyonda önemli bir konu teşkil etmektedir. İki eksenli manipülatörde uç işlvecinin hızının stabilizasyonu için her bir ekseni ayrı ayrı kontrol etmek yeterli olmaktadır. Ancak üç eksenli manipülatörde uç işlevcinin hız bileşenleri birbiri ile etkileşimde olduğu için stabilizasyon işlemi iki eksenli sistemdeki gibi olmamaktadır. Bunu çözmek için Jacobian operatörü kullanımı önerilmiş ve çeşitli bozucu hareketler altında doğrulanmıştır. Anten sisteminin uydu takip kontrol algoritması konum kontrolcüsü ve tarama algoritmasından oluşmaktadır. Konum kontrolcüsü doğrusal PID tipi bir kontrolcü olup istenilen başarım değerleri sağlanmıştır. SOTM antenlerinde uydu sinyalinin seviyesini bozan bir kaç parametre bulunmaktadır. Bunlar düşük çözünürlüklü sensörler, montaj hataları olarak örnek verilebilmektedir. Bu değerler eksenlerin bakış açılarının yanlış hesaplamalarına neden olmaktadır ve sonucunda alınan sinyal seviyesi düşmüş olmaktadır. Sinyal seviyesini iyileştirmek için step-track ve conical scan tarama algoritmaları gerçekleştirilmiş ve sinyal seviyeisinin en yüksek değerleri bulunmuştur. Son olarak da SOTM anteni için en uygun APS modeli karşılaştırılmıştır.

1. INTRODUCTION

1.1 Motivation for Work

Nowadays, the internet has vital necessity in the terrestrial area and has become an important requirement on mobile platforms. This requirement has resulted in development automatic antenna system which can find and track satellite on mobile platforms such as land, air, sea platforms. These systems are called Satcom on the Move (SOTM). They offer broadband satellite communication on land, air and sea platforms. In order to correspond to increasing requirements in both the military and commercial market, SOTM antennas must have a high-speed data rate. Although increasing the size of the antenna can increase the data rate, the larger system has to be supported by the larger mechanical construction. This circumstance is not suitable for mobile SOTM antennas. While the SOTM antenna is designing, the designers have to make the best of performance, size, weight, and cost [1].

Basically, SOTM antennas consist of two main parts which are pedestal and antenna payload. The pedestal, which is also called Inertially Stabilized Platforms (ISP) in the literature, is the robotic structure which has two or more degrees of freedom and can point and stabilize. The antenna payload which consists of active and passive RF components receives and transmits the RF signal. Generally, ISP has two or more rotational axes which have a motor, bearing, and sensor. Moreover, they are designed as a gimbal system. Most of ISP has its own gyroscope sensor to stabilize itself automatically on its payload. ISP is not only used in SOTM antennas but also used in different application areas such as a weapon, camera, and telescope systems as shown in Figure 1.1 [2]. The pointing performances of the SOTM antennas are defined as the ability of the antenna in order to look directly to the satellite during the movement of the vehicle. The pointing error is the radial angular error from the satellite which comes directly from the states of the control system. The pointing error includes all kind of errors caused by atmospheric conditions, sensors, and stabilization. The SOTM antenna must provide under 0.2° pointing error to acquire for the All-Satellite License (ALSAT) from the Federal Communications Commission (FCC). According to FCC

Figure 1.1 : The examples of different application areas of ISP, adapted from (Hilkert, 2008).

standards, if the pointing error is higher than 0.2 degrees, the transmit of the SOTM antenna must be shut down within 100 ms due to damage to adjacent satellite [3]. According to FCC standards, there is no problem if the pointing error is bigger the 0.2° during receiving the RF signal. However, this situation causes a cost increase reflected the user. The pointing error in the SOTM antenna directly affects the price of the rented satellite bandwidth. FCC institution identifies the Effective Isotropically Radiated Power (EIRP) spectral-density limits. While the pointing error is increased, the permissible EIRP density decreases. For this reason, to obtain the same Mbps internet service broader bandwidth rental must be required. As a result, the customer's rental cost is increased. If the pointing error is less than 0.2°, the cost of renting bandwidth is estimated 1300$ while If the pointing error is 0.21°, the cost of renting bandwidth is estimated 1800$. If the pointing error is 0.3°, the cost is increased to 2100$ [4].

The SOTM antenna which contains 2-axes servo mechanical pedestal (ISP) and antenna payload is a simple and cost-effective solution for SATCOM communication. Although SOTM antenna which contains 3-axes servo mechanical pedestal and antenna payload is more expensive than the 2-axes pedestal, it provides better disturbance compensation performance. On the other hand, when the elevation axis is 90° above from horizon in the 2-axes configuration, a problem occurs, which is called

gimbal lock, that the azimuth axis cannot contribute to the end effector orientation [5]. This problem is called singularity in robotics literature [6]. Since the SOTM antenna has float base, it can get into singular position with any satellite look angle and base disturbance. In order to solve this problem, it is a possible solution to try to minimize the elevation angle by using a redundant axis. Therefore, SOTM antenna which has 3-axes is a better solution than 2-axes. It is also expected that 3-axes pedestal maintains pointing accuracy in accordance with FCC standards.

1.2 Purpose of Thesis

During the SATCOM communication for higher data rate, antenna payload needs to be positioned with high accuracy. The SOTM antenna to be examined in this thesis is a shipborne SOTM antenna which designed to operate on the ship platforms. This thesis aims to develop the mathematical model and control system of the 3-axes pedestal to meet the requirements of the shipborne antenna. ENGİN antenna which is designed as a shipborne antenna by Profen Communications Technologies & Services, Inc. is used in this thesis. Antenna Positioning System (APS) which includes stabilization controller, closed-loop controller, and scanning algorithms are developed. The stabilization controller aims to compensate the disturbance forces which are caused by the movement of the mobile platform. With the closed-loop controller, the maximum point of the RF signal is found and maintains. The goals of this thesis to recommend a solution to the antenna pointing system for the shipborne antenna, by:

1. Defining nominal 3-axes APS which is used on sea platforms and pointing requirements.
2. Modeling the kinematics of APS using the Denavit-Hartenberg (DH) method and simplification of the dynamic model of APS.
3. Modeling and torque control the actuator and analyzing the effect on torque ripple in stabilization controller.
4. Developing the stabilization controller and analyzing the performance of it under various disturbance effects.

5. Developing the closed-loop controller and analyzing performance with the stabilization controller.

6. Developing and implementing of the step-track and conical scan algorithms to maximize the RF signal strength.

7. Identify appropriate methods for APS, compare and provide ideas for the shipborne antenna.

1.3 Contributions

This thesis makes the following contributions when successfully complete the goals outlined in Section 1.2:

1. The thesis models and verifies the 3-axes pedestal kinematic model by using the Denavit-Hartenberg (DH) method which is commonly used in robotics. This method can be can to similar pedestals or different robot structures.

2. This thesis models the 3-axes pedestal dynamic by simplifying the normal dynamic model. The complex and nonlinear equations of dynamics of the pedestal can be reduced and simplified by using the advantages of the gimbal structure. This approach can be applied to similar systems.

3. This thesis develops a stabilization controller to compensate the ship movement and point to satellite for the 3-axes APS. This controller can be applied and developed different application areas such as camera, telescope and weapon stabilization.

4. To analyze the performance of the stabilization controller, a Simulink simulation is realized. This simulation can be applied to different SOTM antennas or application areas.

5. This thesis develops a closed-loop controller to maximize the RF signal for the 3-axes APS. This controller can be applied to different SOTM antennas.

6. To analyze the performance of the closed-loop controller, a Simulink simulation is realized. In this simulation, the RF signal is used as a feedback of the controller. This multi-physical control method can provide a different point of view in the control algorithms.

7. This thesis implements step-track and conical scan algorithms into the Simulink simulation and compares both algorithms. This works can be developed and used in the SOTM antennas.

1.4 Thesis Overview

The technologies available to develop an APS system is discussed in Chapter 2. These technologies depend on cost and compactness. The requirements with the commercial standard are examined to build such an APS system to be cost-effective and compact. Thus the first objective is examined in Chapter 2. Second and third objectives are the mathematical model of the antenna are examined in Chapter 3. Chapter 3 also includes the RF model which is obtained from the measured signal of the antenna and specifies the pointing error. The line of sight (LOS) stabilization is designed and implemented in Chapter 4 to confirm the fourth objective. Before stabilization of the 3-axes pedestal, stabilization of the 2-axes pedestal is examined. After that, a Jacobian operator is proposed to stabilize the LOS to confirm the fourth objective. The proposed method is verified under various disturbance affects. To track the satellite, a position controller and scanning algorithm are implemented. In the SOTM, there are a few uncertain parameters which increase the pointing error. Chapter 5 discusses the techniques and algorithms with the verification under various disturbance to accomplish the fifth, sixth objectives and FCC requirements. In the last chapter, the most suitable solution for the APS system is discussed.

2. TECHNICAL BACKGROUND AND SYSTEM ARCHITECTURE

The ISP and pedestal structures vary in order to provide the desired positioning accuracy to meet the different requirements with the given system. In the SOTM antennas, APS points the antenna payload to the satellite in order to establish communication. This chapter examines the modeling of the SOTM antenna and various control system configurations of APS. Finally, this chapter specifies the necessity hardware configuration and pointing requirements of the ENGİN shipborne antenna.

2.1 SOTM Antenna Components

2.1.1 APS components

As mentioned earlier, APS is the robotic structure that points the antenna payload to provide an efficient communication link to the satellite. This robotic structure which is used in the SOTM antenna includes many functional components. This structure comprises antenna payload, GPS sensor, angular position sensors, gyroscope sensor, high-level controller board, low-level controller board, actuators, and robot mechanics. The low-level controller board is responsible for controlling the rate of the axis and reading the angular position sensor. The high-level controller board is responsible for controlling the whole antenna functionality including the closed-loop controller, finding a satellite, kinematic transformations, etc. and reading GPS sensor, gyro sensor, and RF signal strength. Figure 2.1 shows the block diagram of the functional units of the SOTM antenna.

2.1.2 Antenna payload

Aperture is the part of which the antenna receives an RF energy from a satellite or transmits an RF energy to a satellite. In the high bandwidth SATCOM applications, the aperture must be directional. Aperture gain is a measure of how efficiently the

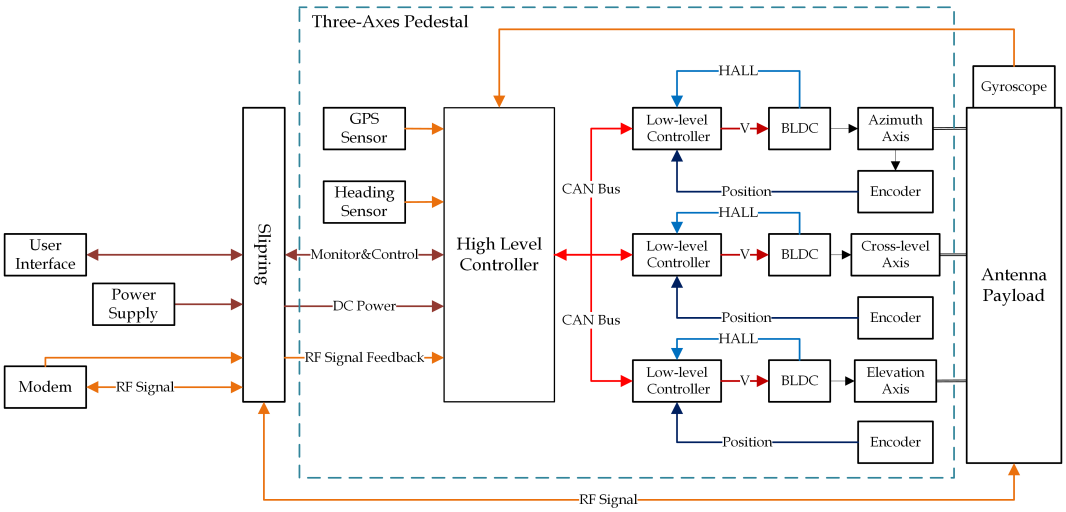

Figure 2.1 : The block diagram of the APS.

aperture reflects the energy. The line of sight (LOS) of the aperture represents the direction of maximum gain. The gain pattern represents the aperture radiation pattern as a function of the pointing angle from the LOS. The gain pattern for the Ku band antenna is represented in Figure 2.2. Most of the dispersed energy is propagated in aperture main beamwidth. The beamwidth of the aperture is the angular width in the main beamwidth at the desired gain level. -3 dB and -10 dB beamwidth can be seen in Figure 2.2. As shown, the place where the gain falls and rises again away from the LOS is called side lobe. In the first side lobe, the gain is enough to maintain an efficient signal. However, side lobe locking is not accepted for the SOTM antennas due to FCC standards. The main beamwidth varies communication frequency and dish diameter. Increasing the frequency and dish diameter reduces the antenna beamwidth as seen in Figure 2.3. The RF pattern in this figure is plotted in one dimension which depends on one axis angle. The gain pattern which depends on 2-axes angles is shown in Figure 2.4. The horizontal axes show the errors of the antenna on elevation and cross-elevation axes [5].

2.1.3 Pedestal, actuators and sensors

The physical characteristics of the servomechanical pedestals are the robotic structures which include motors, sensors, gyroscope, and payload [2]. The most common pedestal type in SOTM antenna systems is the 2-axes azimuth-elevation pedestal. The azimuth-elevation pedestal is stiffer, low-cost and more compact than the 3-axes pedestal. The only disadvantage of the 2-axes pedestal is that when the elevation axis

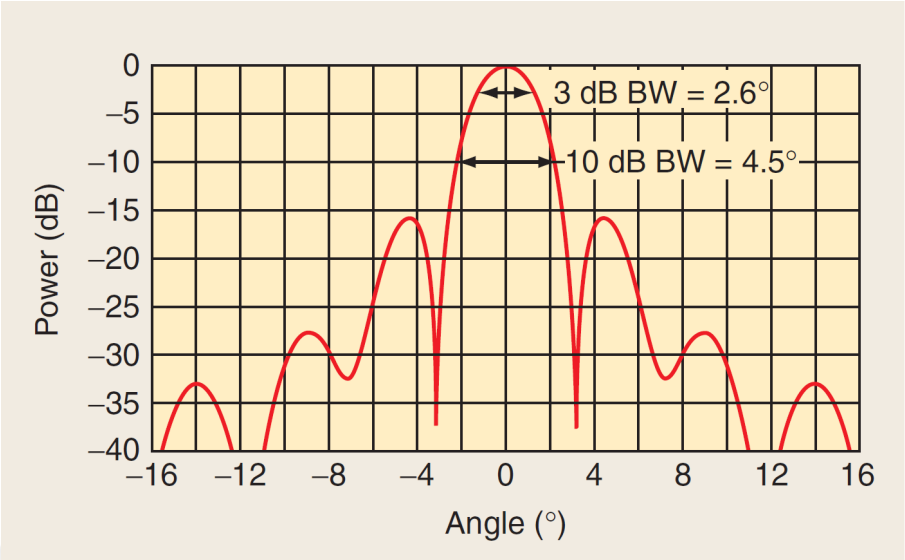

Figure 2.2 : The gain pattern of Ku band aperture, adapted from (Debruin, 2008).

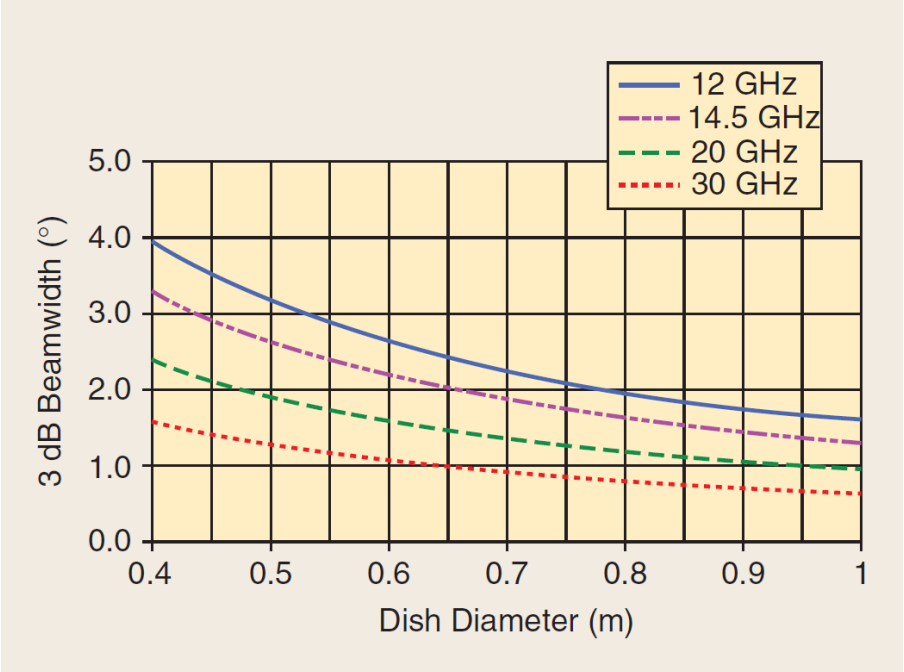

Figure 2.3 : The changing of the beamwidth with respect to frequency and dish size, adapted from (Debruin, 2008).

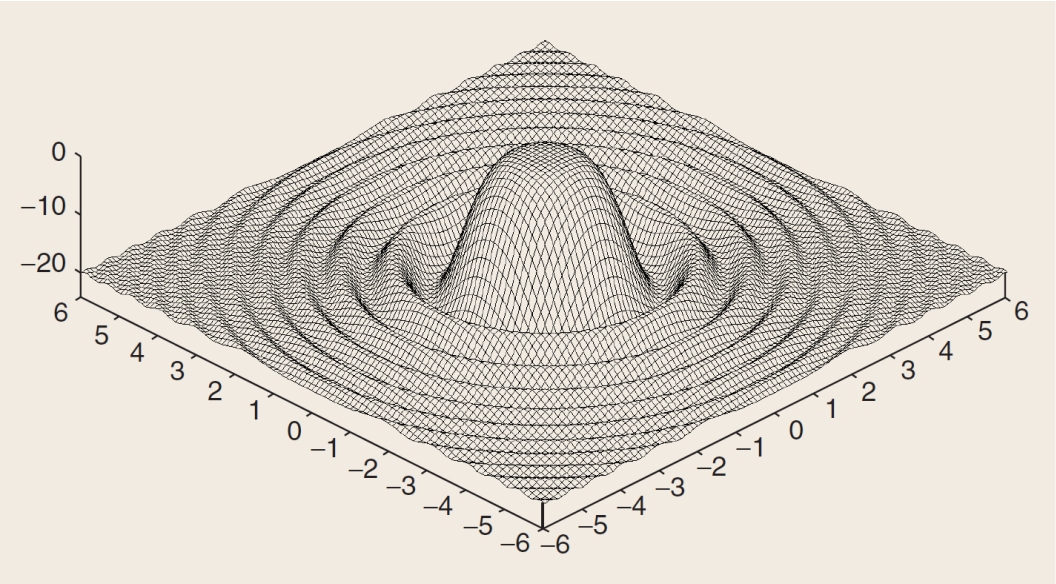

Figure 2.4 : The gain pattern which depends on 2-axes angles, adapted from (Debruin, 2008).

is above 90° from the horizon, the gimbal lock (keyhole) problem occurs. At this point, the azimuth axis cannot contribute to the end-effector orientation. The difficulty of the operation in the keyhole can be explained by the roll coupling. Roll coupling is the circumstance in which the roll axis of LOS coincident to the roll axis of the antenna base depending on the elevation axis angle. Keyhole region is started when the elevation axis angle is bigger than 80°. In this region, the azimuth axis demands twice more torque than nominal needs. The keyhole problem of the 2-axes pedestal can be alleviated by adding a third axis. After adding the third axis, there are 4 different configurations to build 3-axes pedestal by:

1. Azimuth, elevation, cross-elevation

2. Azimuth, cross-level, elevation

3. Azimuth, canted-level, elevation

4. Tilt, azimuth, elevation

The most common approaches are the second and third configurations. In fact, both are the same structure but the only canted-level axis is tilted to increase the stiffness of the mechanical structure are shown in Figure 2.5. The duty of cross-level or canted level axis is to minimize the elevation axis angle. SOTM antenna structure

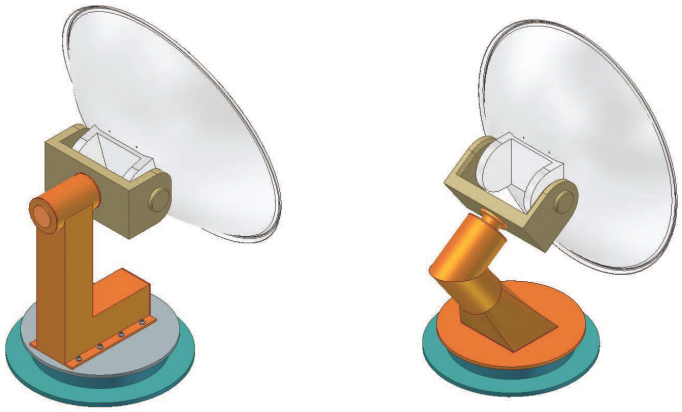

Figure 2.5 : 3-axes pedestal with cross-level axis shown in the left, with canted-level axis shown in the right, adapted from (Debruin, 2008).

has low power requirements due to its gimbal structure and precision manufacturing methods. The azimuth axis motors in azimuth-elevation pedestal require nearly 150W when the elevation angle is 80° which is the starting point of the keyhole [5]. Brushed DC motors are not suitable for the SOTM antennas since they need continuous maintenance due to their brushed. Brushless motors such as Brushless DC Motors (BLDC) and Permanent Magnet Synchronous Motors (PMSM) are suitable for SOTM antenna because of their long life, high efficiency, high dynamic response, and better torque-speed characteristic. However, due to a sinusoidal waveform of the back-emf voltage of the PMSM, PMSM requires a more complex driver circuit, complex controller algorithms, and high-resolution sensor. BLDC can be driven with HALL sensor since they have a trapezoidal waveform of back-emf voltage [7]. It is more convenient to use BLDC motors in SOTM antenna systems due to the low power requirement and easy to implement.

The properties of the gyroscope sensor play a very important role in stabilizing the SOTM antennas. The gyroscope sensor can be Ring Laser Gyro (RLG), Interferomagnetic Fiber-Optic (IFOG), Attitude Heading Reference System (AHRS) and Micro-electro-mechanical sisters (MEMS). The stability and scale factor graph of these sensors is shown in Figure 2.6. It is obviously clear that RLG and IFOG sensors have better stability and scale factor than MEMS sensor although MEMS sensors, which are solid-state inertial sensors, have the advantage of cost, size, and weight. The development of MEMS sensors is constantly evolving but is still retarded from IFOG sensors [8].

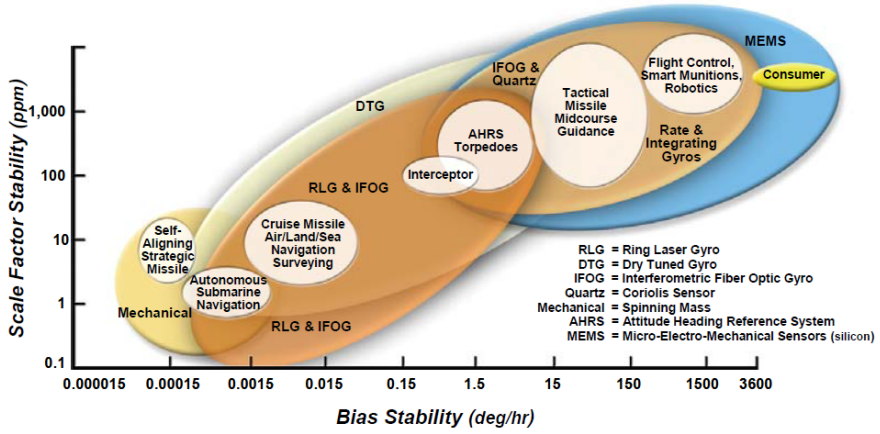

Figure 2.6 : The comparison of the different gyro sensors with respect to the bias stability and scale factor stability, adapted from (Schmidt, 2010).

2.2 Modeling and Control Strategies

In Figure 2.1, APS manages to point, tracking and stabilization of the 3-axes servo mechanical pedestal. APS consists of two main elements which are the low-level controller and the high-level controller board. The Low-level controller board is the electronic board which includes BLDC driver, microcontroller, RS232, CAN Bus communications and several encoder peripherals such as SSI, Quadrature and RS232. In this card, the BLDC driver has been purchased a commercial driver. During the torque control of the BLDC motors, in order to analyze the effect of the torque ripple in APS, the BLDC motor is modeled in Simulink. This torque ripple is added as a white noise into the stabilization controller Simulink file to analyze the effect on the torque controller. The high-level controller board includes low-level controllers, microcontroller, RS232, and CAN Bus communications.

2.2.1 Kinematic and Dynamic Modeling

In order to simulate the stabilization and tracking controller, the kinematics, dynamics and RF model of the SOTM antenna need to be modeled. Euler angles method is commonly used to create the kinematics model of the SOTM antenna. The velocity and acceleration relations of the sequential axes and base frame to end-effector are calculated with Euler angles [9–12]. Another approach developing the kinematic model is to use the Denavit-Hartenberg method which is used in robotics commonly

[13]. The inverse kinematics which used in the positioning of the SOTM antenna and the angular velocity relation between then end effector and base plane in stabilization can be expressed more easily by this method.

Dynamic modeling of the antenna system has a very important role in controller design. The controller of each axis controls the required torque to stabilize the system. Most of the article in the literature use Euler moment equations to describe the relation between torque and angular velocity and acceleration for 2-axes and 3-axes pedestals [9,14,15]. The calculated dynamic has a nonlinear structure and it needs to be linearized to obtain the equations of motion.

2.2.2 Stabilization Controller

Stabilization is a controller that compensates disturbance effects which are caused by vehicle movement in the SOTM antenna. Gyroscope sensor is commonly used in the stabilization of the SOTM antenna. The control method using this sensor is also referred to in the literature as gyroscope nulling or gyro stabilization. The aim of this controller is to sense disturbance movement using the gyroscope sensor and compensate it to maintain the communication link. The orientation of the antenna payload must be the same regardless of disturbance movement. In literature, there are two methods to stabilize the SOTM system. In the first one, also the common one, the gyroscope sensor is placed on the antenna payload. In the literature, it is referred to as LOS stabilization or direct stabilization method. The aim in this method is to stabilize disturbance force resulting vehicle movement by measuring on the end effector which is LOS [2,16–20]. The second one, the gyroscope sensor is placed on the antenna base frame. In the literature, it is called as feedforward stabilization or Indirect Stabilization method. This method is used when there is not enough space to mount the gyroscope sensor on the end effector such as mirror stabilization, camera stabilization, etc. The reason for this, indirect stabilization is less efficient and has more error sources than direct stabilization [21,22].

2.2.3 Closed-Loop Controller

There are two types of position controller in the SOTM antennas. The first one is referred to as Open-loop controller or Point Mode controller in the literature. In this

control structure, precise positioning is provided by using highly sensitive AHRS or Fiber Optic gyro without RF signal feedback. In this structure, the sensor which is placed on the azimuth axis measures the roll, pitch and yaw angles of the azimuth axis to find the correct look angles using inverse kinematics. The second one is referred to as Closed-loop controller or Track Controller in the literature. In this control structure, pointing is provided by measuring the RF signal strength. When this structure is used stabilization controller acts as the inner loop controller and the closed-loop controller acts as the outer loop controller [4, 16, 20, 23].

RF signal measurement cannot be included directly as feedback to the closed-loop controller. The reason for this problem is caused by the antenna pattern which depends on two axes. The decrease in the RF signal strength may be caused by changing of the elevation axis or changing of the azimuth axis or changing of both axes. In order to understand the decrease of the RF signal is to find the maximum the RF signal strength by using scanning algorithms. The most common and easiest one is the step-track algorithm. It is achieved by to move step by step in the direction of the increased signal until the signal strength decrease in any axis. After finding the maximum signal level on the single axis, the same process is performed on the other axis and the maximum signal level of the satellite is found [24–27]. Another method is using the conical scan which is commonly used in radar systems and the big earth stations. This method is more complex than the step-track algorithm. This algorithm plans cosine and sine trajectories to the EL and XEL axes of the antenna payload respectively. The scanning area can be expanded by varying the amplitude of sine and cosine trajectories. During the conical scan, the antenna does not lose any power in the RF signal when the antenna LOS is in the center of the RF signal [28–30].

2.3 APS System Architecture

The hardware of APS is shown in Figure 2.1, will be used in the commercialization project of the ENGİN shipborne SOTM antenna. The aim of the APS is to ensure the best positioning accuracy with a simple and cost-effective system.

APS uses a carbon fiber parabolic dish which diameter is 1 meter. Parabolic dish antennas are commonly used because of high-efficiency and cost-effective. The gain pattern of the dish antenna which depends on the frequency is shown in Figure 2.7. Due

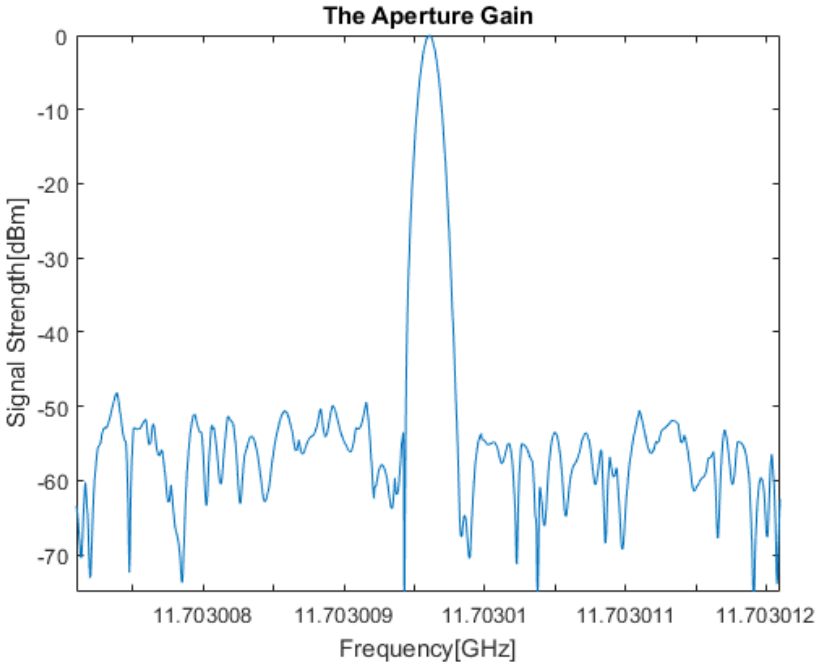

Figure 2.7 : The aperture gain of the ENGİN shipborne SOTM antenna.

to the usage of the parabolic antenna, to compensate the disturbance and to point the satellite a servomechanism pedestal is needed. A 3-axes pedestal which includes the azimuth, canted-level, and elevation axis structure will be used in the APS. Although all axes are operated to stabilize the antenna payload, only azimuth and elevation axes are used in the closed-loop controller. This proves the redundant structure of the 3-axes pedestal. PMSM motors were used which are Beckhoff Servo motors, to provide the necessary orientation of the antenna payload. In case they have good positioning performance, they are very powerful for axis movement and they have complex and large servo drives. Each servo drive can drive two PMSM and its weight is more than 6 kilograms. This isn't a feasible solution for compact SOTM antenna. These motors will have replaced with the BLDC motors which have low power and more compact size. For this purpose, DB56 and DB43 series of motors from Nanotec brand will be used. The ESCON 50/5 BLDC driver of Maxon will be used. It will be assumed that the driver provides the desired torque to the motor in stabilization and tracking simulations. Absolute encoders are available in all axes. The Xsens Mti-30 AHRS sensor is used on the antenna payload to measure both gyro values and roll, pitch and yaw angles. Gyro values are the feedback of the stabilization controller. To find the roll, pitch and yaw angles of base frame roll, pitch and yaw angles of the Xsens are

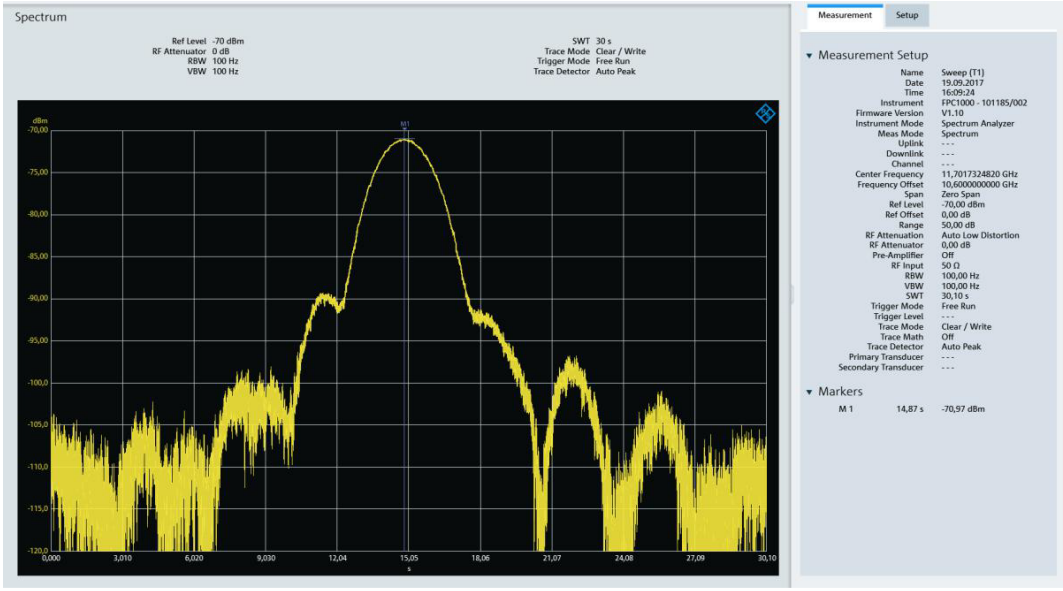

Figure 2.8 : The aperture gain which depends on the azimuth axis of the ENGİN shipborne SOTM antenna.

used in the calculation of look angles.

The aperture gain pattern with respect to the azimuth and elevation axis is shown in Figure 2.8, and 2.9 respectively. Thereby, we are able to determine the -3 dB and -10 dB beamwidth of the aperture. The -3 dB and -10 dB beamwidth of the azimuth axis is calculated 1.664° and 2.954° respectively. Similarly, the -3 dB and -10 dB beamwidth of the elevation axis is calculated 1.684° and 2.888° respectively. It is obvious that there is no pure symmetric but these values are very close to each other. This difference may be caused by the surface quality of the dish or miss alignment on the assembly of the dish. We can assume that the aperture gain pattern has symmetric. -10 dB and -3dB beamwidth is 2.888°, 1.684° respectively. Since the relationships are nonlinear, we can fit a polynomial equation using -3dB and -10 dB values. So, we are able to calculate the pointing error as a function of the RF signal strength. Figure 2.10 shows the fitted polynomial equation, -3dB and -10dB beamwidths.

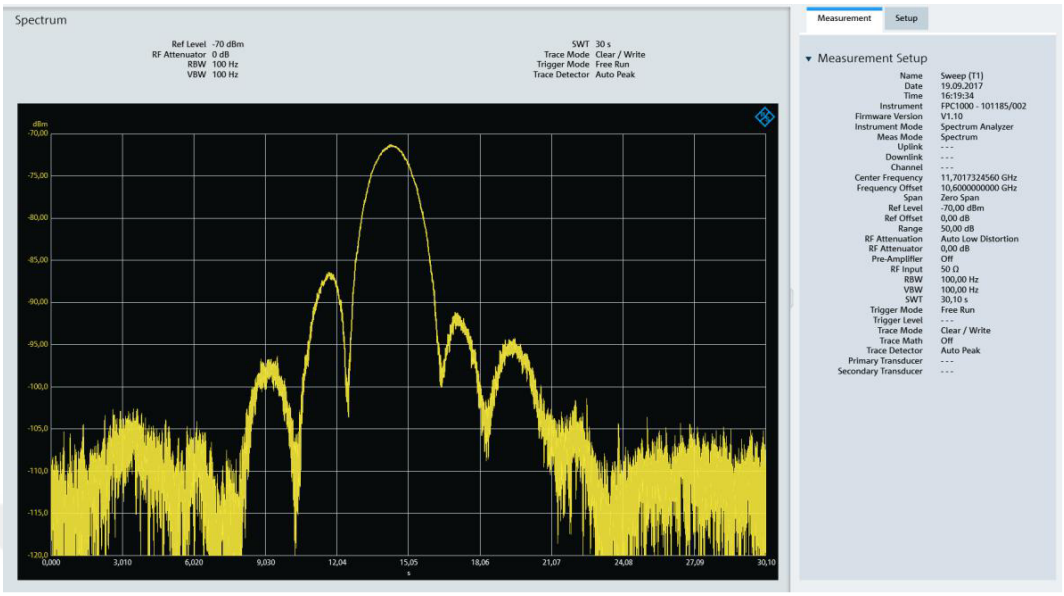

Figure 2.9 : The aperture gain which depends on the elevation axis of the ENGİN shipborne SOTM antenna.

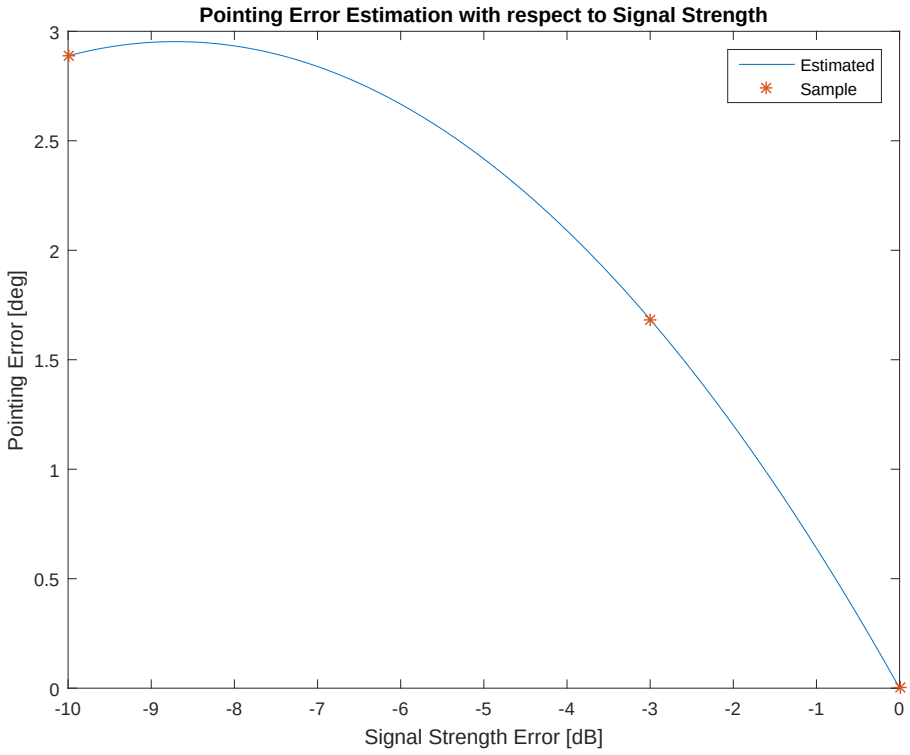

Figure 2.10 : The pointing error changing with respect to RF signal strength.

3. ENGIN SOTM ANTENNA MODELLING

3.1 Kinematic Modelling of the 3-axes Pedestal

In Figure 2.2 and 2.4, the one axis depended on gain and two axes depended gain patterns are shown respectively. In here, the aim of the pedestal kinematic is to possess the orientation which has maximum RF gain. This is the essential relationship between a robotic system and an antenna.

The manufactured ENGIN antenna has four rotational axes which are azimuth, canted-level, elevation and polarization axis as it is shown in Figure 3.1. The polarization axis is related to the RF signal that has linear and circular polarization. This axis is not necessary to use in whole SOTM antennas. While the azimuth and the elevation axes are enough for searching hemisphere during the finding satellite, the azimuth, the canted-level, and the elevation axes are used for stabilizing the LOS. In order to complete the full kinematic of the antenna, the polarization axis has taken into account.

In literature, antenna kinematics is derived by using Euler angles for each axis. Whole axes' frames have the same direction and the difference of them is the changing of the rotation axis. For this reason, in the azimuth axis, the rotation axis corresponds to the z axis of the azimuth frame. In the elevation axis, the rotation axis corresponds to the y axis of the elevation frame. This method is useful for describing the velocity relations of each axis but it makes harder for the inverse kinematic solution because of the different rotation axis [9–12]. To overcome these difficulties, the DH method is used for defining the kinematic of the antenna [6, 13].

3.1.1 Forward kinematics of the antenna

The side drawing of the ENGIN antenna system can be seen in Figure 3.2. Angles of the axes represent the initial position of the antenna system. The $\{x_0, y_0, z_0\}$ frame which is placed with respect to North-East-Down (NED) coordinate system represents the azimuth frame. The NED coordinate system is important to calculate correct

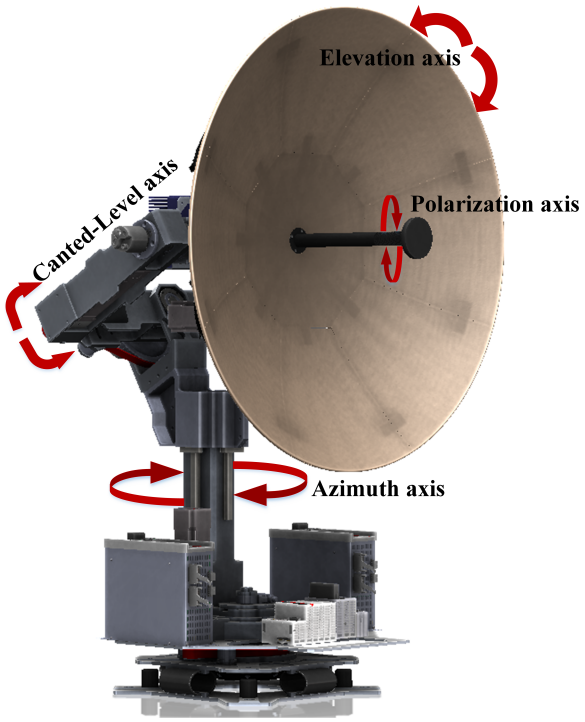

Figure 3.1 : The axes of the ENGIN SOTM Antenna.

orientation with respect to the Global Positioning System (GPS). The z_i axis of the whole frames represents the rotation axis. The x_0 axis of the azimuth frame has to be toward the north in the initial position. β angle is the canted angle which increases the stiffness of the antenna. While this angle offset advances the mechanical properties, the kinematic modeling of the antenna becomes harder. In most robotic systems, the axes of the robots are usually selected with 0° or 90° between sequential axes to simplify the kinematic model. Due to the use of this offset angle, a virtual $\{x_1, y_1, z_1\}$ frame is assigned to correct the relationship between tip and base of the antenna. $\{x_2, y_2, z_2\}$, $\{x_3, y_3, z_3\}$, $\{x_4, y_4, z_4\}$, and $\{x_5, y_5, z_5\}$ frames represent the rotation of canted-level, elevation, polarization and end effector axes respectively. The $\{x_6, y_6, z_6\}$ frame is added to the antenna system for working with GPS sensors and is always the same for each GPS sensor. Therefore, the orientation matrix which is created through collected data from the GPS sensor can be used in the antenna system directly. The DH representation of the antenna that is shown in Table 3.1 can be determined using the axis placement. The DH parameters are created considering GPS data. In Table 3.1, $\beta = 30$, $l_1 = 355.42mm$, $l_2 = 703mm$ and $l_3 = 410.4mm$ for the ENGIN SOTM antenna and they are measured from the CAD assembly of the antenna. The

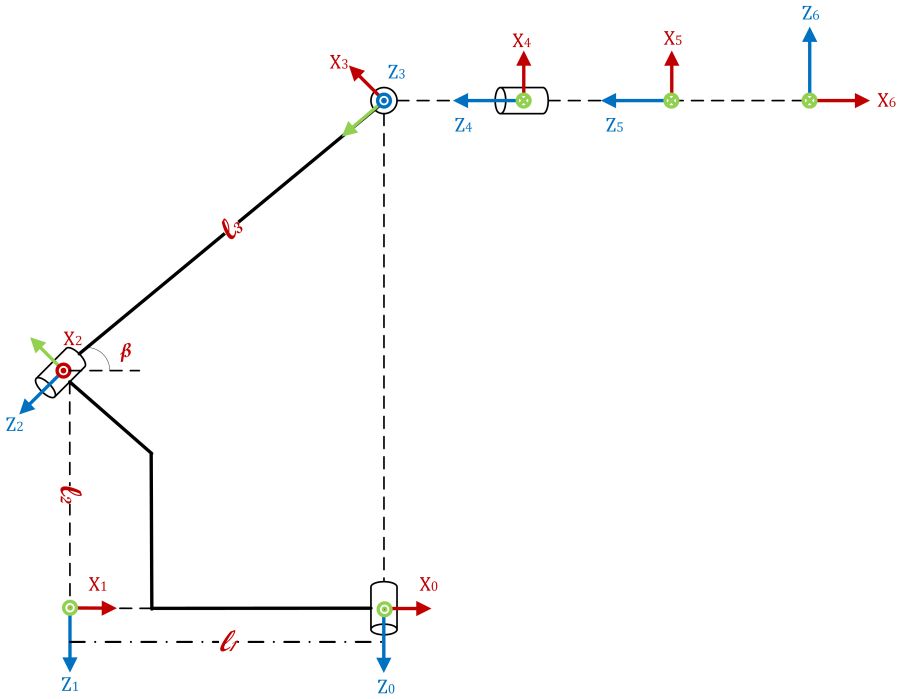

Figure 3.2 : The side drawing of the ENGIN SOTM Antenna.

Table 3.1 : The DH table of the antenna.

i	α_i	a_i	d_i	θ_i
1	0	l_1	0	${\theta_1}^*$
2	$90-\beta$	0	$-l_2$	90
3	-90	0	$-l_3$	${\theta_3}^*-90$
4	90	0	0	${\theta_4}^*+\beta$
5	0	0	0	${\theta_5}^*$

general form of homogenous transformation matrix is given in Equation 3.1. The homogeneous transformation matrices of the links are can be found using DH table as follow: (3.2-3.7).

$$A_i = \begin{bmatrix} \cos(\theta_i) & -\sin(\theta_i)\cos(\alpha_i) & \sin(\theta_i)\sin(\alpha_i) & a_i\cos(\theta_i) \\ \sin(\theta_i) & \cos(\theta_i)\cos(\alpha_i) & -\cos(\theta_i)\sin(\alpha_i) & a_i\sin(\theta_i) \\ 0 & \sin(\alpha_i) & \cos(\alpha_i) & d_i \\ 0 & 0 & 0 & 1 \end{bmatrix} \tag{3.1}$$

$$A_1 = \begin{bmatrix} \cos(\theta_1) & -\sin(\theta_1) & 0 & l_1\cos(\theta_1) \\ \sin(\theta_1) & \cos(\theta_1) & 0 & l_1\sin(\theta_1) \\ 0 & 0 & 1 & 0 \\ 0 & 0 & 0 & 1 \end{bmatrix} \tag{3.2}$$

$$A_2 = \begin{bmatrix} 0 & -\cos(90-\beta) & -\sin(90-\beta) & 0 \\ 1 & 0 & 0 & 0 \\ 0 & \sin(90-\beta) & \cos(90-\beta) & -l_2 \\ 0 & 0 & 0 & 1 \end{bmatrix} \tag{3.3}$$

$$A_3 = \begin{bmatrix} \cos(\theta_3-90) & 0 & -\sin(\theta_3-90) & 0 \\ \sin(\theta_3-90) & 0 & \cos(\theta_3-90) & 0 \\ 0 & -1 & 0 & -l_3 \\ 0 & 0 & 0 & 1 \end{bmatrix} \tag{3.4}$$

$$A_4 = \begin{bmatrix} \cos(\theta_4+\beta) & 0 & \sin(\theta_4+\beta) & 0 \\ \sin(\theta_4+\beta) & 0 & -\cos(\theta_4+\beta) & 0 \\ 0 & 1 & 0 & 0 \\ 0 & 0 & 0 & 1 \end{bmatrix} \tag{3.5}$$

$$A_5 = \begin{bmatrix} \cos(\theta_5) & -\sin(\theta_5) & 0 & 0 \\ \sin(\theta_5) & \cos(\theta_5) & 0 & 0 \\ 0 & 0 & 1 & 0 \\ 0 & 0 & 0 & 1 \end{bmatrix} \tag{3.6}$$

$$A_6 = \begin{bmatrix} 0 & 0 & -1 & 0 \\ 0 & 1 & 0 & 0 \\ 1 & 0 & 0 & 0 \\ 0 & 0 & 0 & 1 \end{bmatrix} \tag{3.7}$$

The forward kinematics model can be calculated using as follow:

$$T_6^0 = A_1A_2A_3A_4A_5A_6 \tag{3.8}$$

3.1.2 Confirmation of the forward kinematic model

The forward kinematics model is confirmed via MATLAB code which is given in Appendix A.2. The first step of the confirmation of kinematic, the position of the end effector at the initial position is calculated. The end effector position according to base with given joint angles in Equation 3.9 is provided in Equation 3.10.

$$q = \begin{bmatrix} 0 & 90 & 0 & 0 & 0 \end{bmatrix}^T \tag{3.9}$$

$$T_6^0 = \begin{bmatrix} 1 & 0 & 0 & 0.0032 \\ 0 & 1 & 0 & 0.0000 \\ 0 & 0 & 1 & -908.2000 \\ 0 & 0 & 0 & 1 \end{bmatrix} \tag{3.10}$$

In Equation 3.10, the position values of the y and z axis are calculated correctly but the x axis is expected to be 0 mm. Although the position value of the x axis is found as 0.0032 mm in the calculation, this is quite small to be neglect. The second step of the kinematic confirmation is an important issue for finding the satellite. This is the comparison between the antenna actual and desired orientation given GPS values. The desired orientation matrix (R_{4A}^{IST}) of the TURKSAT 4A from Istanbul can be seen in Equation 3.11. The joints' angles which cover the expectation of the orientation matrix are given in Equation 3.12.

$$R_{4A}^{IST} = \begin{bmatrix} -0.7148 & 0.1664 & 0.6792 \\ 0.2520 & 0.9673 & 0.0281 \\ -0.6524 & 0.1913 & -0.7334 \end{bmatrix} \tag{3.11}$$

$$q = \begin{bmatrix} 160.60 & 90.00 & 0.00 & 40.72 & 165.40 \end{bmatrix}^T \tag{3.12}$$

If these joints' angles are substituted in the forward kinematics model, the transformation matrix is found as shown in Equation 3.13. Consequently, it is clear that the kinematic model of the antenna system is true because the results are highly familiar with the desired orientation matrix (3.11).

$$T_6^0 = \begin{bmatrix} -0.7149 & 0.1663 & 0.6792 & 0.0030 \\ 0.2517 & 0.9674 & 0.0281 & 0.0011 \\ -0.6524 & 0.1910 & -0.7334 & -908.2000 \\ 0 & 0 & 0 & 1 \end{bmatrix} \tag{3.13}$$

3.1.3 Inverse kinematics model of the antenna

While the transformation matrices (3.8) are used for solving the inverse kinematics in ordinary robotics system problem, the orientation matrices (3.14) are used for the inverse kinematic solution of this antenna. Because the end-effector position is not important in pointing. Since the antenna is similar to the wrist of the industrial robot, it is only important to possess the correct orientation.

$$R_{desired} = R_1 R_2 R_3 R_4 R_5 R_6 \tag{3.14}$$

The second transformation matrix is an imaginary axis so that there is no joint variable. For this reason, it is a constant matrix in any joints configuration. $\cos(90 - \beta) = 0.866$

and $\sin(90-\beta)=0.5$ are the constant values. The antenna system has a canted-level joint to avoid singularity regions. During the pointing to the satellite, the azimuth, and the elevation axes are enough for pointing so that the canted-level axis is 0° ($\theta_3=0$). Actually, the canted-level axis has a small amount of movement during the stabilization but this movement is assumed that the axis is stationary. Therefore, A_3 transformation matrix becomes a constant and the amount of variable in the forward kinematics decrease. To solve the inverse kinematics, the desired orientation matrix must be equal to the forward kinematics of the antenna system (3.14). The inverse kinematic solution for the elevation angle (θ_4) is then:

$$\theta_4 = atan2(-0.866, 0.5) + atan2(\pm\sqrt{1-r_{31}^2}, r_{31}) \tag{3.15}$$

The inverse kinematic solution for the azimuth angle (θ_1) is:

$$\cos(\theta_1) = \frac{r_{11}}{0.5\sin(\theta_4+\beta)+0.866\sin(\theta_4+\beta)} = a \tag{3.16}$$

$$\sin(\theta_1) = \frac{r_{21}}{0.5\sin(\theta_4+\beta)+0.866\sin(\theta_4+\beta)} = b \tag{3.17}$$

$$\theta_1 = atan2(b,a) \tag{3.18}$$

And the inverse kinematic solution for the polarization angle (θ_5) is found as:

$$\cos(\theta_5) = \frac{r_{33}}{0.5\sin(\theta_4+\beta)+0.866\sin(\theta_4+\beta)} = a \tag{3.19}$$

$$\sin(\theta_5) = \frac{r_{32}}{0.5\sin(\theta_4+\beta)+0.866\sin(\theta_4+\beta)} = b \tag{3.20}$$

$$\theta_5 = atan2(b,a) \tag{3.21}$$

There are two solution sets for the inverse kinematic solutions (a,b) due to the positive and negative solutions of θ_4. The correct solution set in our case is selected such that θ_4 must be between 0° and 90°.

3.1.4 Confirmation of the inverse kinematic model

The forward kinematic is be used to confirm inverse kinematics. To accomplish this confirmation, the forward kinematic model of the antenna system was created with given joint values in (3.12). Also, the orientation matrix of the end effector would be an input of the inverse kinematics. The result of the calculation in matrix form is shown in

Equation 3.22. These calculated angles are elevation, azimuth and polarization values respectively and have the same values with respect to the reference values (3.12).

$$q = \begin{bmatrix} 40.7207 & 160.6000 & 165.4000 \end{bmatrix}^T \tag{3.22}$$

3.2 Dynamic Modelling of the 3-axes Pedestal

The dynamic of the serial robots is specified by the relation between the torques generated by the joints' actuator and position, velocity and acceleration with respect to time. Thus, the dynamic of the robot has to be modeled to analyze and optimize the desired controller performance. Generally, there are two methods that are Lagrange-Euler and Newton-Euler in the robotic literature to develop the dynamic model of the robot [31]. However, these methods have not been tried in the SOTM antenna yet. In literature, the Euler equations are used the describe the dynamics. This method is very useful the transform the LOS velocity to the angular torques which make easier the gyroscope stabilization [9, 14, 15].

The dynamic model of the 3-axes pedestal shall be obtained using the Newton-Euler method. Since the Newton-Euler method is a recursive method, firstly the velocity and acceleration relationship of each sequential link must be calculated using the forward calculations. Secondly, the force and torque relationship of each sequential link must be calculated using backward calculations. Combining the backward and the forward calculation, the dynamic of the robot is conducted. In Equation 3.23, the general torque equation of the i link is shown. In here, ${}^{i}N_i$ is the torque value which occurs while the rotation of the i axis inertia. ${}^{i+1}n_{i+1}$ is the torque value which is applied torque by the $i+1$ link to the i link. ${}^{i}P_{C_i} \times {}^{i}F_i$ is the torque value which is generated by the force on the center of gravity of the i link to the rotation axis. ${}^{i}P_{i+1} \times {}^{i}_{i+1}R^{i+1} f_{i+1}$ is the torque value is generated by the force which is on the $i+1$ link.

$$n_i^i = {}^{i}N_i + {}^{i}_{i+1}R^{i+1} n_{i+1} + {}^{i}P_{C_i} \times {}^{i}F_i + {}^{i}P_{i+1} \times {}^{i}_{i+1}R^{i+1} f_{i+1} \tag{3.23}$$

Since the mechanical structure of the antenna is gimbal structure, the antenna has a more compact and robust design than serial robots. Additionally, the main aim in the mechanical design is to coincident the center of gravity with the rotation axis of each link which is named as perfect balance. If there was no friction and loses in the antenna, the antenna would automatically stabilize itself without actuator in this design. This

also is referred to as a mass stabilization of the system. However, it is not possible in the practice and the stabilization of the antenna is provided by low power actuators.
Basically, to create the dynamic model of the antenna the forward and the backward calculations should be calculated. In addition, the dynamic model of the antenna can be simplified because of the mechanical structure. Firstly, if the torque equation of the elevation axis is written with respect to the Newton-Euler, the $i+1$ torque and force values equal to zero due to movement in the free space. The antenna is covered by the composite structure which is conductible for RF signal and solid for the disturbances such as wind, rain, etc. Since the center of gravity and the rotation axis are coincident, the torque that generated by the force on the center of gravity equals to zero. To sum up, for the elevation axis, the torque equals the just the torque generated by the inertia of the elevation axis.
This simplification can be applied to other axes. The dynamical modeling of the 3-axes SOTM antenna is examined in [32]. The Matlab SimMechanics model and the single input single output (SISO) model of the SOTM is compared. The result of this comparison is outputs of both models are almost the same. In fact, the computational demands of the SISO model are lower than the SimMechanics model. To conclude, the whole axis is to be modeled using a SISO system by the help of the perfect balance and pedestal structure..

3.2.1 Simplified dynamical axis model of the antenna

In order to make up the dynamical equation of the antenna, we have to concern both the torques which are caused by the rotation and the torques which are caused by the friction. Equation 3.24 describes the relationship between the torques and motion of the simplified axis. This equation describes the equation of the axis motion. So, the whole parameters must be the axis parameters.

$$\tau = I\dot{\omega} + B\omega + Tsign(\omega) \tag{3.24}$$

Where;

- I: axis moment of inertia [kg.m2]
- B: viscous friction coefficient [N.m.s]
- T: dry friction coefficient [N.m]

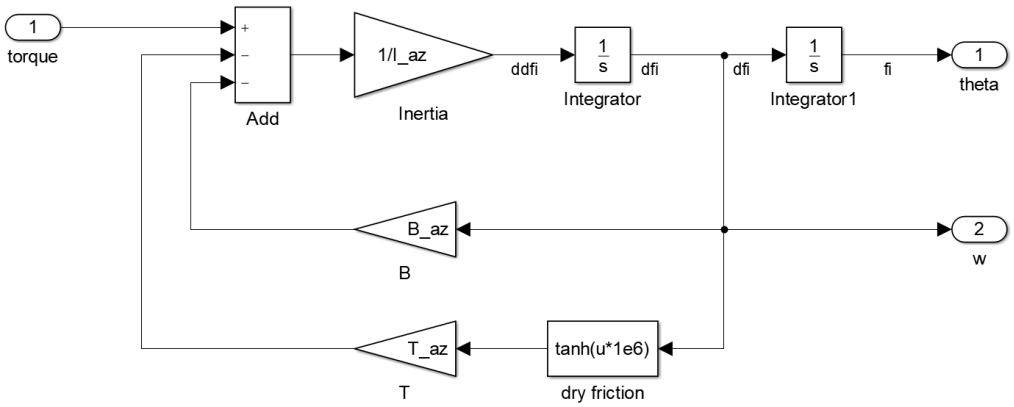

Figure 3.3 : The simplified axis model of the azimuth axis.

Table 3.2 : The parameters of the dynamic equations.

Axis	Inertia	Viscous friction
Azimuth	2.5359	0.2
Canted-level	1.4250	0.2
Elevation	1.6759	0.2

- τ: total axis torque [N.m]
- ω : axis velocity [rad/s]

Equation 3.24 can be modelled using the differential equation as shown in Figure 3.3. This represents the dynamical model of the azimuth axis. The other axes can be modeled using the same approach. The inertia of each axis is taken from the CAD part of each axis. In order to derive this value, it is important to coincident the rotation axis with the inertia calculation axis. Otherwise, the inertia and torque values are calculated wrong. Viscous friction is estimated by the ball bearing reference manual. In the model, the dry friction is added. In order to estimate the dry friction is hard and this value is taken zero in the dynamics of the antenna. If there was dry friction in the axis, it would be suggested to use feedforward control compensates for the dry friction. The parameters of the dynamic equation for each axis can be shown in Table 3.2. The whole dynamic model of the antenna is shown in Figure 3.4. The inputs of the axis are limited by the saturation blocks to implement the physical limitations.

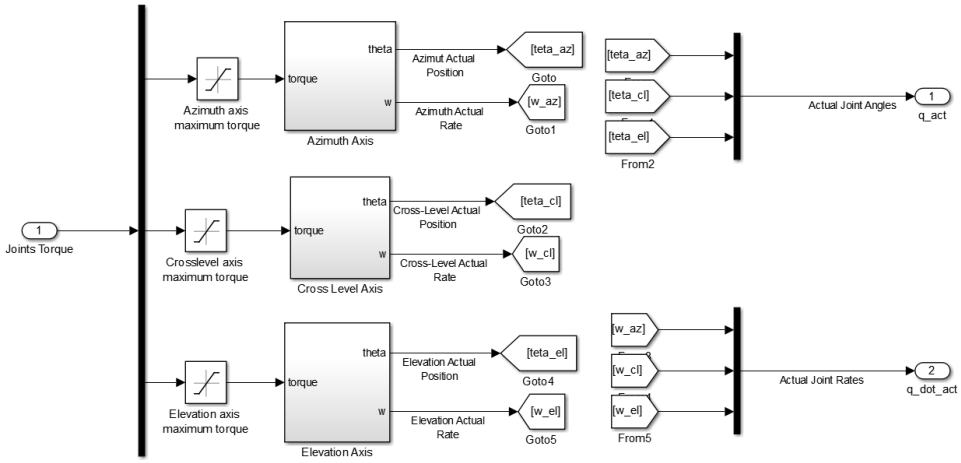

Figure 3.4 : The dynamic model of the antenna.

3.3 Actuator Modelling of the 3-axes Pedestal

Brushless DC Motor (BLDC) is the best choice for SOTM antenna because of their long life, high efficiency, high dynamic response, torque-speed characteristic, and cost-efficiency. Since the controlling of the BLDC is easier than the PMSM, it is more reasonable to use BLDC motor on each axis. In the market, there is a lot of the BLDC shelf driver to implement on the low-level controller. Generally, this shelf controller drives the BLDC motor with HALL sensor-based. HALL sensor-based control method is the detect the rotor position using the HALL sensor and switching the necessary MOSFETs to change the commutation. Using this method in the driver there are ripples in the electrical torque of the BLDC motor. In order to analyze the effect of the torque ripple on the stabilization and tracking the BLDC motor is modeled and controlled like a shelf driver. The torque ripple which observed in the torque control is added to the dynamics as white noise. In order to examine the torque ripple of a BLDC motor Simscape model is used as shown in Figure 3.5.

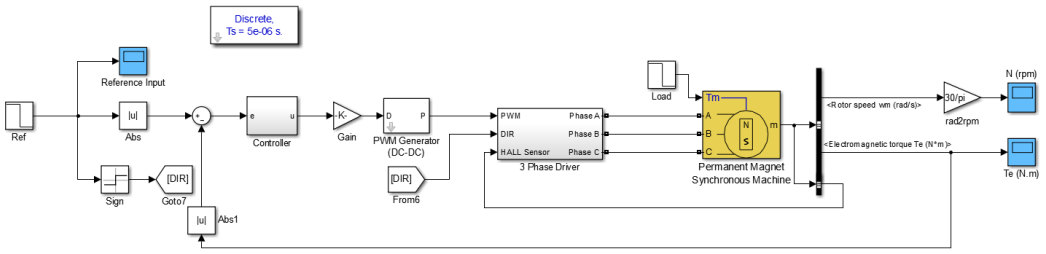

Figure 3.5 : The Simscape model of the BLDC motor.

3.3.1 The simulation of the BLDC motor

The BLDC motor model and the inverters are used of the Simscape library to simulate the BLDC motor. Actually, this model can be constructed with mathematical equations of the BDLC motor. The fact that the BLDC motors have both electrical angle and mechanical angles. The electrical angle is rotated pole pair times faster than mechanical angles. If the pole pairs of the motor are 4, the electrical angles rotate 4 times faster than mechanical angle. To simulate the operation at high speed, the sample time of the simulation must be capable to sample the electrical angle rotation. In Simulink, it can be done by using s-function. Since developing the driver and the motor mathematically in the s-function takes more time, using Simulink libraries are more reasonable.

Because the BLDC motor has trapezoidal back-emf form, the HALL sensor output of the motor model is read by the function which in the script. This function takes the HALL sensor outputs and switches MOSFETs of the inverter to commutates correctly. The controller output is directly connected Pulse Width Modulation (PWM) block which generates PWM signal with 2 kHz. The PWM signal is subjected to in the and gates with switches' signals. Thus, the MOSFET is controlled with the PWM signal which is really close to the real driver. To develop a torque controller, the torque feedback is measured on the motor block is added on the motor. A simple PI control method is used and implemented [7]. Our aim is not the development of the BLDC controller, is to see the noise caused by the driver. The torque controller performance is seen in Figure 3.6. The figure shows us, there is 10% torque ripple on the BLDC electrical torque.

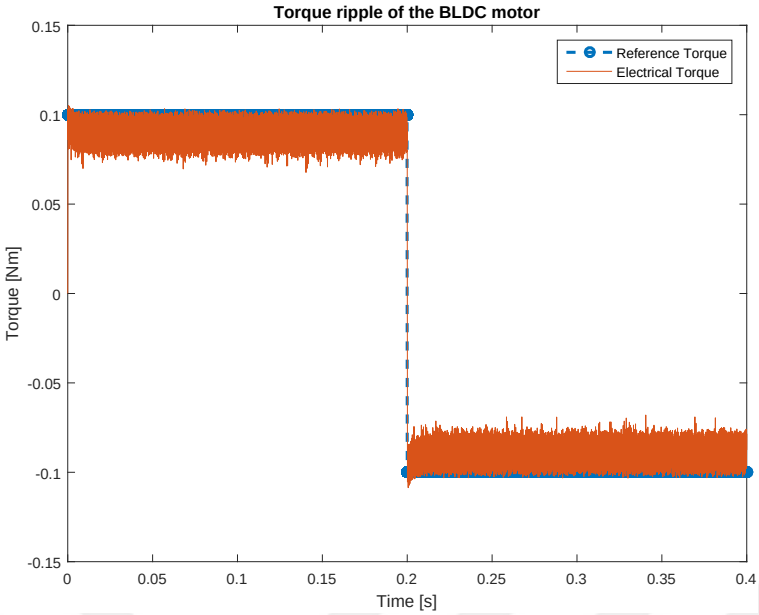

Figure 3.6 : The torque ripple of the BLDC motor.

3.4 RF Modelling of the Antenna Aperture

The aperture gain model is important to simulate the closed-loop algorithm and measuring the pointing error. Theoretically, the aperture gain model has highly nonlinear equations and is harder to simulate in the controller. The aperture model depends on several factors but it can be represented using Gaussian wave. We assume that the aperture has an ideal form. The second assumption in the simulations, we are only interested in the main beamwidth of the aperture. Thus, axes' angle is limited between +5° and -5°. So that, reduce to complexity a simple Gaussian waveform is created in Figure 3.7. The coefficients of the wave are calculated as the 10dB beamwidth of the aperture is 2.888°. Thus the simulated aperture gain is identified with the experiments of the aperture gain (Figure 2.8 and 2.9).

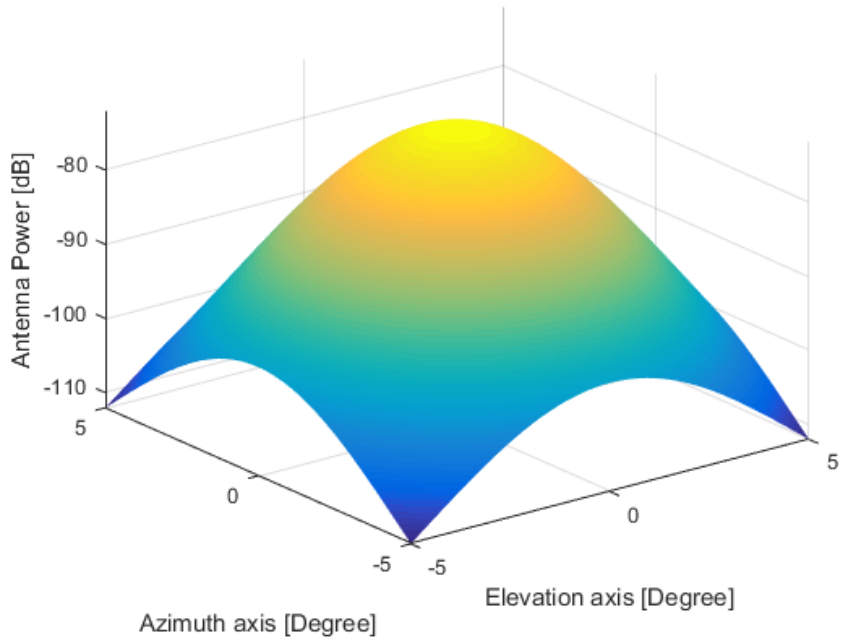

Figure 3.7 : The simulated mainlobe of the aperture gain.

4. LINE OF SIGHT STABILIZATION OF THE 3-AXES PEDESTAL

LOS stabilization consists of two main parts which are an axis controller that is responsible to control the axis rate by applying the torque reference to the BLDC, and kinematic transformations that is responsible to transform the gyroscope sensor values to the axis rate as feedback. These transformations are related to the pedestal structure and vary on different structures.

4.1 Design of the Axis Controller

In order to control the dynamics of the axis, a linear Proportional-Integral (PI) based control is used. Because of the noise of the gyroscope sensor, derivate control isn't used to avoid the growth of the error and giving the bigger torque reference. The PI controller provides low bandwidth and eliminates steady-state error on the output. In addition, the PI controller reduces the phase of the frequency that is lower than the crossover frequency. Thus, the PI controller improves disturbance rejection and reference tracking properties [33]. Closed-loop bandwidth of the controller depends on the type of mobile platforms. Land SOTM antennas have the biggest bandwidth due to off-road conditions in different types of SOTM antennas. The closed-loop bandwidth of the controller of a SOTM antenna is 10 Hz for land vehicle [16]. This frequency is bigger than the required frequency which on the sea platforms, but 10 Hz is used in the design of the controller. The dynamics of the axes were examined in section 3.2. After the simplification whole axes are linear and this makes the designing of the controller easier. The azimuth axis has one pole which is -0.0789 rad/s as shown in root locus of the azimuth axis in Figure 4.1. This states that the system has a slow response. This situation is proved by the step response in the same figure. The rise and settling time of the azimuth axis are 27.9 second and 49.6 seconds respectively. The Bode diagram of the azimuth axis is shown in Figure 4.2. This diagram shows the 3 dB bandwidth of the azimuth and the value of it is 0.554 rad/s. PI controller parameters are tuned which the closed-loop has the 10 Hz (62 rad/s) bandwidth,

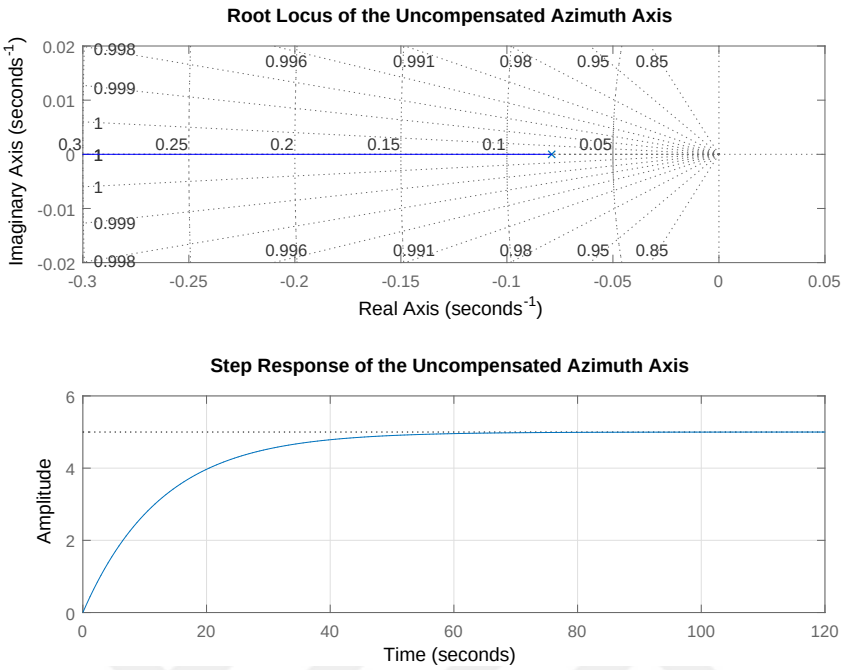

Figure 4.1 : The Root Locus of the uncompensated azimut axis(top), the step response of the uncompensated azimuth axis(bottom).

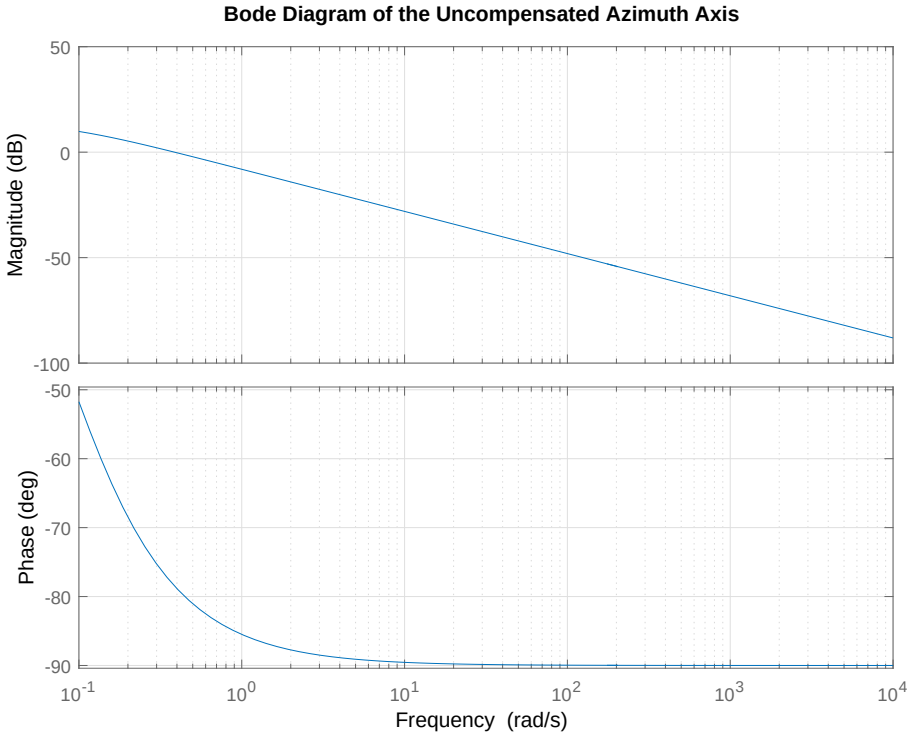

Figure 4.2 : Bode diagram of the uncompensated azimuth axis.

Table 4.1 : Rate controller requirements and estimated parameters.

Axis	Bandwith (rad/s)	Steady State Error	Phase margin °	Kp	Ki
Azimuth	63.71	0	172.52	160.55	99.67
Canted-level	64.13	0	170.27	90.20	100.75
Elevation	64.83	0	170.95	107.55	99.50

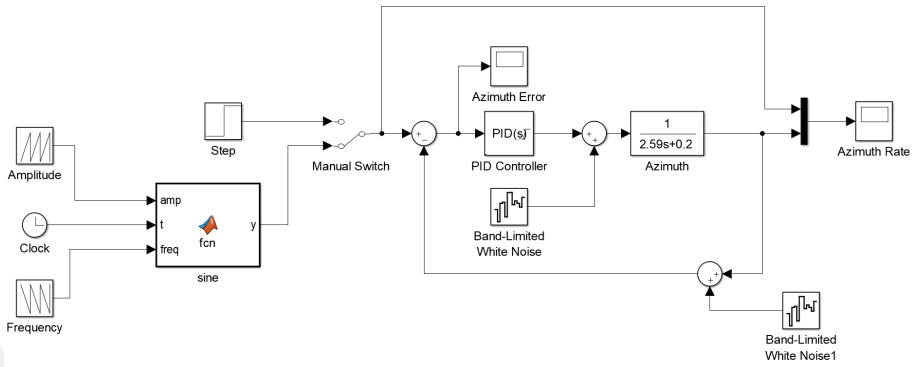

Figure 4.3 : The block diagram of the controlled azimuth axis.

no steady-state error, and more than 170° phase margin requirements. Closed-loop bandwidth defines the maximum disturbance frequency. The phase margin reduces settling time. The canted-level and elevation axes controller parameters are tuned using the same requiremenrs. The whole controller parameters and the requirements of all axes can be shown in Table 4.1. In order to test the performance of the controller, a Simulink file is created as shown in Figure 4.3. The controller structure, the ship movement simulation, and disturbance noises can be seen. The controller structure is the PI controller with back-calculation anti-windup. The parameters of the controller are used in Table 4.1. The controller is saturated between +40 and -40 to limit the controller output. Since the controller output directly defines axis torque, after this limit physical system cannot achieve this reference. This situation gives us knowledge about the motor torque and speed requirements. Selection on the motor and gear this controller output must be overviewed. There are two disturbance noises which are the torque ripple caused by BLDC torque ripple and gyroscope sensor noise. In Figure 4.4, as it is shown in the step response of each axis, the output settles the reference value quickly and no steady-state error. The ship movement is a disturbance movement but this disturbance is sensed by the gyroscope sensor. Instead of giving step reference, the ship movement simulation can be given as a reference to the axis. The sea waves can be modeled using a sine wave that has 0.7 rad/s frequency and 10 amplitude [34].

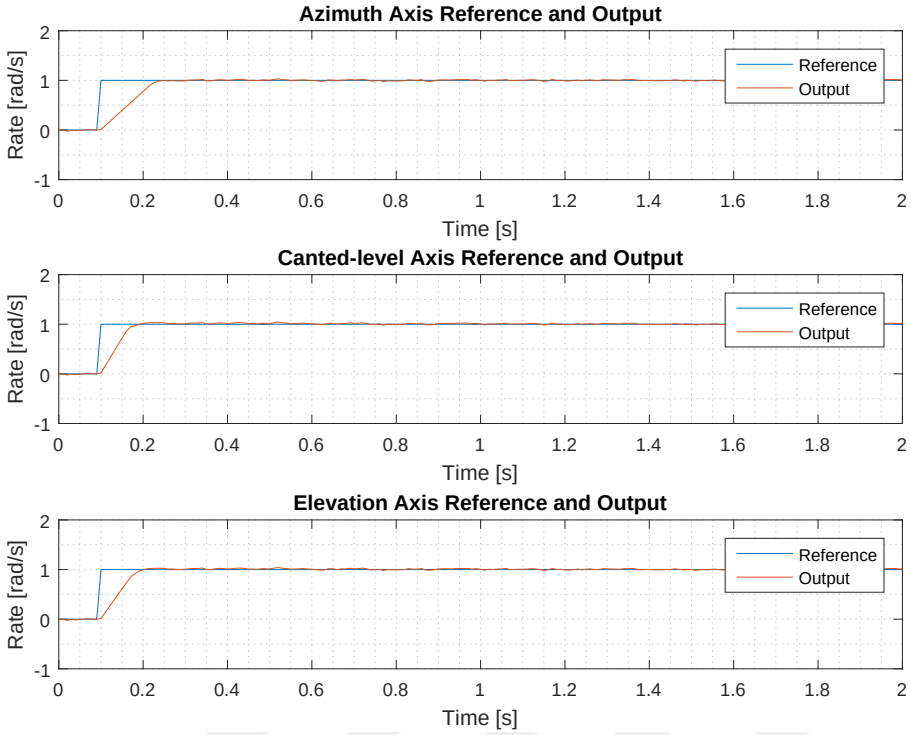

Figure 4.4 : The step response of the each axis.

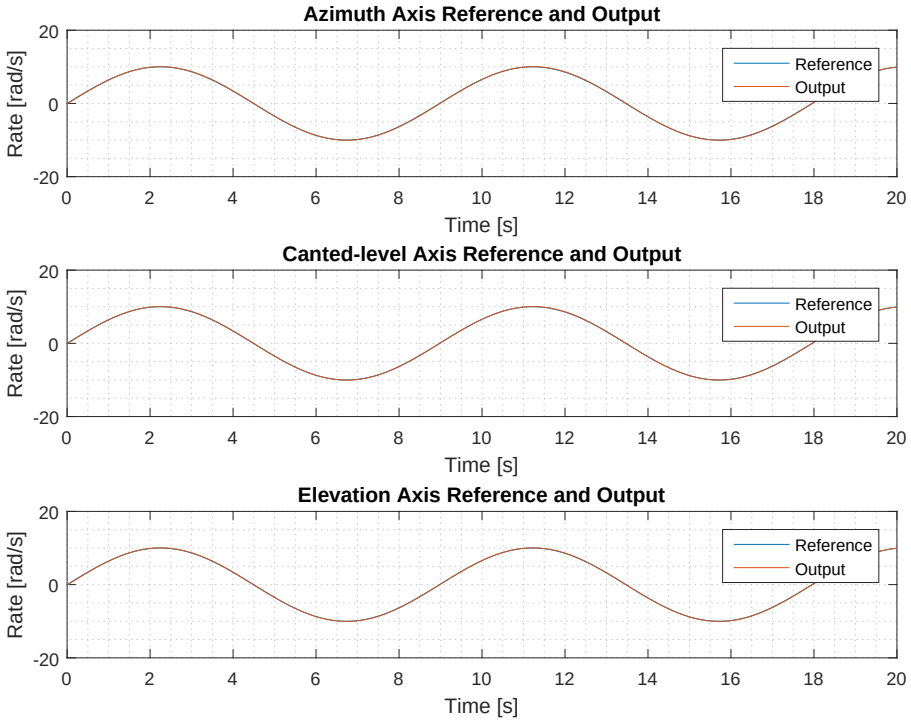

Figure 4.5 : The tracking response of the each axis.

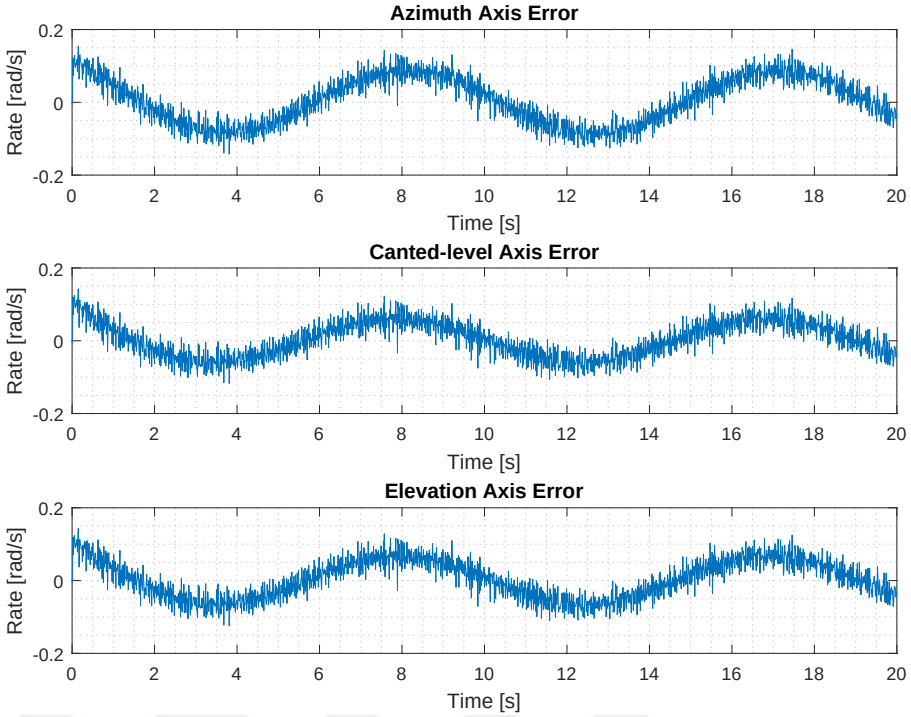

Figure 4.6 : The tracking error of the each axis.

The sine references which is the model of the ship movement of each axis can be seen in Figure 4.5. It is clear that the designed controller of each axis can track the sine reference under gyroscope and torque ripple noises. The tracking error of each axis is shown in Figure 4.6.

4.2 LOS Kinematics of the 2-axes Pedestal

To derive the correct solution for LOS stabilization of the 3-axes pedestal, the LOS simulated of the 2-axes pedestal must be examined in detail. In most application, the 2-axes solution is enough for the LOS stabilization. Analyzing the kinematics of 2-axes pedestal, Euler transforms is used to transform the rotation and velocity with respect to each sequential axis. Since the type mechanism of the pedestal is a gimbal mechanism, Euler transforms make easier the solution for stabilization. The three Euler matrices which depend on the rotation direction are given below respectively the x, y and z axis [2].

$$E_x(\psi) = \begin{bmatrix} 1 & 0 & 0 \\ 0 & \cos(\psi) & \sin(\psi) \\ 0 & -\sin(\psi) & \cos(\psi) \end{bmatrix} \tag{4.1}$$

$$E_y(\theta) = \begin{bmatrix} \cos(\theta) & 0 & -\sin(\theta) \\ 0 & 1 & 0 \\ \sin(\theta) & 0 & \cos(\theta) \end{bmatrix} \tag{4.2}$$

$$E_x(\phi) = \begin{bmatrix} \cos(\phi) & \sin(\phi) & 0 \\ -\sin(\phi) & \cos(\phi) & 0 \\ 0 & 0 & 1 \end{bmatrix} \tag{4.3}$$

If we examine in detail the 2-axes gimbal mechanism, we can explain two different gimbals such as inner gimbal and outer gimbal. For the antenna systems, the outer gimbal is supposed as the azimuth axis and the inner gimbal is supposed as the elevation axis. P (roll), Q (pitch), and R (yaw) are body disturbance rates (velocities) which are measured by a gyroscope that mounted on the mainframe. This gyroscope senses both disturbance and axis rate (which is not required for stabilization but in order to simulate in Matlab we have to define the base disturbance). The other gyroscope which is mounted at the inner gimbal senses angular velocity of the end effector and attempts to hold the LOS steady in spite of the kinematic coupling torques. The first equation of angular velocity for the azimuth axis frame (4.4) written in terms of the body frame rates P, Q and R. The relative gimbal motor rate $\dot{\theta}_{az}$ is added to the vehicle rate to account for gimbal rotation because of the place of the gyroscope.

$$\omega_{\theta_{az}} = \begin{bmatrix} \cos(\theta_{az}) & \sin(\theta_{az}) & 0 \\ -\sin(\theta_{az}) & \cos(\theta_{az}) & 0 \\ 0 & 0 & 1 \end{bmatrix} \begin{bmatrix} P \\ Q \\ R + \dot{\theta}_{az} \end{bmatrix} \tag{4.4}$$

The inner gimbal rates are calculated similarly to the outer gimbal. The rates of the line of sight must be kept as zero to provide the stabilization. It suffices to control only the motion of the two axes orthogonal to the LOS. The movement of the LOS is affected by two rotations thus the endpoint can be stabilized to control just these two axes. The relative gimbal motor rate $\dot{\theta}_{el}$ is added to the azimuth axis rate to account for gimbal rotation.

$$\omega_{\theta_{el}} = \begin{bmatrix} \cos(\theta_{el}) & 0 & -\sin(\theta_{el}) \\ 0 & 1 & 0 \\ \sin(\theta_{el}) & & \cos(\theta_{el}) \end{bmatrix} \begin{bmatrix} \omega_{\theta_{azx}} \\ \omega_{\theta_{azy}} + \dot{\theta}_{el} \\ \omega_{\theta_{azz}} \end{bmatrix} \tag{4.5}$$

$$\omega_{\theta_{el}} = \begin{bmatrix} \cos(\theta_{el})(P\cos(\theta_{az}) + Q\sin(\theta_{el})) - \sin(\theta_{el})(R + \dot{\theta}_{az}) \\ Q\cos(\theta_{az}) - P\sin(\theta_{az}) + \dot{\theta_{el}} \\ \sin(\theta_{el})(P\cos(\theta_{az}) + Q\sin(\theta_{el})) - \cos(\theta_{el})(R + \dot{\theta}_{az}) \end{bmatrix} \tag{4.6}$$

4.3 LOS Simulation of the 2-axes Pedestal

In section 4.2, the angular velocity of the inner gimbal is represented with respect to base disturbance rates, axes' angular rates and angular positions using Euler notation. In order to stabilize the antenna, two orthogonal axes are sufficient for the most application. These orthogonal axes in here are *y* and *z* axes of the inner gimbal. These orthogonal axes are related to the elevation axis or the end-effector. The equation of the *y* axis of the inner gimbal is shown in equation 4.7. This equation specifies that the angular speed of the *y* axis depends on a geometric function of the base disturbance that is dependent on the azimuth angle and the elevation axis rate. In order to stabilize the *y* axis, the elevation motor rate can be controlled.

$$\omega_{\theta_{ely}} = Q\cos(\theta_{az}) - P\sin(\theta_{az}) + \dot{\theta}_{el} \tag{4.7}$$

The *y* axis of inner gimbal stabilization is shown in Figure 4.8. This block diagram is constructed in Simulink and the parameters do not represent the actual system. In this case, our aim is to prove the stabilization of the LOS. The block diagram aims to stabilize the *y* axis using elevation axis motor. The gimbal rate is the same as the elevation rate. To calculate LOS, we have to add the effect of the disturbance of the base. In here, the feedback sensor is coming from gyroscope which is mounted inner gimbal or LOS. The equation of the *z* axis of the inner gimbal is shown in Equation 4.8. This equation specifies that the angular speed of the *z* axis depends on a geometric function of the base disturbance that is dependent on azimuth and elevation angle

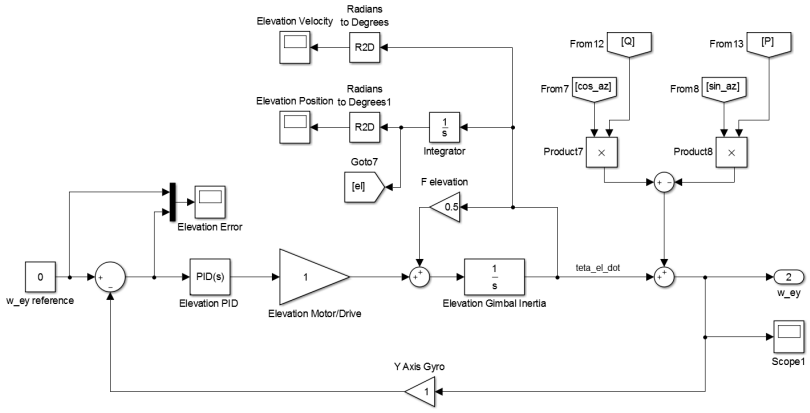

Figure 4.7 : Block diagram of the inner gimbal stabilization.

and azimuth axis rate. In order to stabilize the z axis, the azimuth motor rate can be controlled.

$$\omega_{\theta_{el_z}} = \sin(\theta_{el})(P\cos(\theta_{az}) + Q\sin(\theta_{el})) - \cos(\theta_{el})(R + \dot{\theta_{az}}) \tag{4.8}$$

The z axis of inner gimbal stabilization is shown in Figure 4.9. The block diagram aims to stabilize the z axis using the azimuth motor. This block diagram is more complex than the y axis block diagram. The complexity is caused by the kinematic coupling. The rate of the azimuth axis has directly related the cosine of the elevation angle. Also, this kinematic coupling expresses the gimbal lock problem. When the elevation angle goes to 90°, the cosine of elevation angle goes to zero. This causes the singularity when the elevation angle reaches 90°. There is a different point in here, the gimbal rate is the sum of the azimuth and yaw rate of the disturbance. So, in order to calculate the azimuth motor rate, we have to deduct the yaw rate. To calculate LOS, we have to add the effect of the disturbance. In here, the feedback sensor is coming from gyroscope which is mounted inner gimbal or LOS. The disturbances of the base are created using a sine wave. The disturbance can be seen in Figure 4.9. The y and z axes stabilization results can be seen in Figure 4.10 and 4.11 respectively. It's clear that the controllers compensate for the disturbance movement and stabilize the LOS.

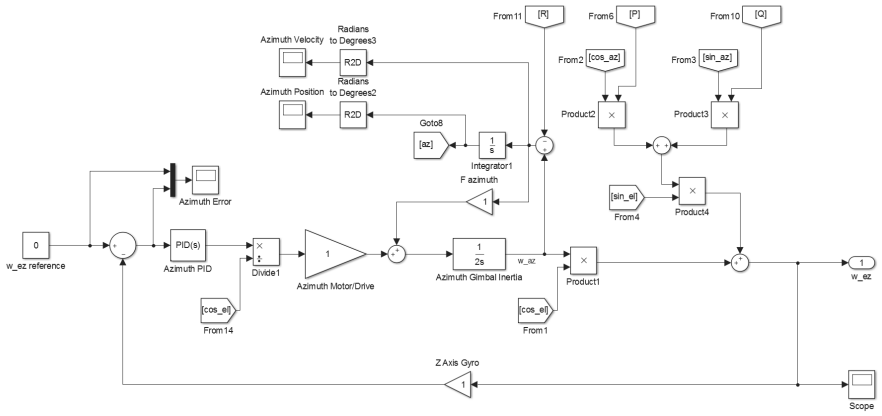

Figure 4.8 : Block diagram of the outer gimbal stabilization.

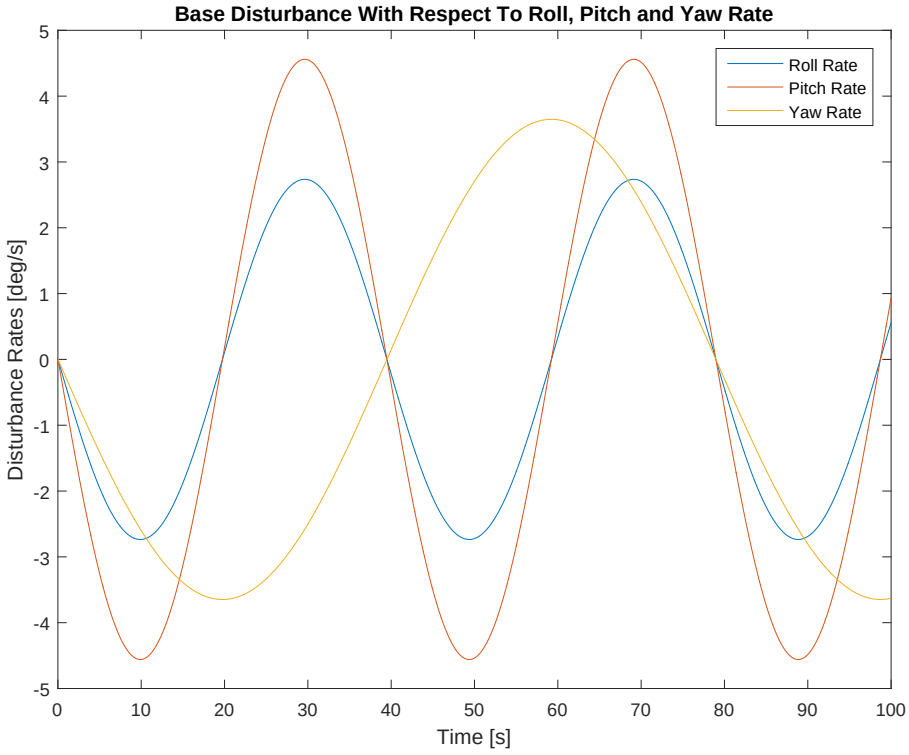

Figure 4.9 : Simulated base motion of the mobile platform.

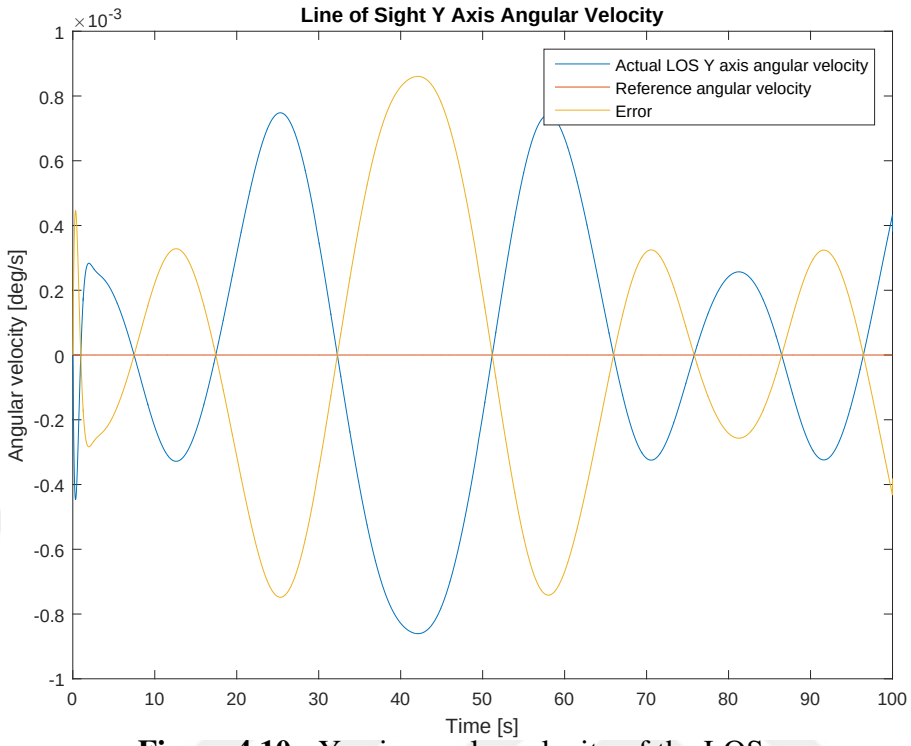

Figure 4.10 : Y axis angular velocity of the LOS.

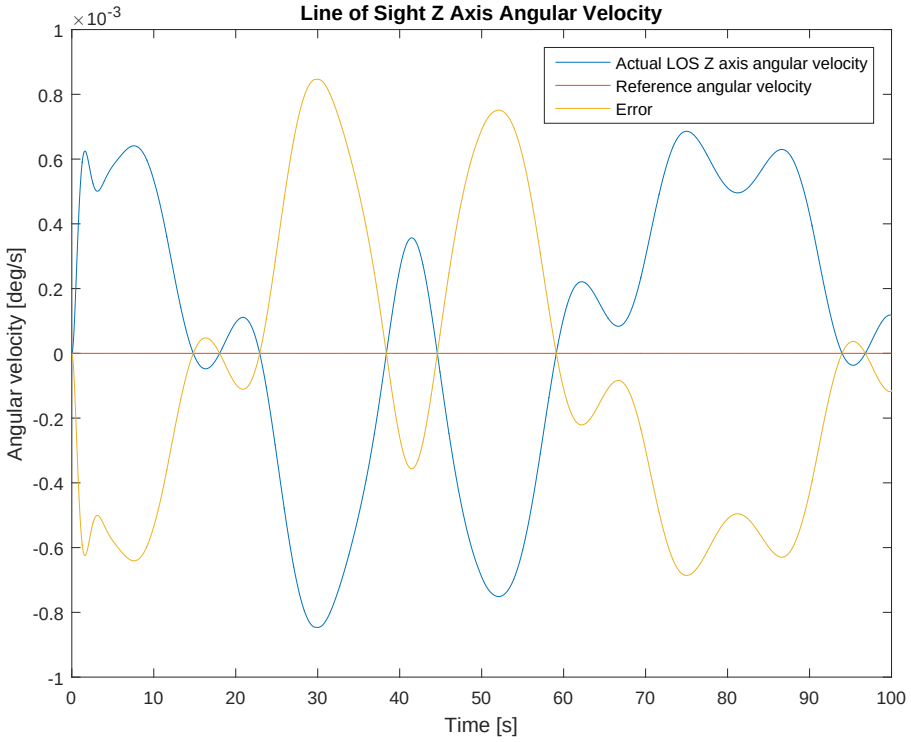

Figure 4.11 : Z axis angular velocity of the LOS.

4.4 LOS Kinematic of the 3-axes Pedestal

In sections 4.2 and 4.3, the LOS kinematic of the 2-axes was examined and simulated. Because of the simplicity of the 2-axes pedestal structure, the y axis of the end effector angular velocity depends on just elevation motor rate and the z axis of the end effector angular velocity is dependent on just azimuth motor rate. In order to control y and z axis of the end effector, controlling of the elevation and azimuth motor is needed respectively. This leads to developing and implement controller more easily. However, in the 3-axes pedestal structure, the angular velocity of the end effector which is elevation axis is more complex than two-axis structure. The y and z axis of the end effector angular velocity depend on two axes motor rate parameters. Thus we are not able to use a control structure such as 2-axes pedestal.

In order to stabilize the 3-axes gimbal, the Jacobian operator is proposed to transform the kinematic relations. The aim of stabilization is to compensate for the end effector angular rates. A Jacobian operator which transform the end effector angular rates to the axis rate is a matrix. Before the calculating angular velocities antenna axis frames must be assigned. The axis coordinate frames are shown as in Figure 3.2. In the Figure, the azimuth, canted-level and the elevation axis can be seen respectively. In here, the polarization axis is not used due to there is no effect on the LOS stabilization. So that the kinematic modeling is ended on the elevation axis. The rotation matrices that are used in the kinematic equations come from Section 3.2.

The angular velocity for the azimuth frame is written in terms of the body frame rates P, Q, and R which is base disturbance respectively roll, pitch and yaw rates and azimuth actuator speed in Equation (4.9).

$$\omega_{az} = R_1^0 \begin{bmatrix} P \\ Q \\ R \end{bmatrix} + \begin{bmatrix} 0 \\ 0 \\ \dot{\theta}_{az} \end{bmatrix} \tag{4.9}$$

The angular velocity for the canted-level frame is written in terms of the azimuth axis frame rate and canted-level actuator speed in Equation (4.10). The rotation of canted-level axis is tilted by mechanically. So that to transform correctly the imaginary

and canted-level axis are added in the equation.

$$\omega_{cl} = R_3^2 R_2^1 \begin{bmatrix} \omega_{\theta_{az}} \\ \omega_{\theta_{az}} \\ \omega_{\theta_{az}} \end{bmatrix} + \begin{bmatrix} 0 \\ 0 \\ \dot{\theta}_{cl} \end{bmatrix} \tag{4.10}$$

The angular velocity for the elevation frame is written in terms of the canted-level axis frame rate and elevation actuator speed in Equation (4.11).

$$\omega_{el} = R_4^3 \begin{bmatrix} \omega_{\theta_{cl}} \\ \omega_{\theta_{cl}} \\ \omega_{\theta_{cl}} \end{bmatrix} + \begin{bmatrix} 0 \\ 0 \\ \dot{\theta}_{el} \end{bmatrix} \tag{4.11}$$

After calculation of the end effector angular rates, we have to define this rate with respect to the base frame as in Equation 4.12.

$$\omega_{el}^{base} = R_4^0 \omega_{el} \tag{4.12}$$

Now, we can calculate Jacobian operator using Equation 4.12 via partial derivative with respect to axes' rate as in Equation 4.13.

$$J_\omega = \begin{bmatrix} \frac{(\partial \omega_{el}^{base})_x}{\partial \dot{\theta}_{az}} & \frac{(\partial \omega_{el}^{base})_x}{\partial \dot{\theta}_{cl}} & \frac{(\partial \omega_{el}^{base})_x}{\partial \dot{\theta}_{el}} \\ \frac{(\partial \omega_{el}^{base})_y}{\partial \dot{\theta}_{az}} & \frac{(\partial \omega_{el}^{base})_y}{\partial \dot{\theta}_{cl}} & \frac{(\partial \omega_{el}^{base})_y}{\partial \dot{\theta}_{el}} \\ \frac{(\partial \omega_{el}^{base})_z}{\partial \dot{\theta}_{az}} & \frac{(\partial \omega_{el}^{base})_z}{\partial \dot{\theta}_{cl}} & \frac{(\partial \omega_{el}^{base})_z}{\partial \dot{\theta}_{el}} \end{bmatrix} \tag{4.13}$$

Equation 4.13 only depends on joint angles and it's too complex the write on the document. In Simulink file, the Jacobian operator is calculated with Matlab Symbolic toolbox and transformed with using String library to the Matlab function file which is given in the Appendix.

4.5 LOS Simulation of the 3-axes Pedestal

As in Figure 4.12, a Simulink file that has two dotted areas which are the main functions of the simulation file, has been constructed. The first area contains the Jacobian operator which is calculated using Equation 4.13 and is implemented using Symbolic Toolbox. This is the main function also it has to be implemented in the high-level controller. The second area contains the base movement and LOS velocity. The base movement can be generated using a sine wave or pulse signal. These parameters can be set in the mask with frequency, the amplitude for the sine wave and amplitude, duty cycle for pulse signal. In LOS calculation with disturbance function, Equation 4.12 is implemented using Symbolic Toolbox as the Antenna Model Block.

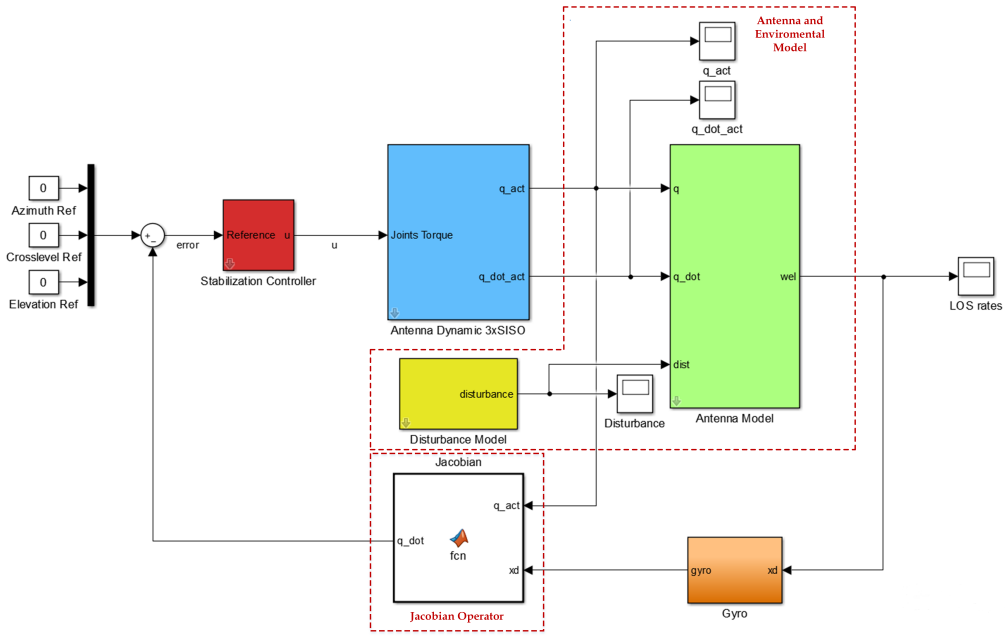

Figure 4.12 : The screenshot of the Simulink file.

This block takes the angular position, velocity, disturbance and calculates the end effector velocity. The output of this function is the LOS angular rates. "Antenna Dynamic 3xSISO" block diagram contains the azimuth, canted-level, and elevation axis dynamics. Totally, this block includes three single input single output system to describe the antenna dynamics. This block takes the reference torque value and calculates the angular position and velocity of each axis as shown in Figure 4.13. In order to analyze the performance of the controller, the various disturbances are applied to the system to show that the system maintains the LOS angular speed at the reference value. Also, the gyroscope noise and BLDC torque ripple noise are added on the simulation.

In the first case just roll disturbance that shown in Figure 4.14 is added on the system. In the second case just pitch disturbance that shown in Figure 4.16 is added on the system. In the third case, just yaw disturbance that is shown in Figure 4.18 is added on the system. In the fourth case roll, pitch and yaw disturbance that is shown in Figure 4.20 are added on the system. In the fifth case roll, pitch and yaw disturbance that is shown in Figure 4.22 are added on the system. It is clear that the angular rates of LOS prove the axis controller and Jacobian operator under all disturbance cases in Figure (4.14 - 4.23). While there are only two axes contributes to LOS angular velocity in case 1-3, the whole axis contributes to the LOS angular velocity in case 4 and 5. The

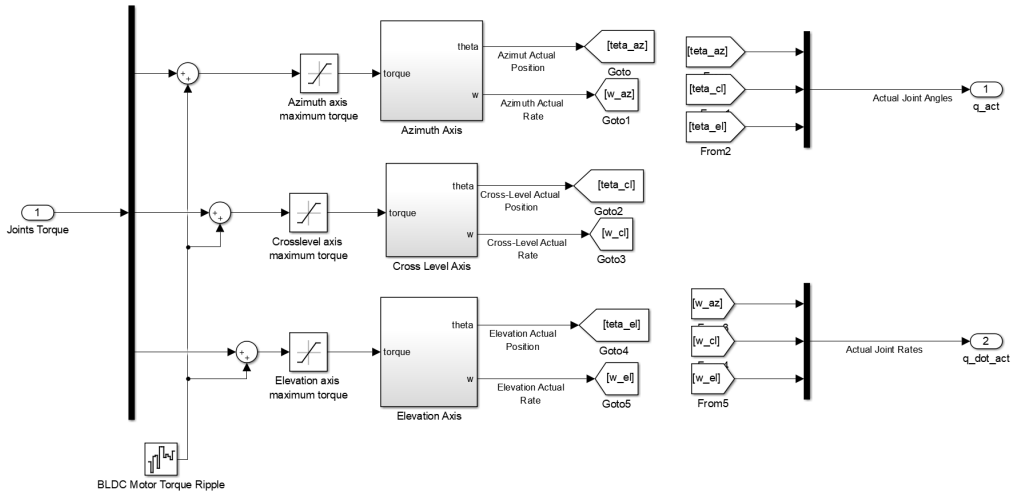

Figure 4.13 : Block diagram of the antenna dynamic.

difference between case 5 and 4 is the analyze the maximum angular velocity changing of the axis motor. In here, the azimuth axis reaches 0.3 rad/s (18 deg/s) and this value can be taken limit speed value of the motor. The other motors can be selected with this limit value.

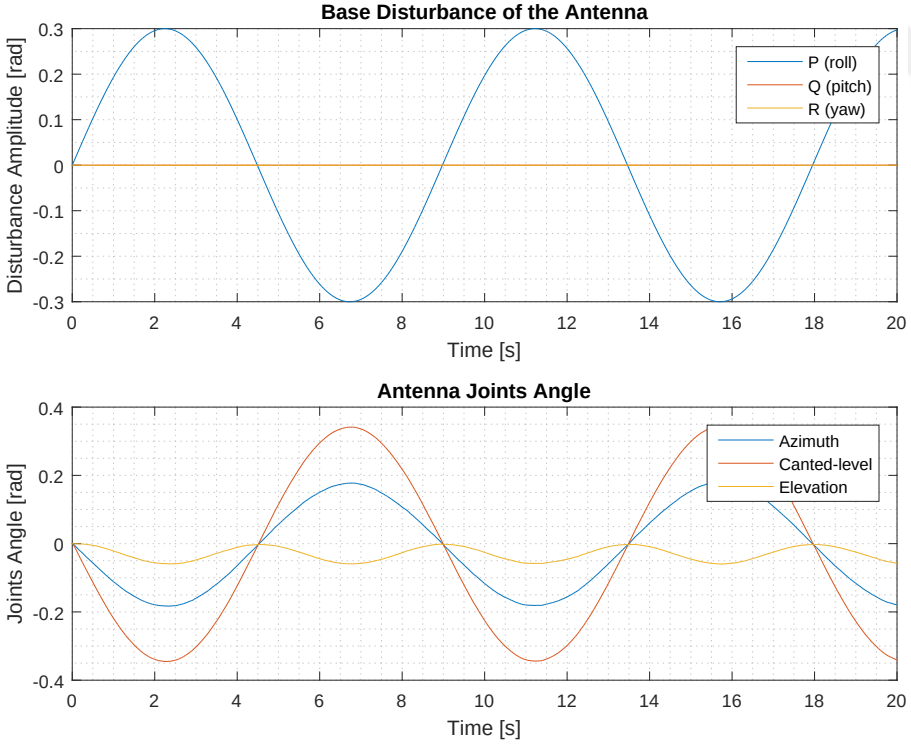

Figure 4.14 : Roll base disturbance (top), Antenna joints angle during stabilization (bottom).

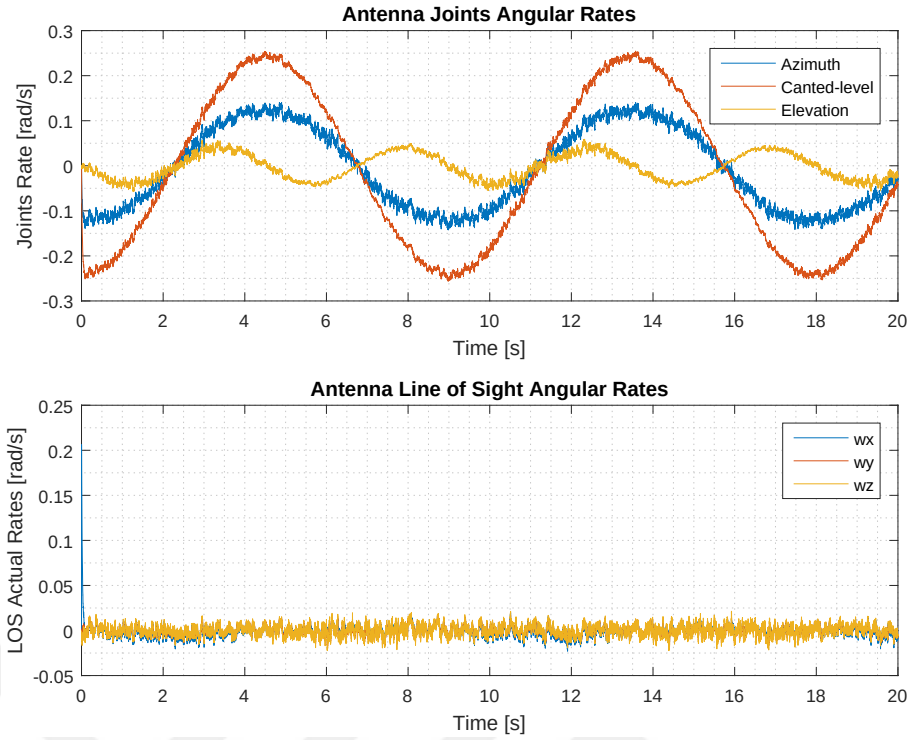

Figure 4.15 : Antenna joints angular rates during stabilization (top), LOS angular rates during stabilization (bottom) under roll disturbance.

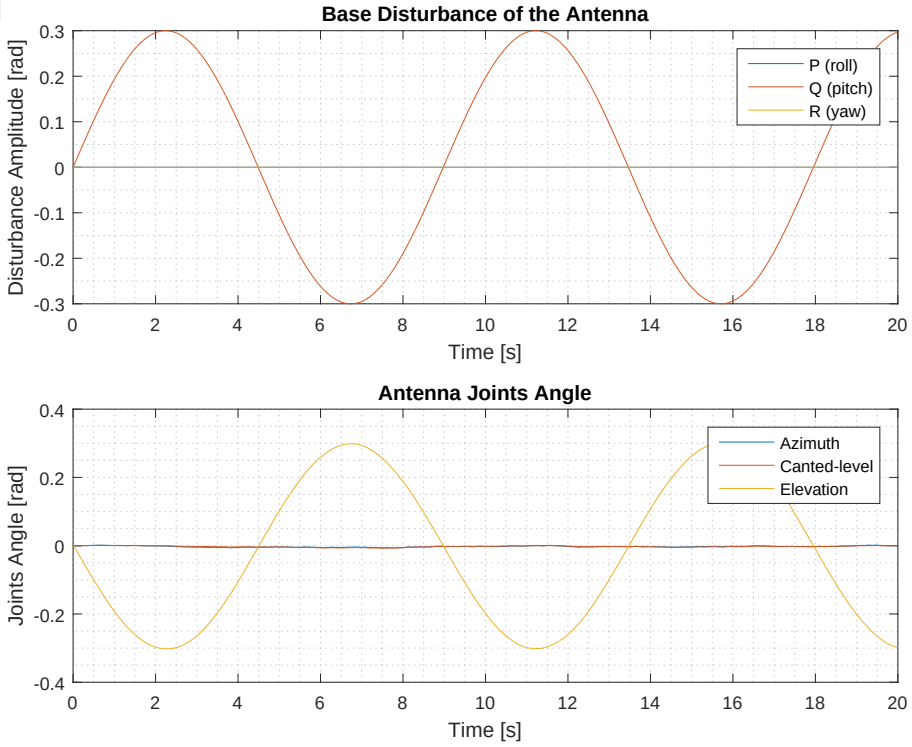

Figure 4.16 : Pitch base disturbance (top), Antenna joints angle during stabilization (bottom).

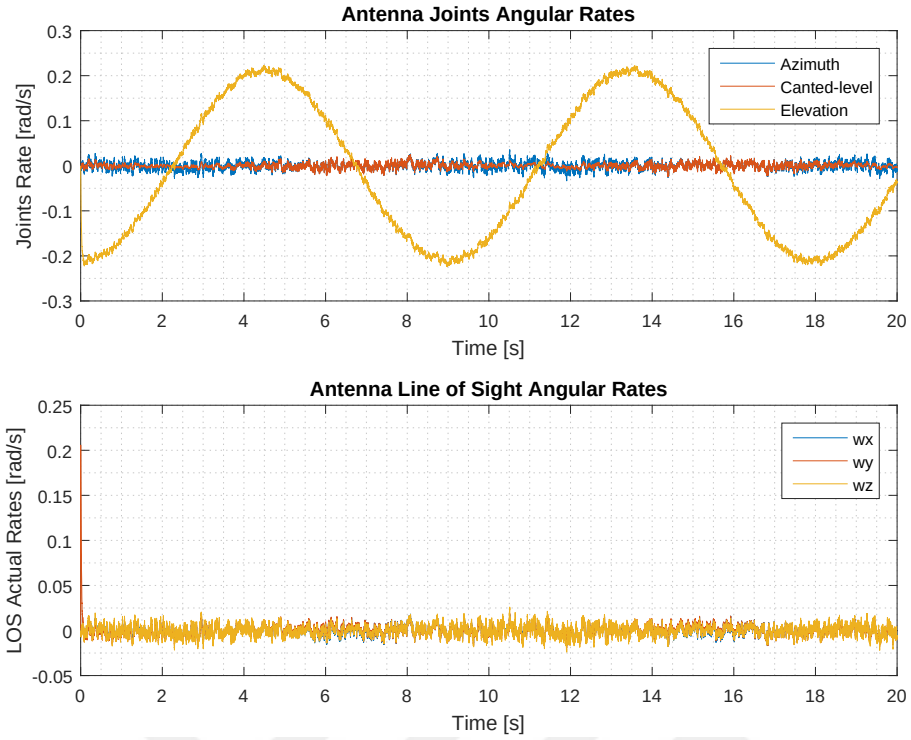

Figure 4.17 : Antenna joints angular rates during stabilization (top), LOS angular rates during stabilization (bottom) under pitch disturbance.

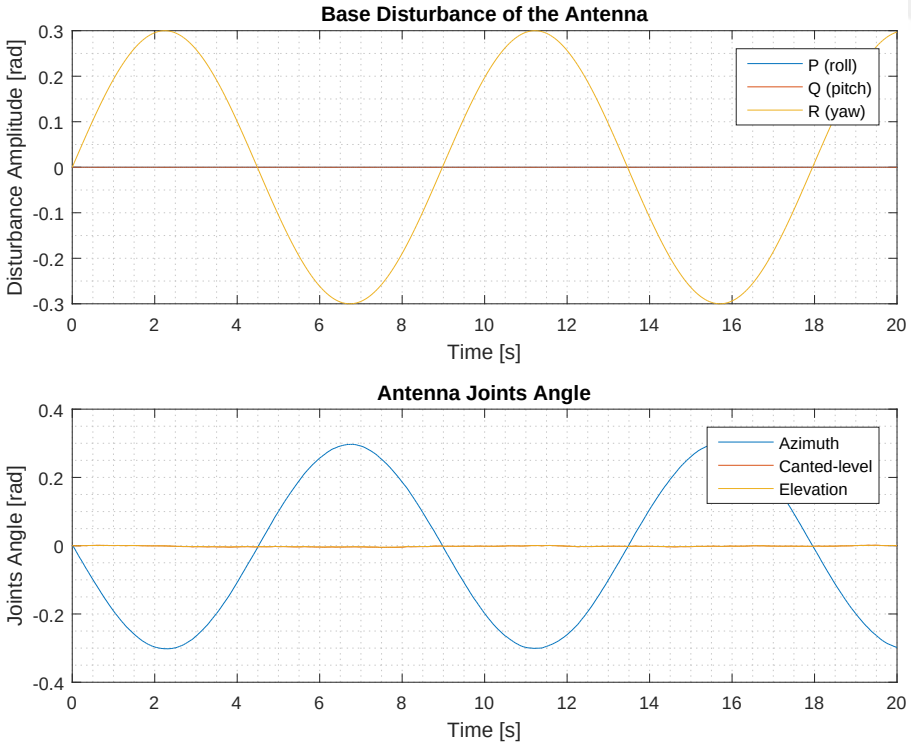

Figure 4.18 : Yaw base disturbance (top), Antenna joints angle during stabilization (bottom).

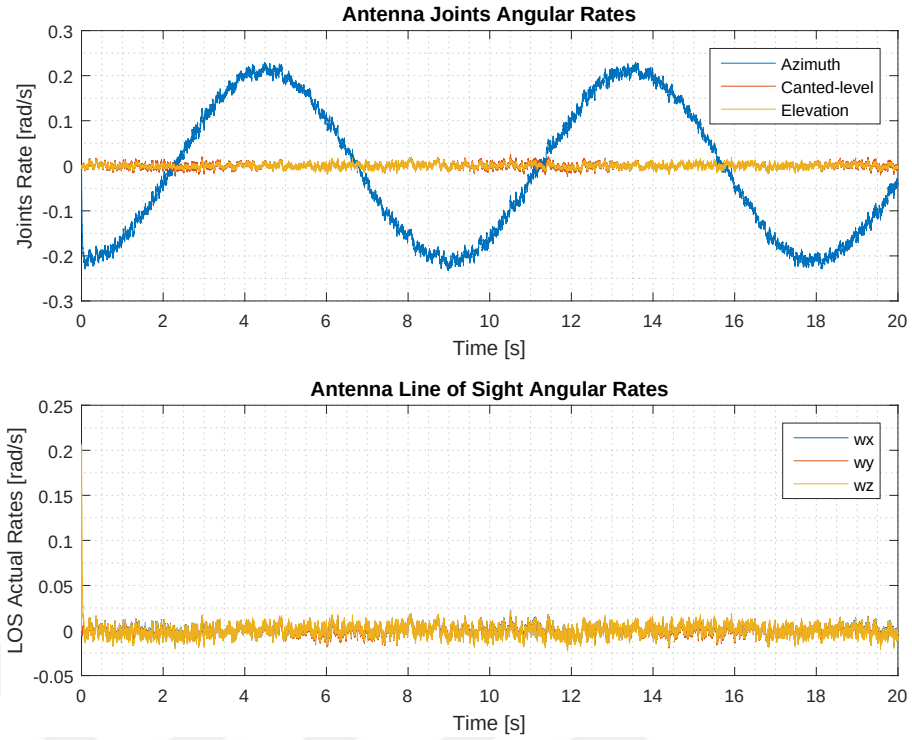

Figure 4.19 : Antenna joints angular rates during stabilization (top), LOS angular rates during stabilization (bottom) under yaw disturbance.

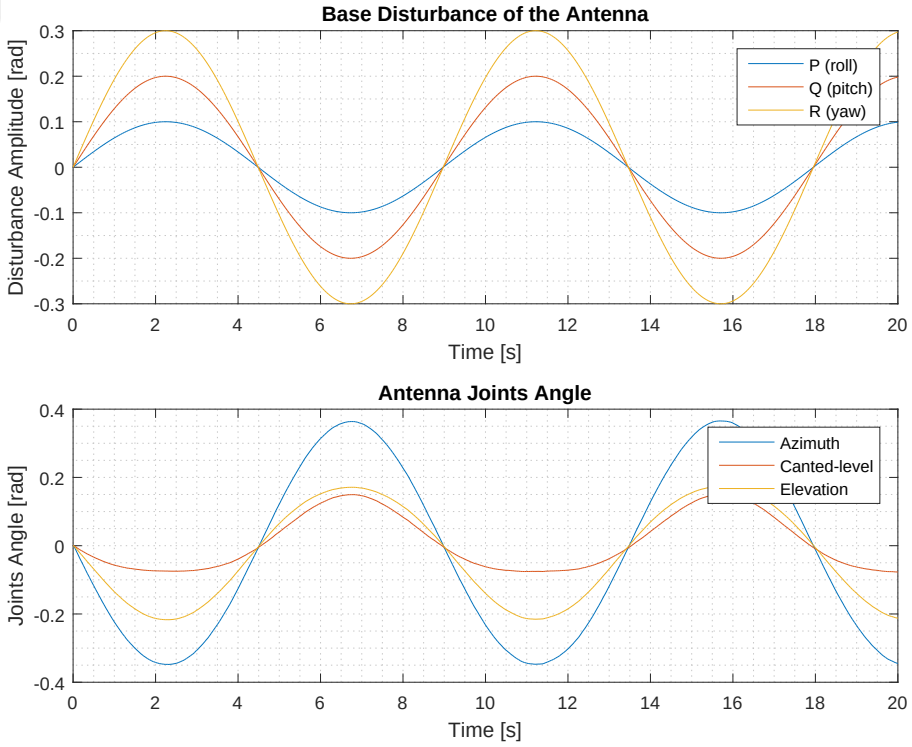

Figure 4.20 : Roll, pitch, and yaw base disturbance (top), Antenna joints angle during stabilization (bottom).

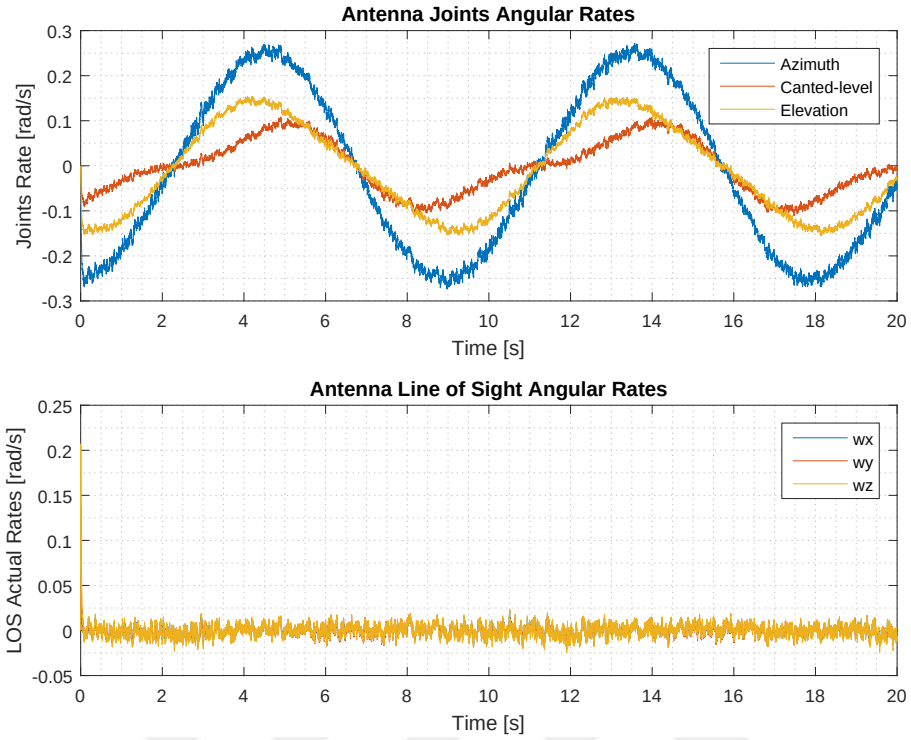

Figure 4.21 : Antenna joints angular rates during stabilization (top), LOS angular rates during stabilization (bottom) under roll, pitch and yaw disturbance.

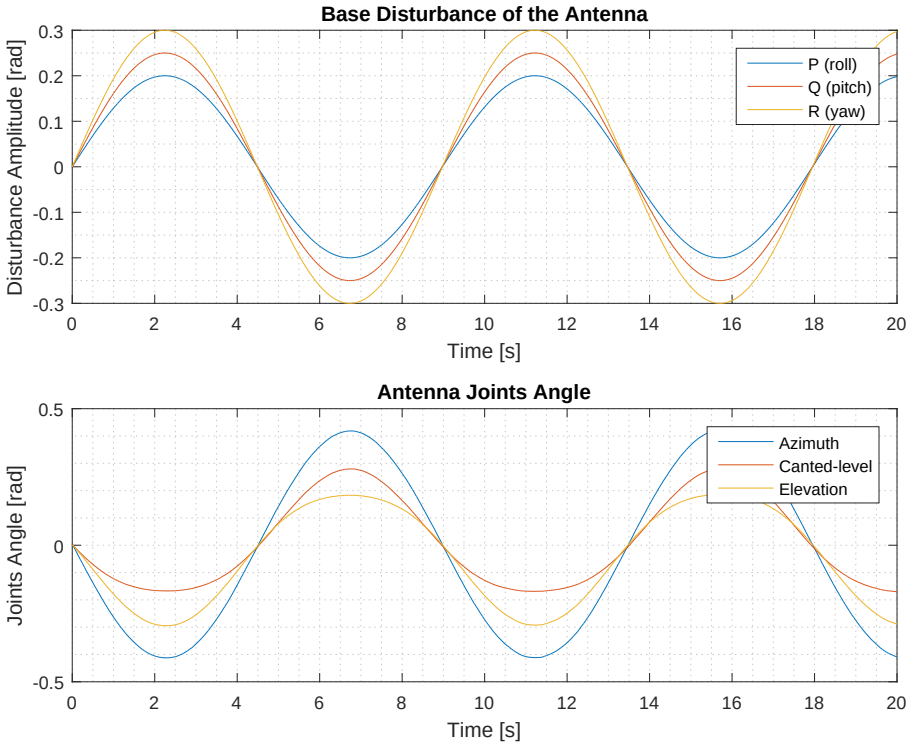

Figure 4.22 : Roll,pitch, and yaw base disturbance (top), Antenna joints angle during stabilization (bottom).

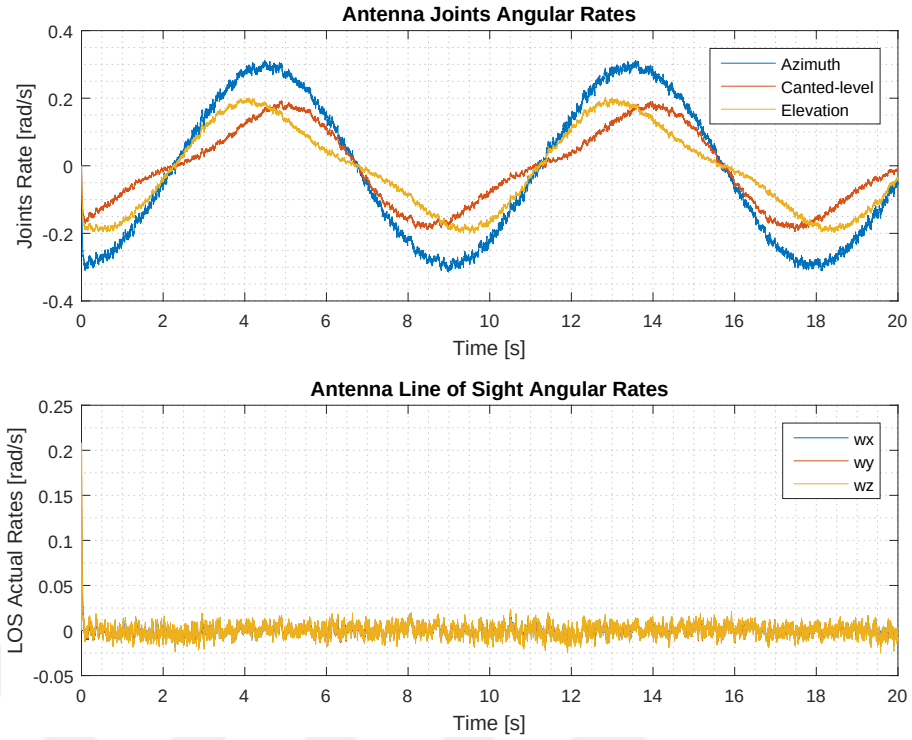

Figure 4.23 : Antenna joints angular rates during stabilization (top), LOS angular rates during stabilization (bottom) under roll, pitch and yaw disturbance.

5. CLOSED - LOOP CONTROLLER OF THE 3-AXES PEDESTAL

Closed-loop can be considered as a combination of the position controller which is responsible to control the axis position by applying the position reference to the LOS controller and the scanning algorithm which is responsible to plan a trajectory to find the maximum signal level. Since just the azimuth and elevation axes are enough to search the full hemisphere, the canted-level reference must be always zero to obtain the correct rotation matrix. However, just the position controller is not enough to obtain and hold the maximum RF signal level. There are many error sources which affect the maximum signal level, such as weather conditions, GPS sensor error, antenna misalignment, gyro bias error, and IMU bias error. Therefore, a scanning algorithm which finds the maximum signal level must be implemented to maximize the RF signal.

5.1 Position Controller Design

In order to control axis position, a linear Proportional-Integral-Derivative (PID) based control is used. The proportional controller increases the error level to make the system faster response to follow the reference, but also it can increase the overshoot. The derivative controller increases the error as the same as the proportional controller by taking the derivative of the error. This tends to add damping and into the system, therefore the overshoot and settling time are decreased. Integrator controller eliminates the steady-state error and the system output settles the with no error [33]. The closed-loop bandwidth of the designed stabilization controller was 10 Hz. So that the bandwidth of the closed-loop tracking controller is designed with 2 Hz to control the position reference. The system equation (Equation 3.24) is modified by adding the integrator to the closed-loop transfer function of each axis.

The PID controller parameters which have the 2 Hz (12 rad/s) bandwidth, no steady-state error requirements, and more than 150° phase margin requirements are tuned. The whole controller parameters and the requirements of all axes can be shown in Table 5.1. The stabilization controller parameters are different due to the different

Table 5.1 : Position controller requirements and estimated parameters

Axis	Bandwith (rad/s)	Steady State Error	Phase margin °	Kp	Ki	Kd
Azimuth	12.08	0	150.81	12.03	25.75	0.37
Canted-level	12.16	0	151.51	12.21	24.58	0.36
Elevation	12.28	0	150.35	12.22	26.65	0.36

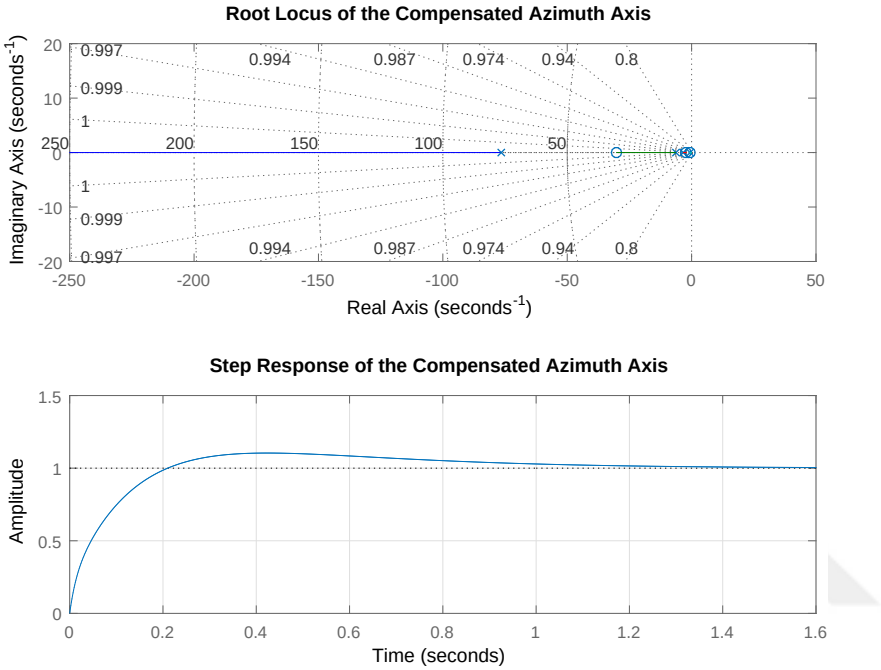

Figure 5.1 : The Root Locus of the compensated azimut axis(top), the step response of the compensated azimuth axis(bottom).

dynamics parameters of each axis. Since the designed stabilization controllers have the same performance, parameters of the position controller for each axis estimated with the close values. The performance of the controllers is the same each other. The root locus and the step response of the azimuth axis position controller are shown in figure 5.1. In order to test the position performance of the controller, a Simulink file is created as shown in Figure 5.2. The controller structure and the disturbances can be seen in the figure. There are three disturbance noises which represent the torque ripple, gyroscope sensor noise, and IMU sensor noise. In Figure 5.3, as it is shown in the sine response of each axis, it is clear that the designed controller can track the sine reference with a low error. The tracking error of the designed controller of each axis is shown in Figure 5.4. In Figure 5.3 and 5.4, the performance of the position controller of each axis is simulated and analyzed individually. In Figure 5.5, the position controller

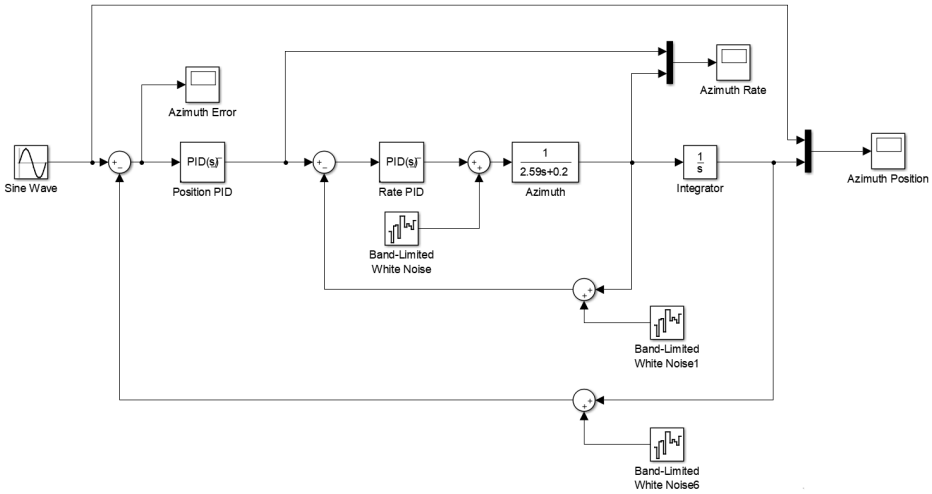

Figure 5.2 : The block diagram of the controlled azimuth axis.

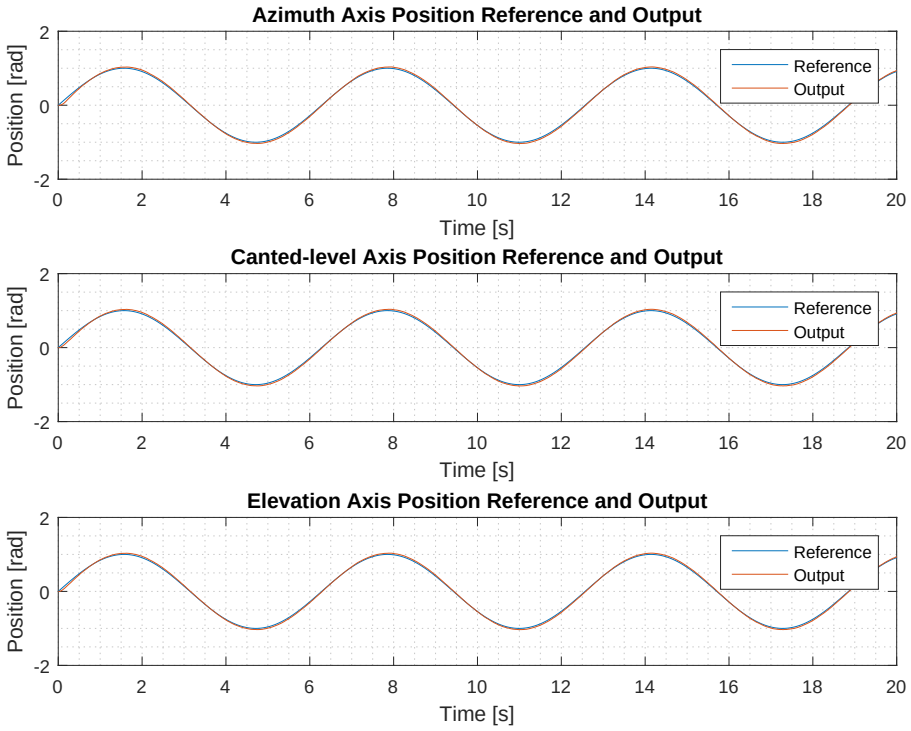

Figure 5.3 : The position tracking response of each axis.

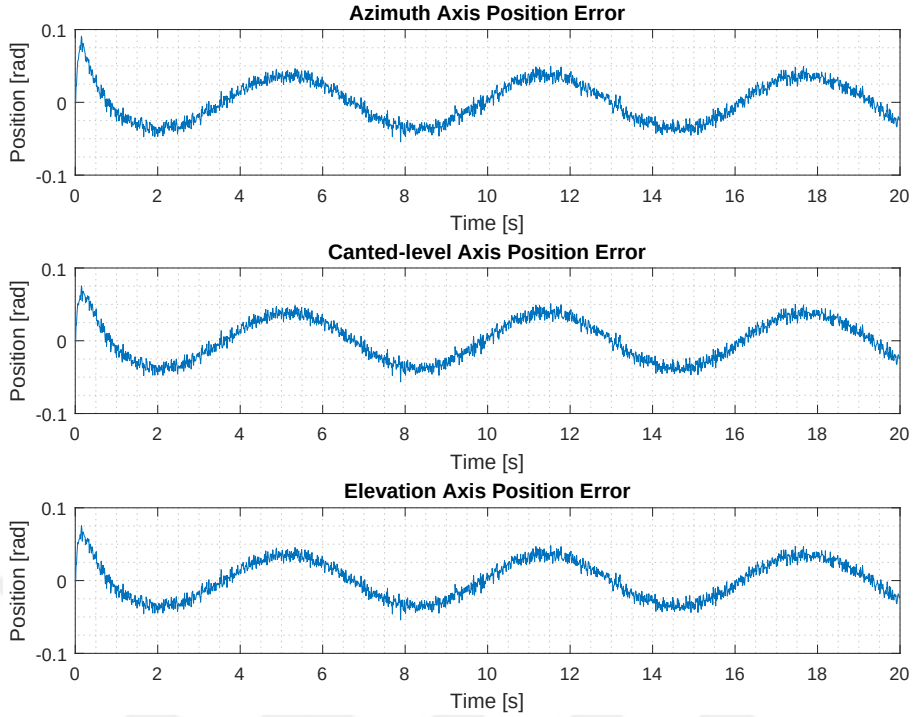

Figure 5.4 : The position tracking error of each axis.

of all axis are added into the LOS simulation file. The position controllers in the design are the outer loop of the cascade controller structure. To calculate the correct look angles, the inverse kinematics of the antenna is added before the reference. Also in the antenna model, the conversion between RF signal level and pointing error is added. The relationship between each other was examined in Chapter 2. The satellite references are assumed as 60.6° azimuth angle and 40° elevation angle. The inverse kinematic takes the disturbance values and calculates the desired look angels as in Equation 5.1.

$$R_d = R'_{dis} R_{sat} \tag{5.1}$$

In this diagram, R_{dis} is the roll, pitch, and yaw matrix of the disturbance and R_{sat} is the satellite desired matrix which is calculated using forward kinematics. R_d is the desired matrix for the calculation of the correct look angles and it is the input of the inverse kinematics. Before the calculation, the IMU noise is added on the disturbance to see the effects of the IMU sensor variation on the positioning controller. In this design, there is a sensor is used for reading both gyro, roll, pitch, and yaw values. Since the location of the sensor on the antenna payload, the kinematic transformation is needed to measure the base roll, pitch, and yaw angle. In the simulation, while the control algorithm was implementing, the disturbance was implemented as a base disturbance

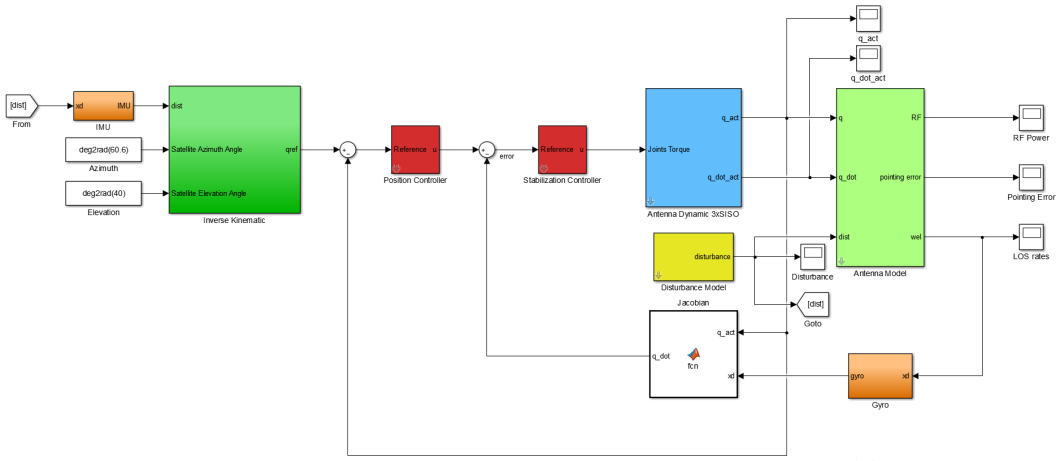

Figure 5.5 : The block diagram of the controlled azimuth axis.

and the angular velocity of the LOS was calculated using the kinematic transformation. Due to this design, there is no need to add a transformation matrix to convert roll, pitch and yaw angles. In order to analyze the performance of the position controller, the various disturbances are applied to the system and it is shown that the controllers keep the LOS angular speed at the reference value and the actual axes' position at the position references. The aim of the position controller is to keep the pointing error as low as possible. There are four cases examined to analyze the performance of the controller. In each case, the initial position of the antenna joints' angle is assumed that the RF signal level is at the maximum point.

In the first case, just roll disturbance that shown in Figure 5.6 is applied on the antenna. In the second case, just pitch disturbance that shown Figure 5.9 is applied on the antenna. In the third case, just yaw disturbance that is shown in Figure 5.12 is applied on the antenna. In the fourth case, roll, pitch and yaw disturbance that is shown in Figure 5.15 are applied on the antenna. In all cases, the controllers maintain the LOS stabilization and hold the pointing error below the FCC limitation as shown in Figures (5.6- 5.17). However, the IMU and gyro sensor have a bias value. This bias value is not a constant value and varies within the limitation of the sensor. This bias value wasn't included in the four cases to analyze the performance of the controller. These bias values of the sensor caused the wrong calculation in the kinematic transformations and result in the higher pointing error than the limitation. In the last case roll, pitch and yaw disturbance that is shown in Figure 5.18 are applied on the antenna including bias value of them. The bias value of the IMU sensor is taken 0.2° for roll axis, 0.1°

for pitch axis, 0.5° for yaw axis. The bias value of gyroscope sensor error $0.1^\circ/s$. These values mean that the sensor measuring the disturbance position and rate with adding bias error. In Figure 5.19 the angular rate of joints and angular rates of LOS are changing to compensate for the disturbance movement. The angular rates of LOS prove the controller and Jacobian operator under this disturbance with working with the position controller. In Figure 5.20, the RF signal level and pointing error are shown and the designed controller and algorithm keeps the pointing error as low as possible. Due to bias error on the sensor, the kinematic equations are calculated wrong and the controllers try to stabilize the system with the wrong reference value. This situation has resulted in signal reduction and exceeded the FCC limitation.

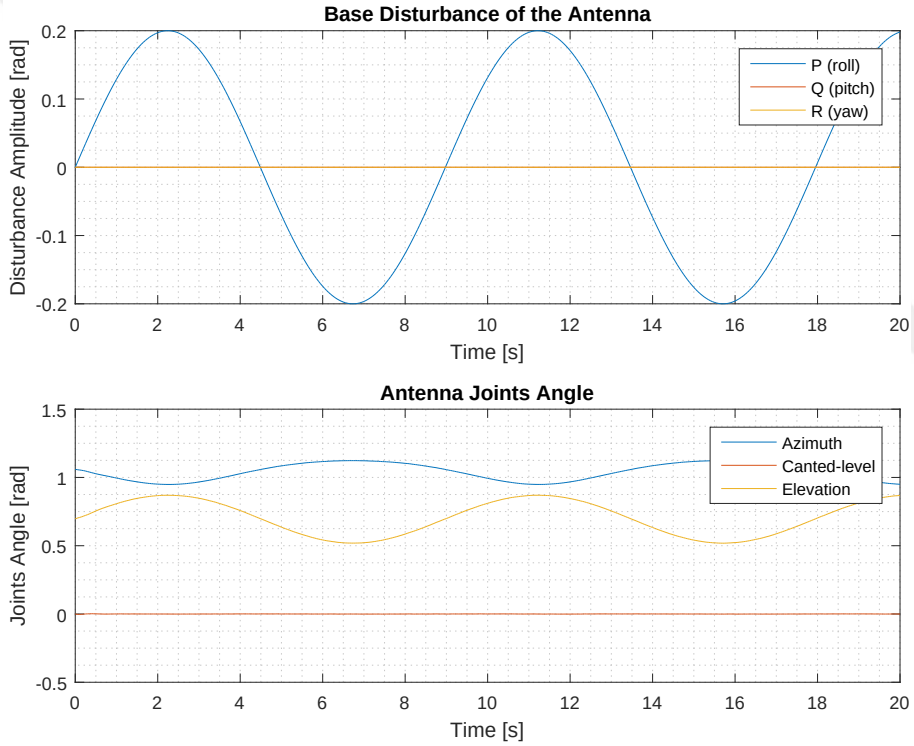

Figure 5.6 : Roll base disturbance (top), Antenna joints angle during pointing (bottom).

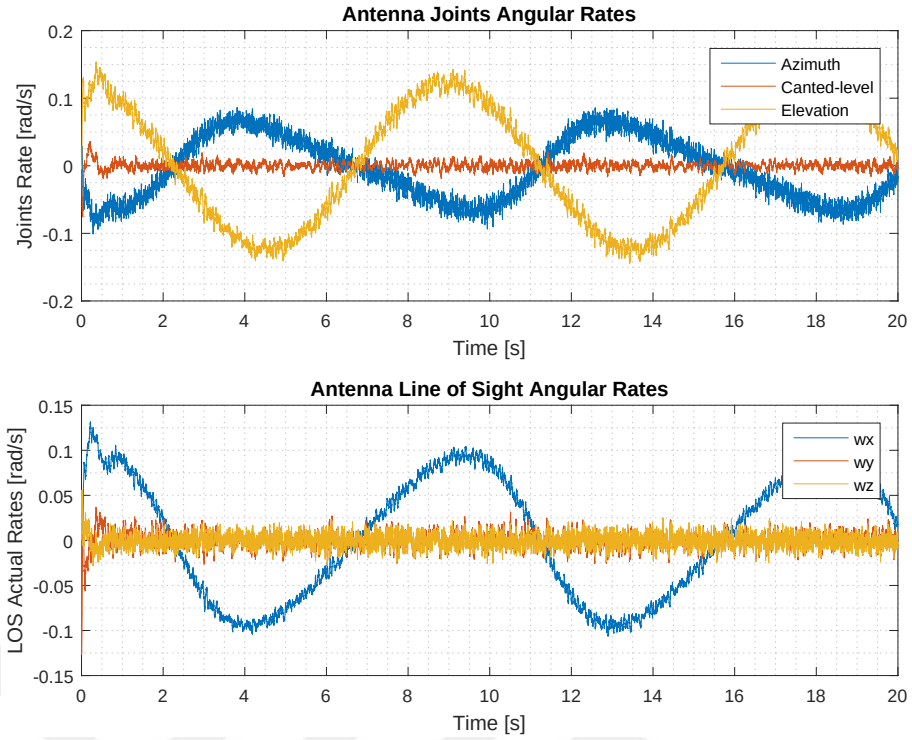

Figure 5.7 : Antenna joints angular rates during stabilization (top), LOS angular rates during stabilization (bottom) under roll disturbance.

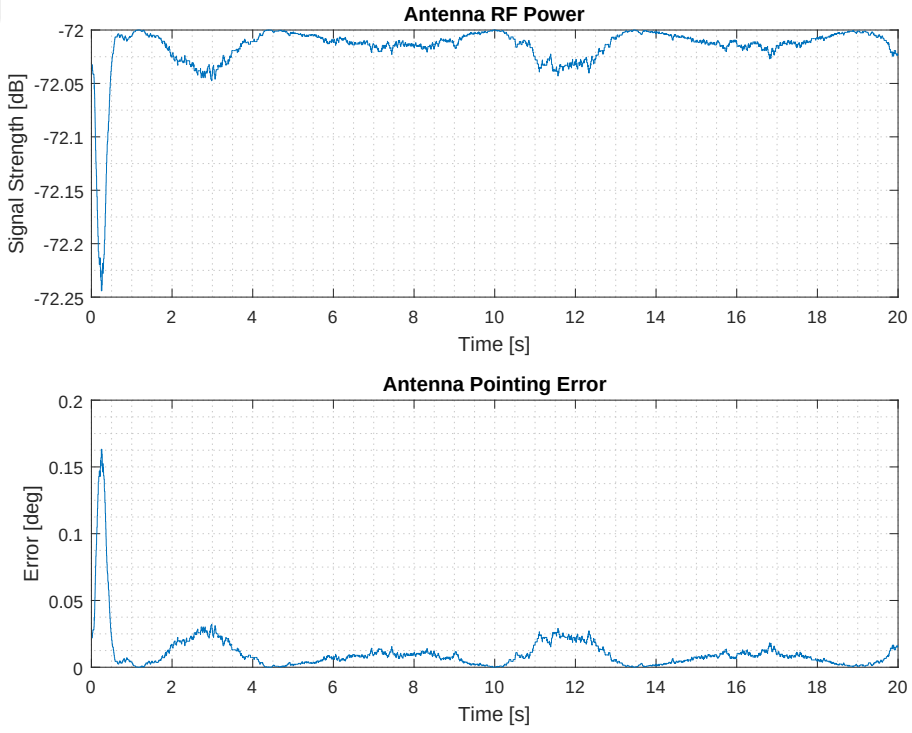

Figure 5.8 : Antenna RF signal level during pointing (top), Antenna pointing error (bottom) during pointing under roll disturbance.

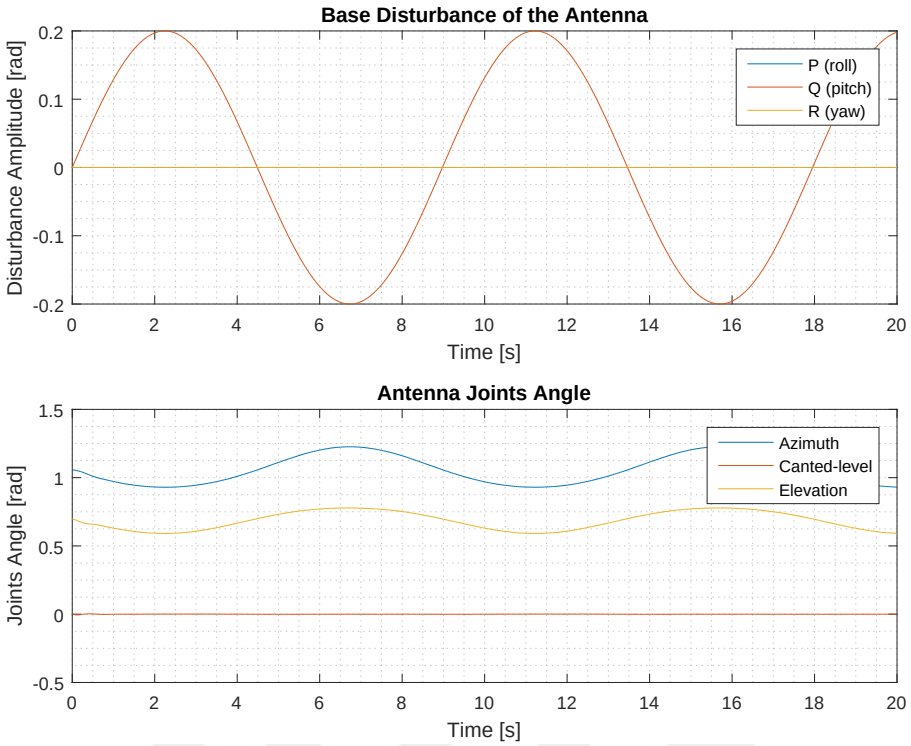

Figure 5.9 : Pitch base disturbance (top), Antenna joints angle during pointing (bottom).

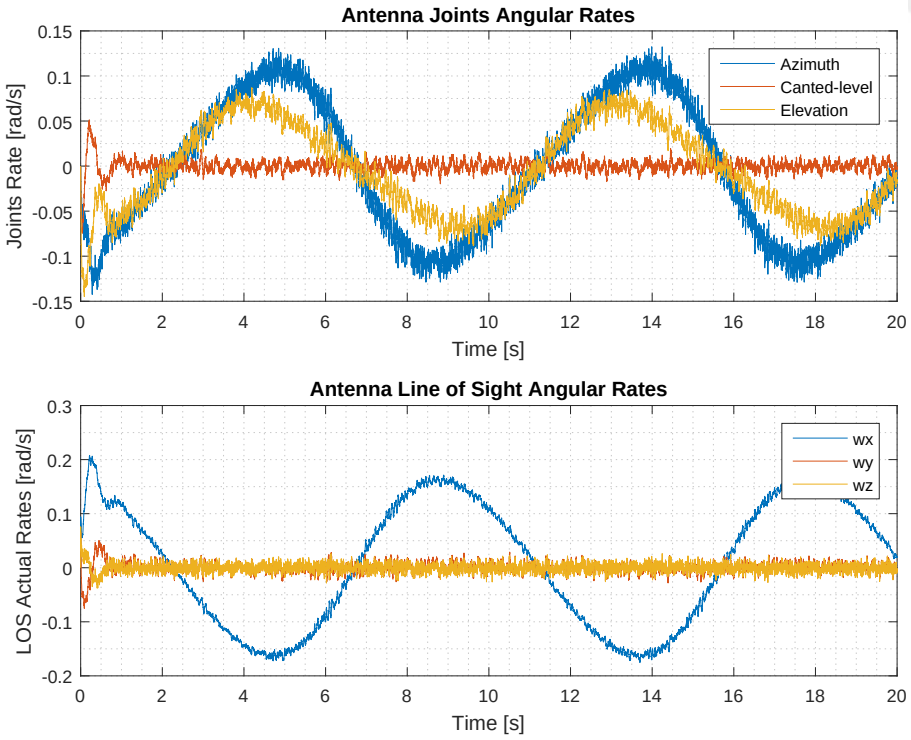

Figure 5.10 : Antenna joints angular rates during stabilization (top), LOS angular rates during stabilization (bottom) under pitch disturbance.

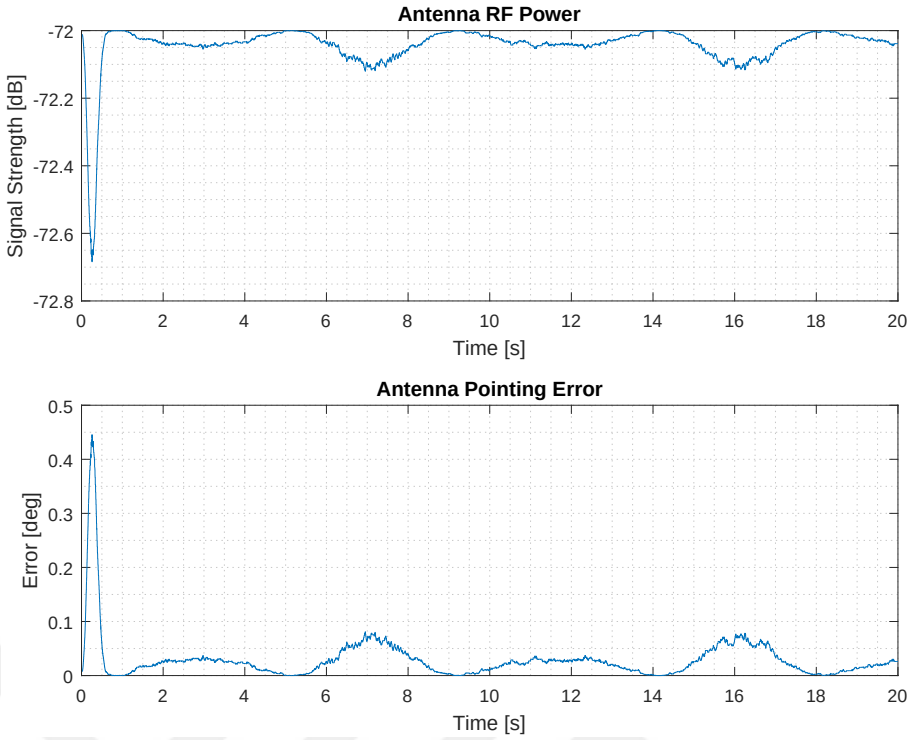

Figure 5.11 : Antenna RF signal level during pointing (top), Antenna pointing error (bottom) during pointing under pitch disturbance.

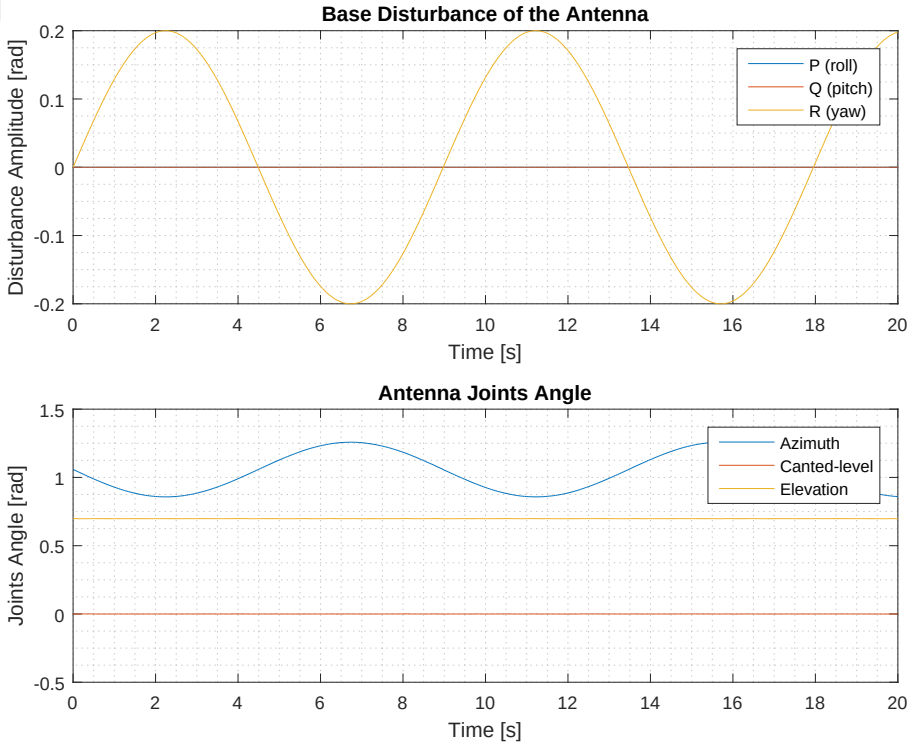

Figure 5.12 : Yaw base disturbance (top), Antenna joints angle during pointing (bottom).

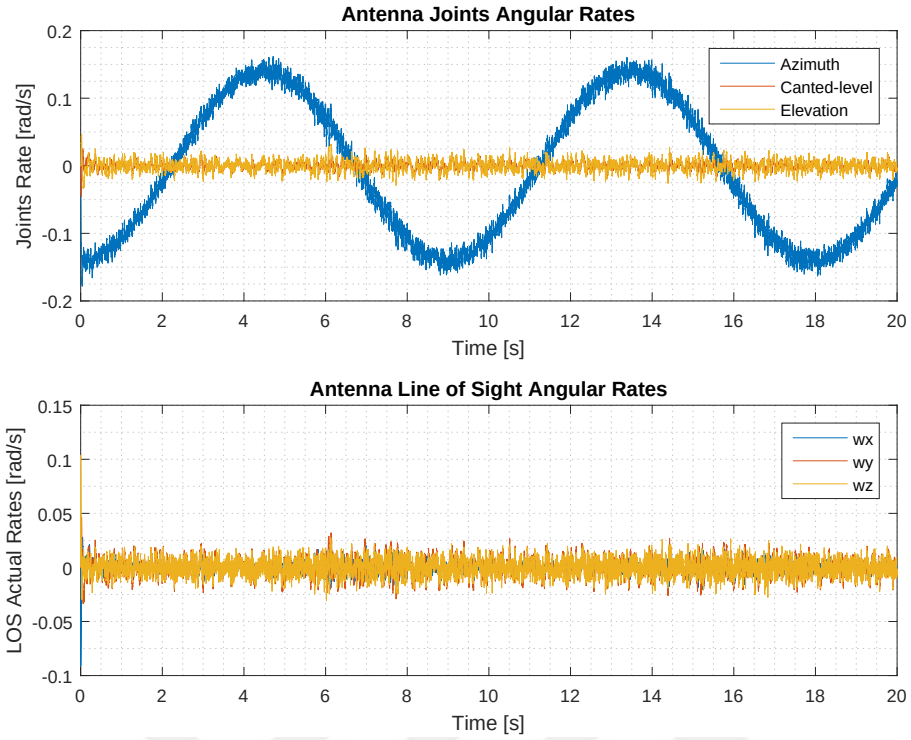

Figure 5.13 : Antenna joints angular rates during stabilization (top), LOS angular rates during stabilization (bottom) under yaw disturbance.

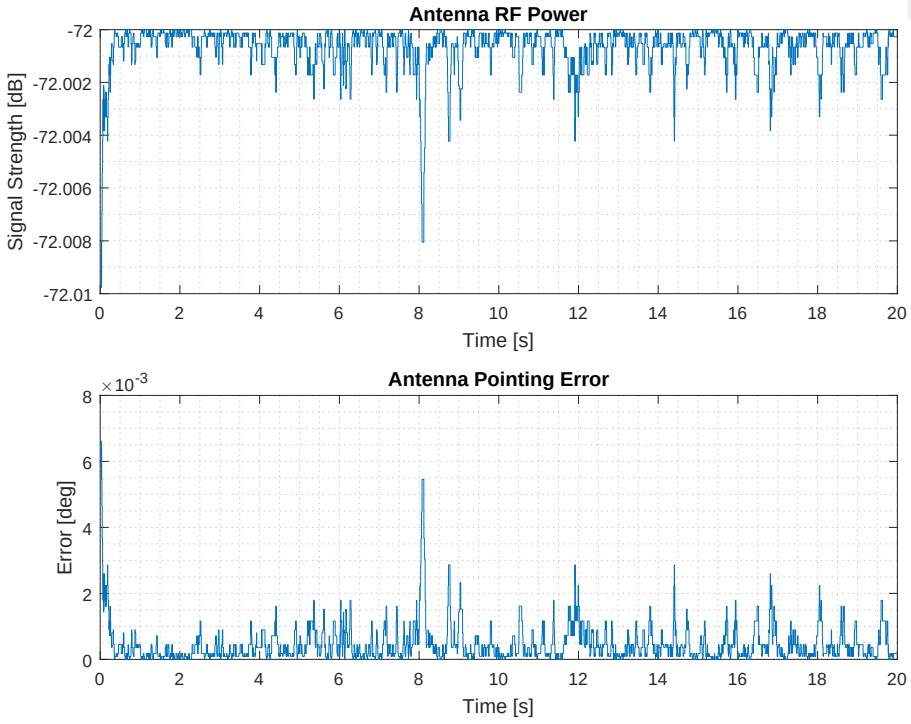

Figure 5.14 : Antenna RF signal level during pointing (top), Antenna pointing error (bottom) during pointing under yaw disturbance.

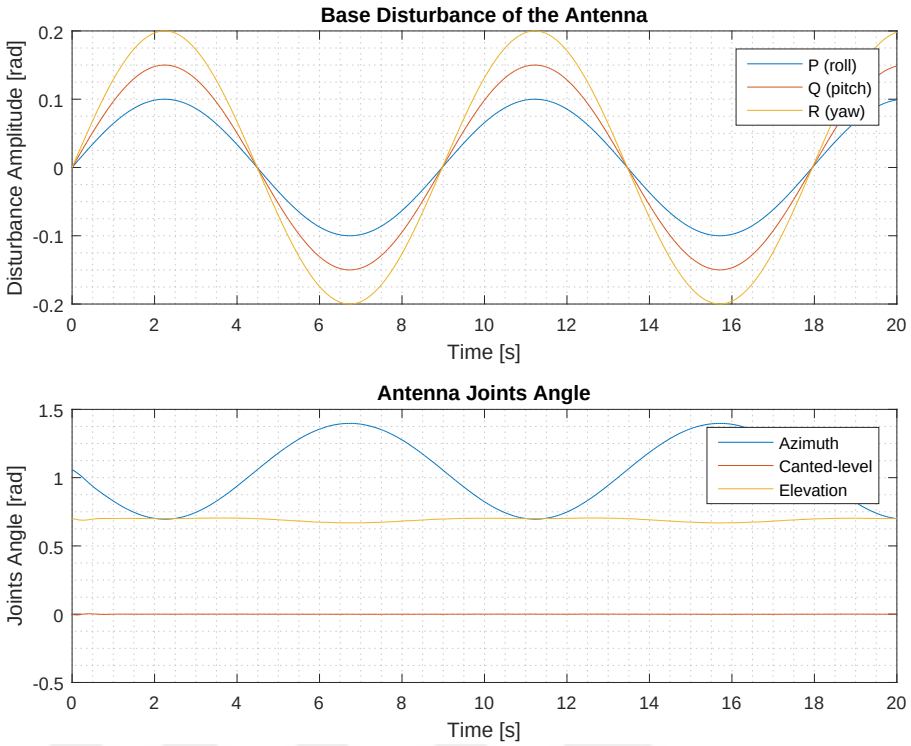

Figure 5.15 : Roll, pitch, and yaw base disturbance (top), Antenna joints angle during pointing (bottom).

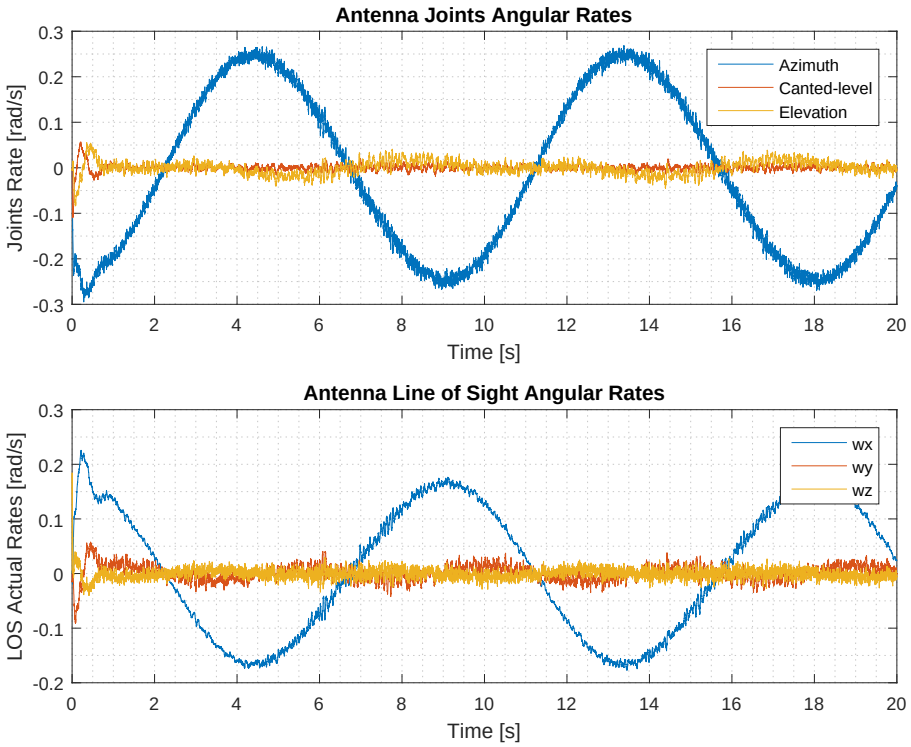

Figure 5.16 : Antenna joints angular rates during stabilization (top), LOS angular rates during stabilization (bottom) under roll, pitch and yaw disturbance.

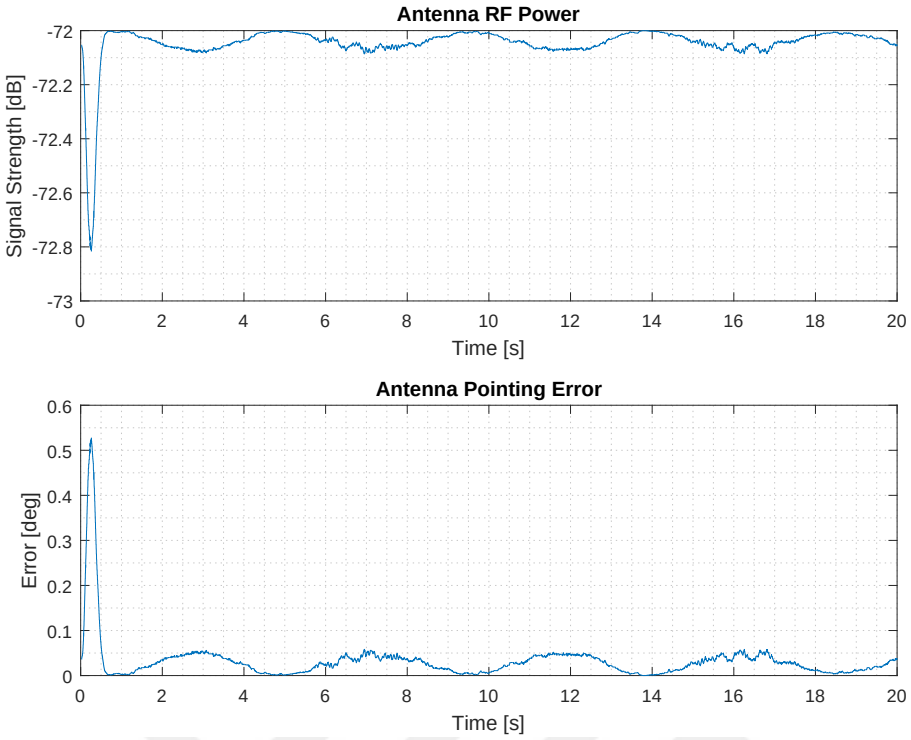

Figure 5.17 : Antenna RF signal level during pointing (top), Antenna pointing error (bottom) during pointing under roll, pitch and yaw disturbance.

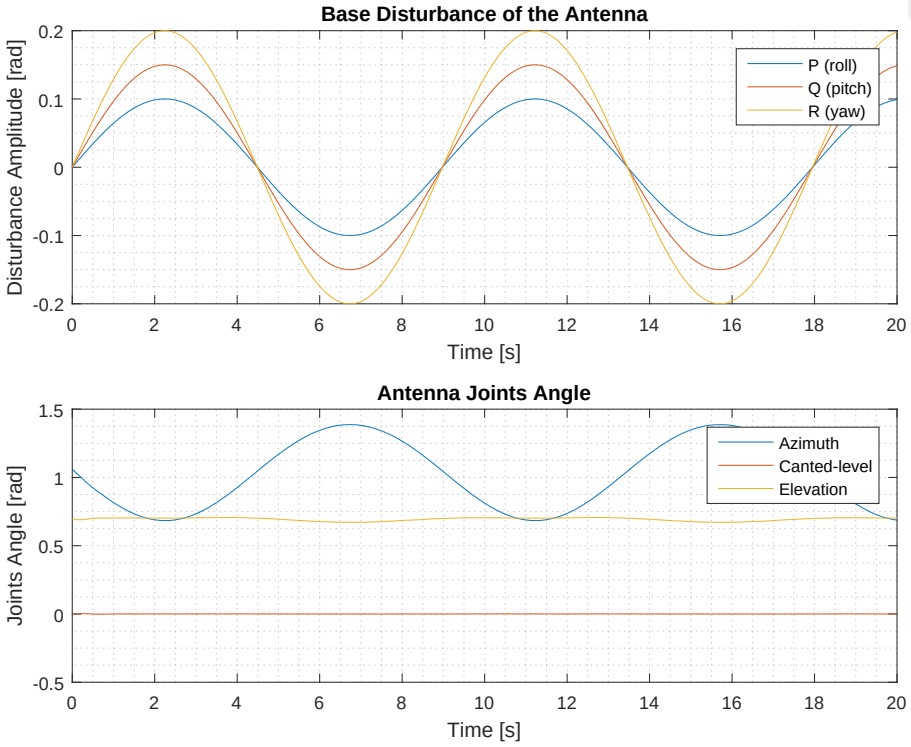

Figure 5.18 : Roll, pitch, and yaw base disturbance (top), Antenna joints angle during pointing (bottom) with IMU bias error.

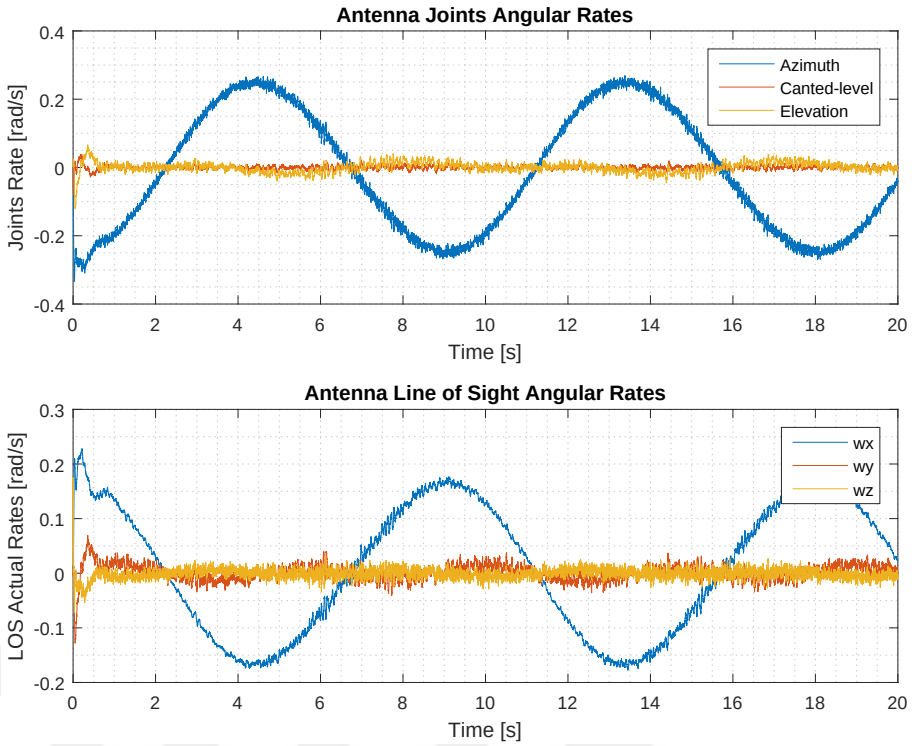

Figure 5.19 : Antenna joints angular rates during stabilization (top), LOS angular rates during stabilization (bottom) under roll, pitch and yaw disturbance with IMU bias error.

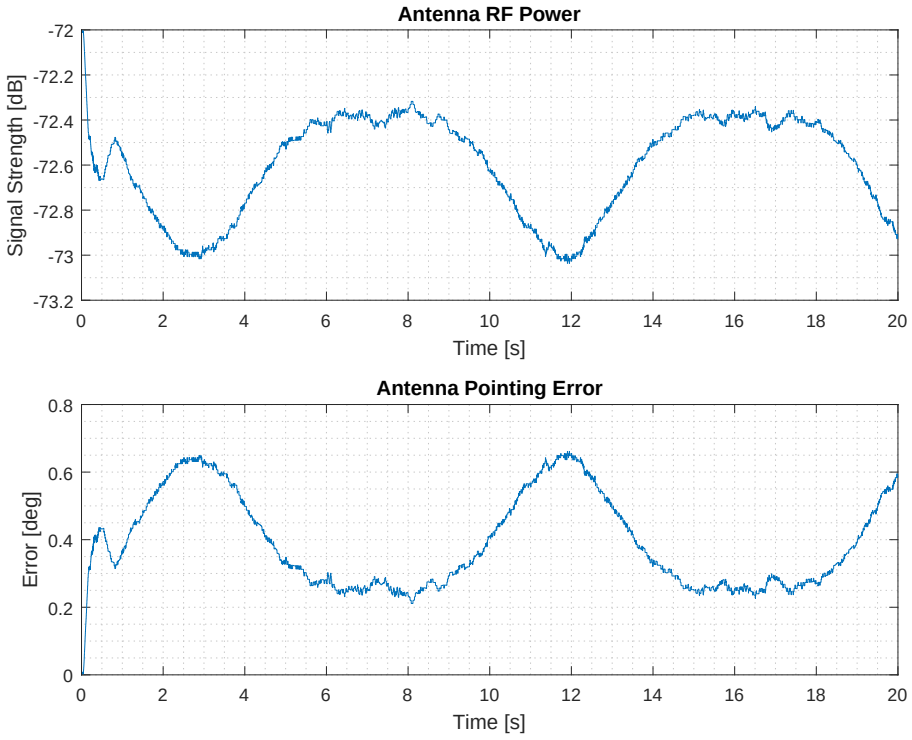

Figure 5.20 : Antenna RF signal level during pointing (top), Antenna pointing error (bottom) during pointing under roll, pitch and yaw disturbance with IMU bias error.

5.2 Scaninng Algorithms for SOTM Antennas

In section 5.2, the performance of the controllers is examined in different cases. If there is an error, the controllers point the satellite with pointing error. The satellite position with respect to earth is typically calculated with high accuracy, and the look angles which point to this satellite is implied to the antenna command. However, due to environmental disturbances and errors, such as antenna movement, temperature gradient, gravity forces, sensors accuracy such as GPS, IMU, gyroscope ... , and manufacturing imperfections, the antenna points towards the satellite with some error. These disturbances are difficult or impossible to predict and, therefore, they must be measured before compensatory measures can be taken. These measurements cannot be taken while the antenna on the operation and are too expensive to build a compact system [30]. In any case, the antenna always points to the satellite with an error because of the disturbance. In order to eliminate this disturbance, the scanning algorithm must be implemented the antenna.

A scanning algorithm is a special trajectory planning which helps to find the maximum signal level, for the end effector or antenna payload. After finding the maximum signal, the reference of the position controller is taken the finding value and the controller tries to provide maximum signal level. The trajectory is planning to antenna payload which means the elevation axis. The y axis of the elevation frame is represented the EL or elevation and the z axis of the elevation frame is represented XEL or cross-elevation as shown in Figure 5.21.

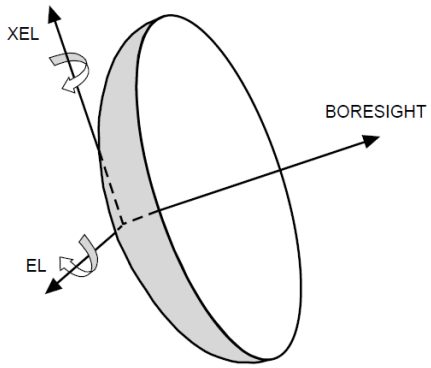

Figure 5.21 : The EL and XEL axes of the antenna payload adapted from (Gawronski, 2001).

5.2.1 Designing and implementation of the step-track algorithm

The step-track algorithm provides is a basic solution to find the maximum signal level. It is commonly used in earth stations with medium size antennas because of simple design, low cost, and need for just RF signal feedback [24, 25]. Although It's generally used in the earth stations which the antenna has fixed base, it can be used in the SOTM antennas. There are a few techniques to implement step-track, the most common of which are: hill-climbing technique, curve fitting, and gradient algorithm method. The most effective strategy that has been used so far is the gradient method [26]. In this thesis, only the gradient step-track algorithm is implemented. Just two axis of the elevation is enough for finding the maximum signal level. Basically, the cross-elevation axis is the same as the azimuth axis when the elevation angle is zero. Increment on the elevation axis also increases the ratio between the azimuth angle and the cross-elevation angle. When the elevation angle is zero the ratio equals to one but when the elevation angle is bigger than zero, the ratio is divided by the cosine of the elevation angle. In order to make simpler, we assumed that the cross-elevation axis is the same as the azimuth axis in the step-track algorithm.

The algorithm starts with initial conditions such as initial axis and initial increment direction. In this algorithm the logical high value is taken the positive rotation, the logical low value is taken negative rotation. The algorithm makes step reference in the active axis with the initial direction. This step reference is always repeated if the RF signal value of the new position is higher than the previous position. If the RF signal is below than the previous one, the algorithm changes the active axis and direction. These conditions are repeated when the counter equals the specified value [27]. In Figure 5.22, the algorithm is implemented using the user-defined function as the input of the inverse kinematic model. (The function code is given in the Appendix.) The step-track algorithm implemented is a function that takes the actual angles, the RF signal level, the step angle, the initial azimuth direction, the initial elevation direction, and initial active axis and calculates the reference azimuth and elevation axis positions. Since the azimuth and elevation axes are enough to search full hemisphere, only azimuth and elevation axis is used in the scanning algorithm. The canted-level axis is set zero. The satellite look angles of the inverse kinematic are entered with a small error to make the pointing error. The aim here is to find the maximum RF signal level with the wrong

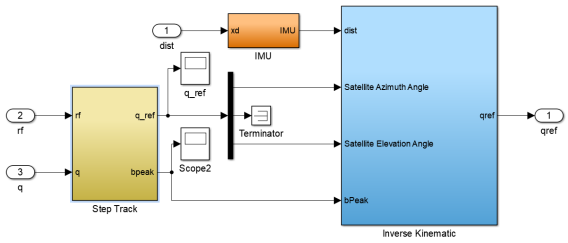

Figure 5.22 : The implementation of the step-track algorithm.

error and IMU bias error. There are two cases are implemented to simulate step-track algorithm performance. In the first case, it's assumed that there is no disturbance on the antenna. In Figure 5.23, the step-track algorithm reference and the changing of the angle of joints with a step reference are shown. In Figure 5.24, the RF signal level and pointing error are shown and the step-track algorithm finds the maximum RF signal as close as possible.

In the second case, there is a small disturbance on the roll, pitch, and yaw axis. In Figure 5.25, the step-track algorithm reference and the changing of the angle of joints with a step reference are shown. In Figure 5.26 the angular rate of joints and angular rates of LOS are changing to compensate for the disturbance movement. In Figure 5.27, the RF signal level and pointing error are shown. Even if the step-track algorithm works correctly, the algorithm cannot find the maximum point and cannot draw a gradient trajectory. Both changing in the disturbance and both changing in the reference, the antenna cannot reach the maximum RF signal level as shown in Figure 5.27.

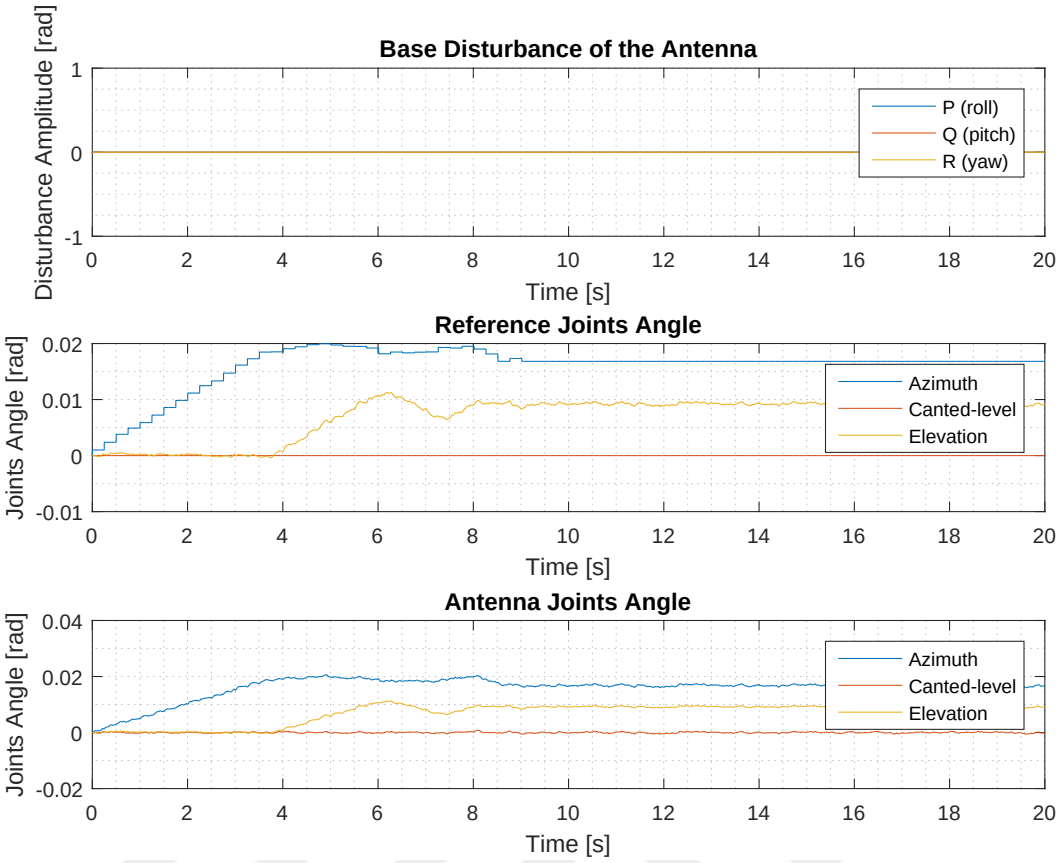

Figure 5.23 : The disturbance on the antenna (top), The step-track algorithm reference (middle), The actual joints angle (bottom).

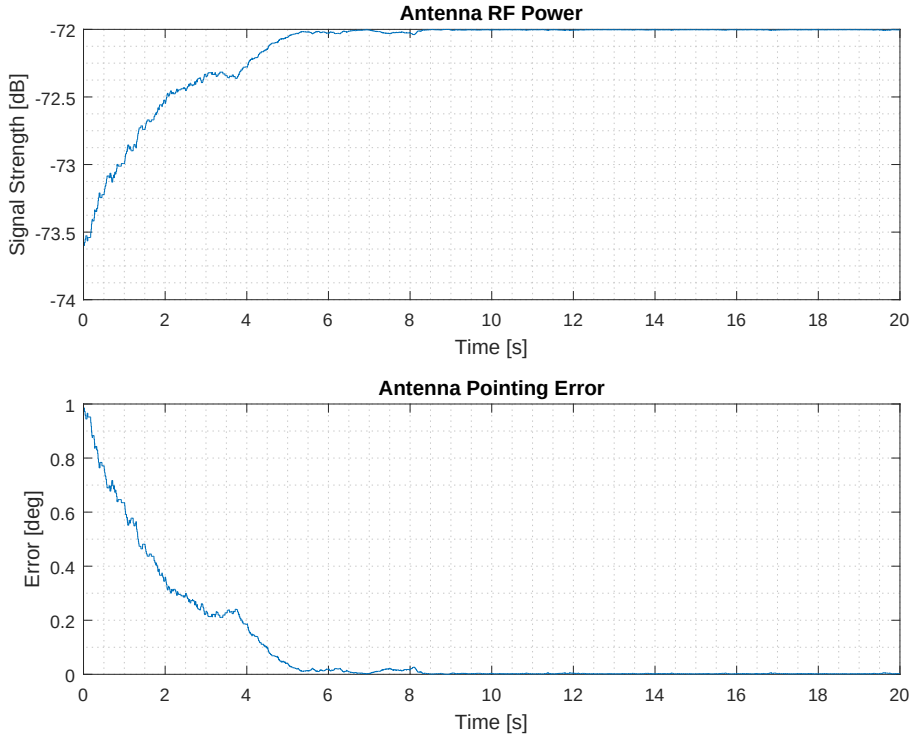

Figure 5.24 : Antenna RF signal level during scanning (top), Antenna pointing error during scanning (bottom).

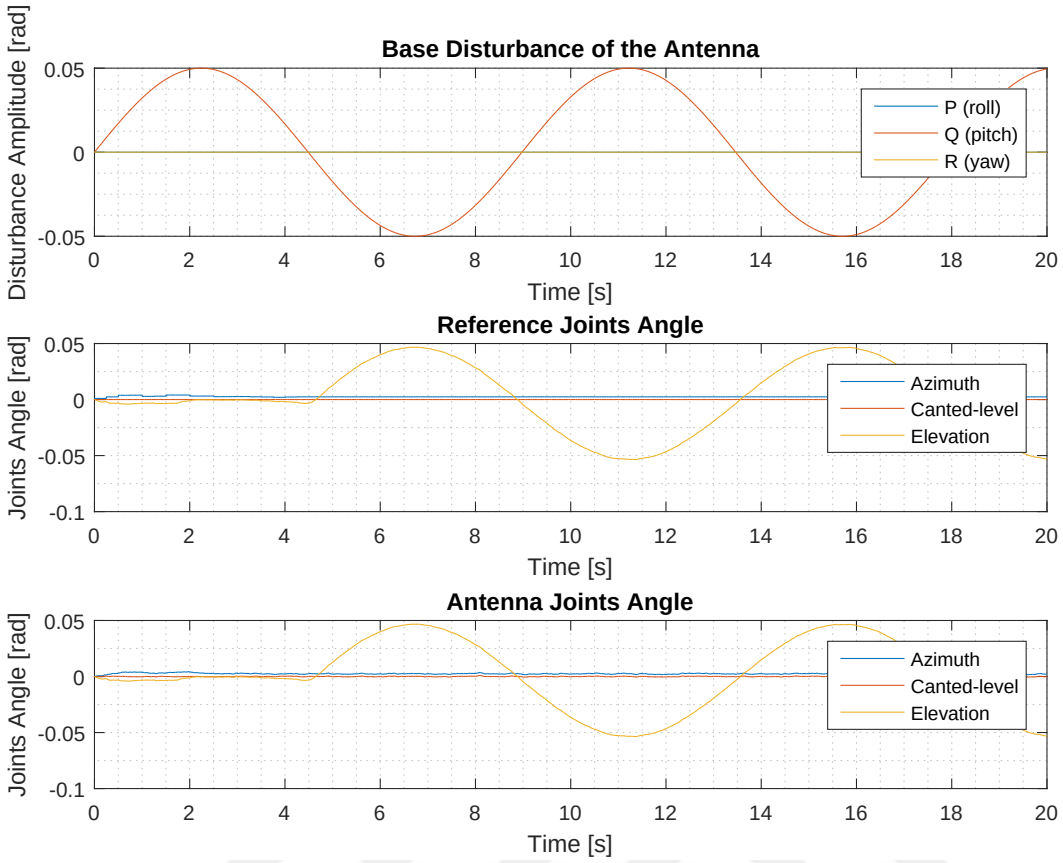

Figure 5.25 : The disturbance on the antenna (top), The step-track algorithm reference (middle), The actual joints angle (bottom).

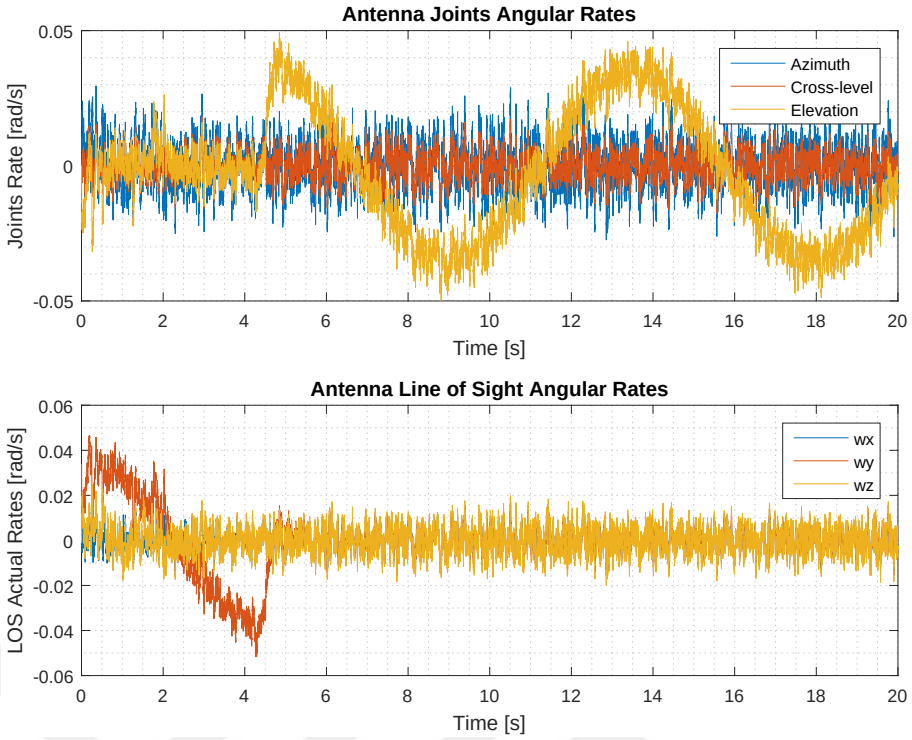

Figure 5.26 : Antenna joints angular rates during stabilization (top), LOS angular rates during stabilization (bottom) under pitch disturbance with IMU bias error.

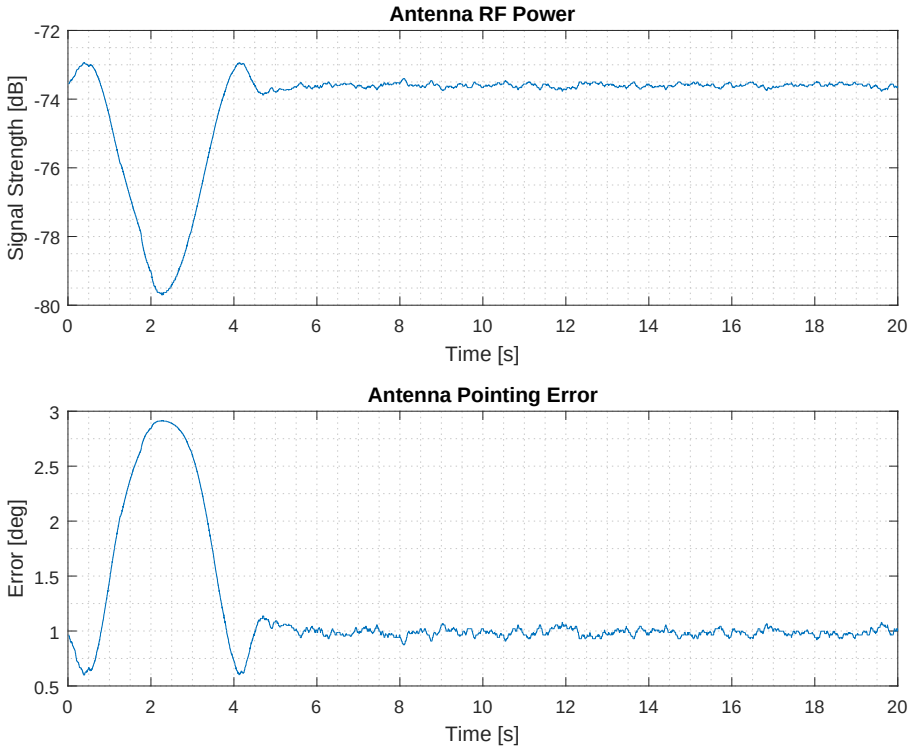

Figure 5.27 : Antenna RF signal level during scanning (top), Antenna pointing error during scanning (bottom). under pitch disturbance.

5.2.2 Designing and implementation of the conical scan algorithm

The other algorithm which helps to find the maximum signal level is the conical scan algorithm. This algorithm implies a sine trajectory for the EL axis and a cosine trajectory for the XEL axis. Due to 90° phase shift between sine and cosine, end effector draws a circular movement. This movement tracks the satellite maximum level, finally, the maximum point is found. The amplitude of the cosine and sine specifies the radius of the circular movement. This amplitude can be changeable to optimize and maintains the maximum signal level. Also, if the disturbance movement which comes from IMU is bigger than the threshold, the bigger amplitude can help to maintain the maximum signal level. The changeable radius may improve the tracking properties but in this thesis fixed amplitude is used. The flow of the conical scan algorithm is different from the step-track. In the step-track algorithm, the algorithm plans a trajectory for the azimuth and elevation axis. However, in the conical scan algorithm plans a trajectory for the antenna payload. This situation helps the find maximum signal level more efficiently than the step-tracking. The algorithm can be explained in a few steps as follow;

- The first step in the algorithm is to plan one period a sine and cosine trajectory for XEL and EL axis of the antenna payload frame.
- The second step in the algorithm is to increase the amplitude and to decrease the frequency of the sine and cosine. This makes the bigger circular movement on the antenna payload.
- The third step in the algorithm is to repeat one period of the sine and cosine with increased amplitude and decreased frequency until the specified counter value.
- These steps draw a circular movement for the antenna payload but in each step, the azimuth and elevation values must be calculated including the base disturbances. Also, the signal measurement is saved for finding the maximum signal point with respect to the azimuth and elevations axis [28].

In Figure 5.28, the algorithm is implemented using the user-defined function as the input of the inverse kinematic model. The conical scan algorithm implemented is a function that takes the actual angles, the RF signal level, sine frequency, radius, time

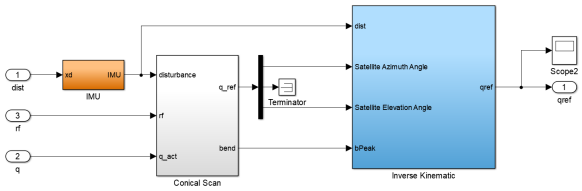

Figure 5.28 : The implementation of the conical-scan algorithm.

difference, and disturbance and calculates the reference azimuth and elevation axis positions (The function code is given in the Appendix.). As in the step-track algorithm, the reference of the canted-level is set to zero. The satellite look angles of the inverse kinematic are entered with a small error to make the pointing error. The aim here is to find the maximum RF signal level with the wrong error and IMU bias error under base disturbance. In all cases which will be examined, the axis of the pointing error figure is scaled between zero and FCC limits to see the performance of the system. Because the conical scan has a trajectory which has increasing amplitude, the pointing error during the scanning is too bigger than the FCC limitation. There is no need to examine the pointing error during the finding maximum signal level. Until two seconds, the conical-scan plans a trajectory with increasing amplitude. The measured signal level is both increasing and decreasing in trajectory planning. The azimuth and elevation angles which have maximum signal level is saved with the disturbance values. Using the saved values, the actual joints angle which has the maximum signal level and IMU bias are calculated with kinematic equations. After trajectory planning is completed, the controller stabilizes the actual joints angle values.

In the first case, it's assumed that there is no disturbance on the antenna. In the second case, there is a disturbance on the roll axis. In the third case, there is a disturbance on the pitch axis. In the fourth case, there is a disturbance on the yaw axis. In the fifth case, there is a disturbance on roll, pitch and yaw axes. In Figure 5.29, the conical scan trajectory planning is shown. In all cases, the conical scan algorithm finds the maximum RF signal as close as possible and the controllers stabilize the system within the FCC limits as shown in Figure (5.30 - 5.44)

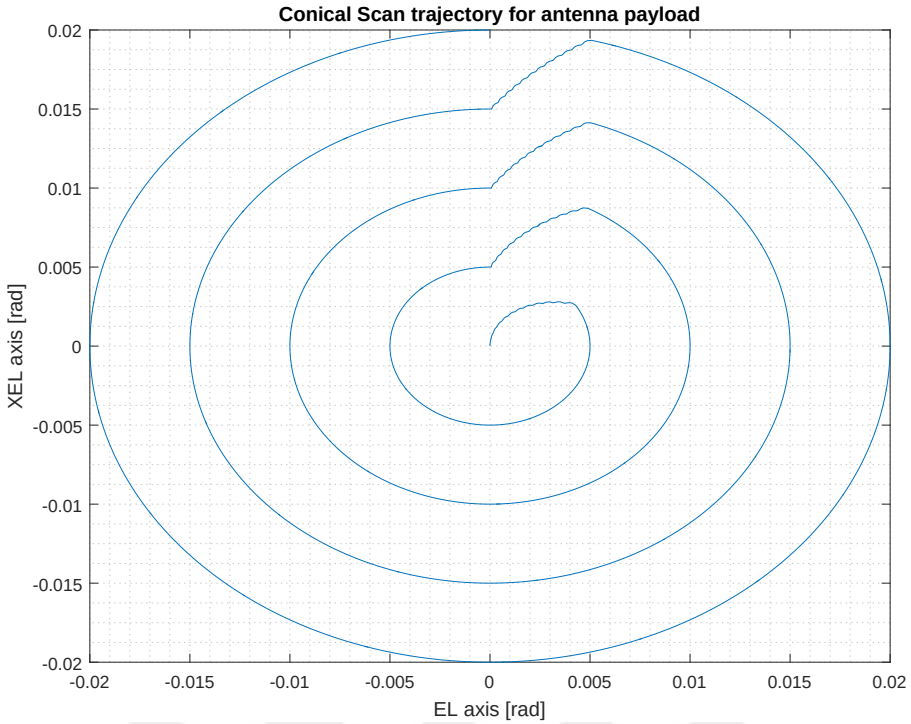

Figure 5.29 : The planned trajectory of the conical-scan.

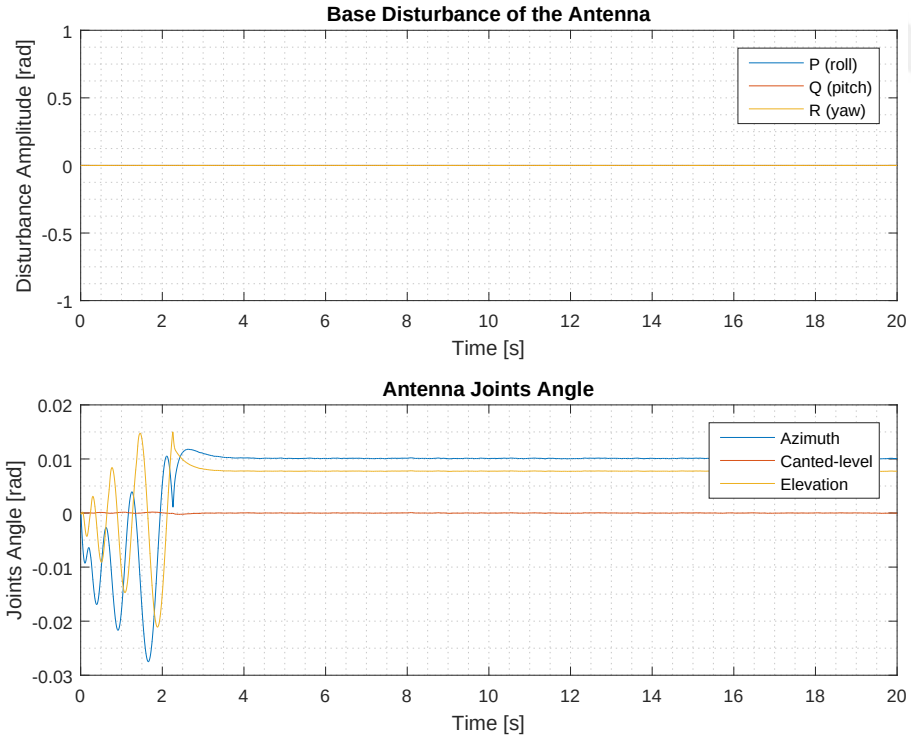

Figure 5.30 : The disturbance on the antenna (top), The actual joints angle (bottom).

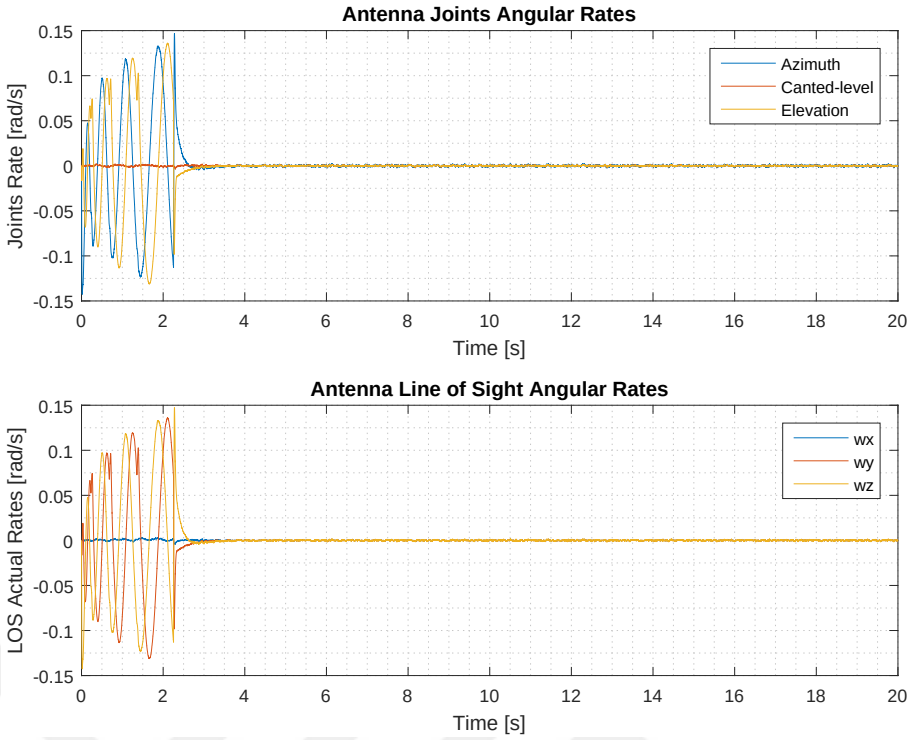

Figure 5.31 : Antenna joints angular rates during stabilization (top), LOS angular rates during stabilization (bottom) with IMU bias error.

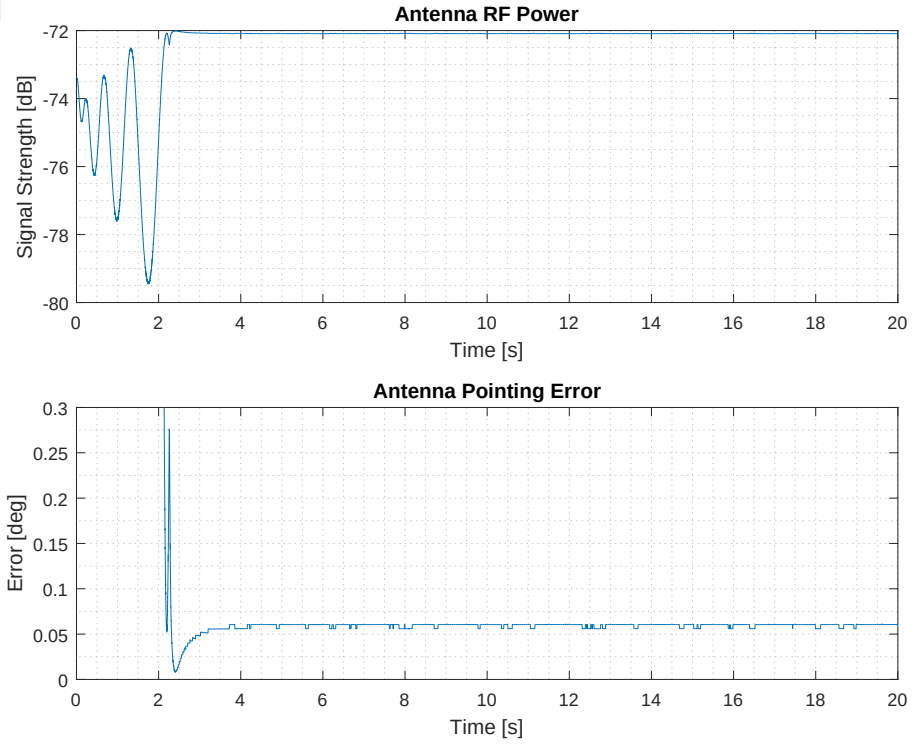

Figure 5.32 : Antenna RF signal level during scanning (top), Antenna pointing error during scanning (bottom) with IMU bias error.

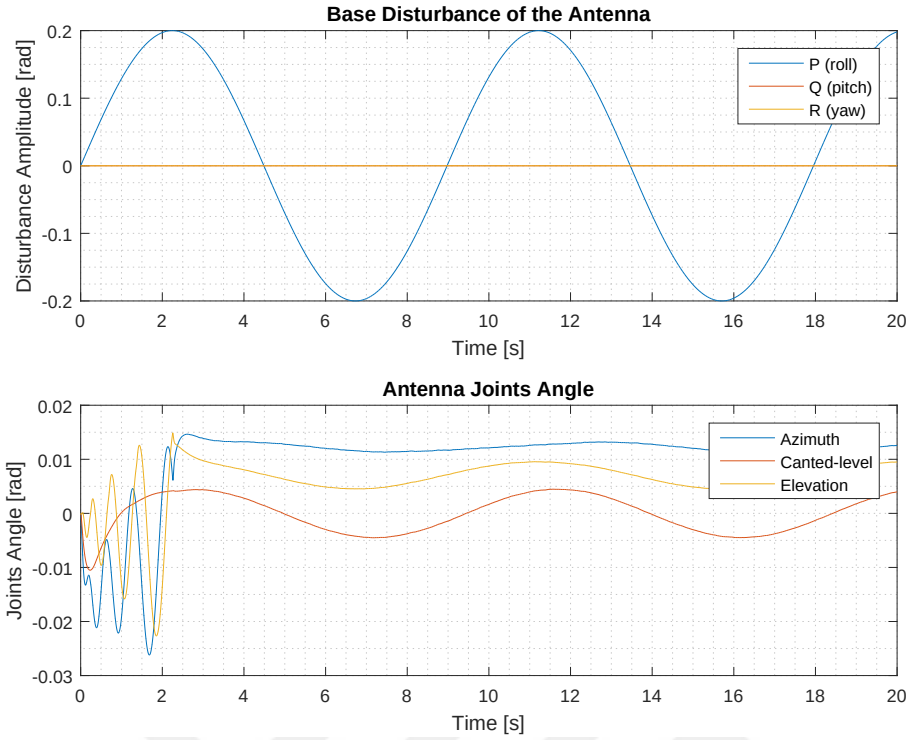

Figure 5.33 : The disturbance on the antenna (top), The actual joints angle (bottom).

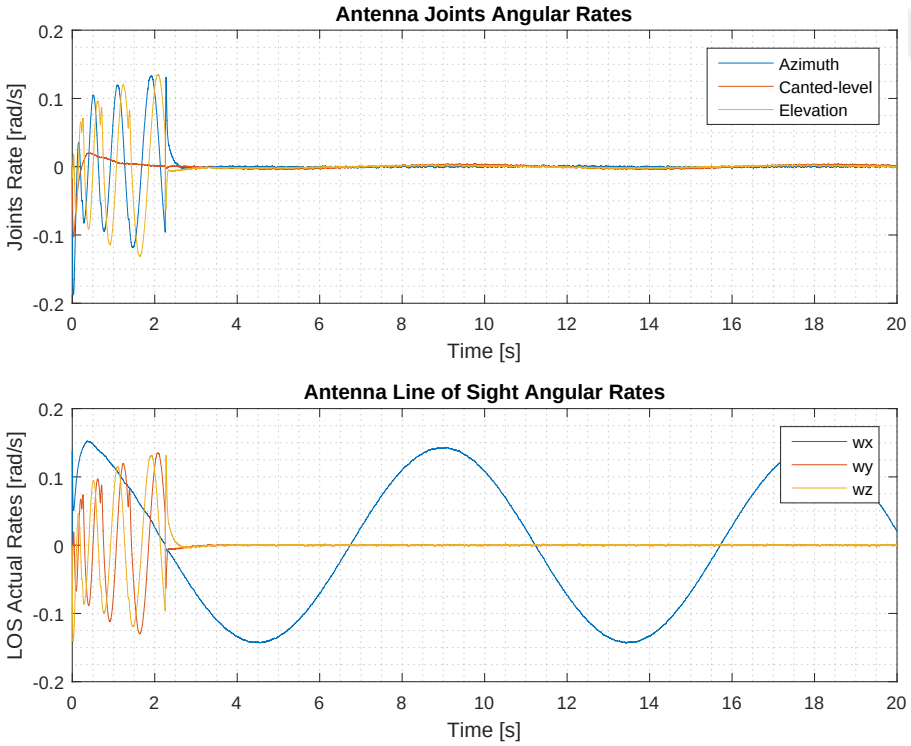

Figure 5.34 : Antenna joints angular rates during stabilization (top), LOS angular rates during stabilization (bottom) under roll disturbance with IMU bias error.

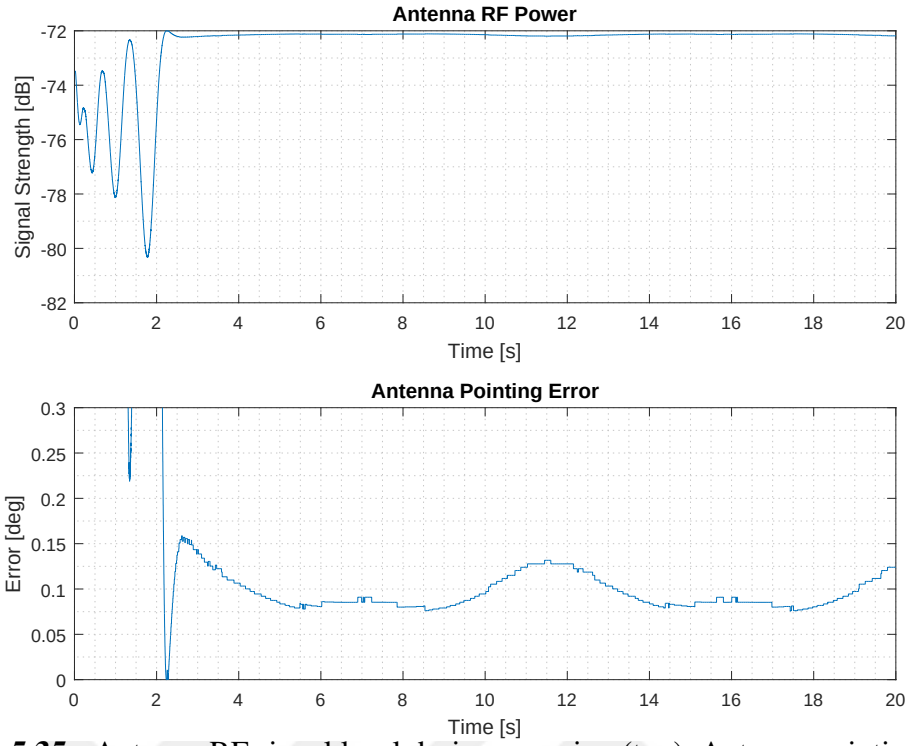

Figure 5.35 : Antenna RF signal level during scanning (top), Antenna pointing error during scanning (bottom) under roll disturbance with IMU bias error.

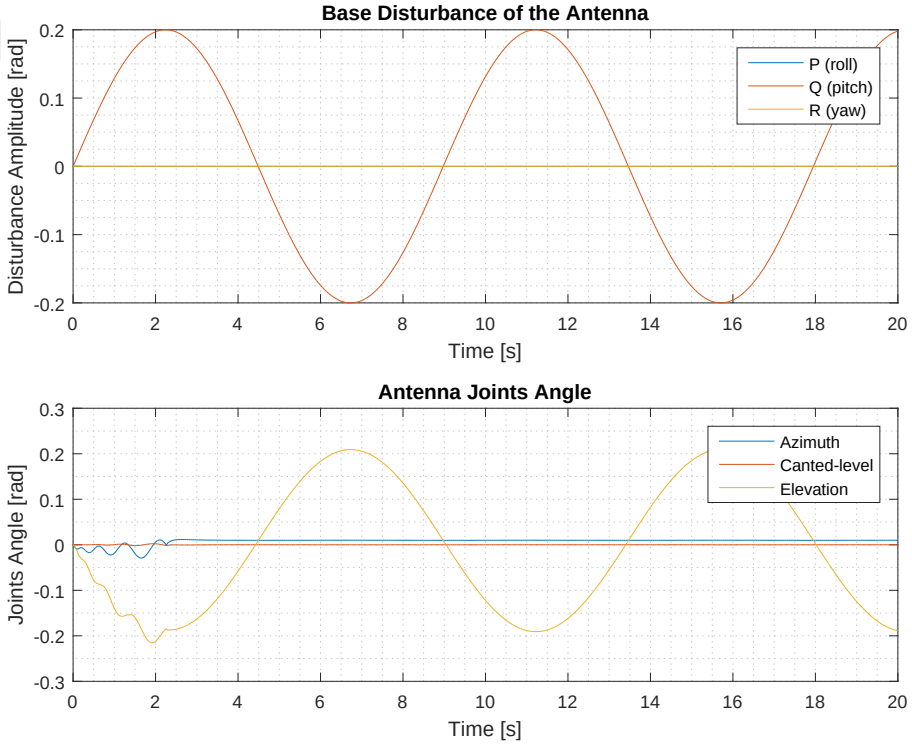

Figure 5.36 : The disturbance on the antenna (top), The actual joints angle (bottom).

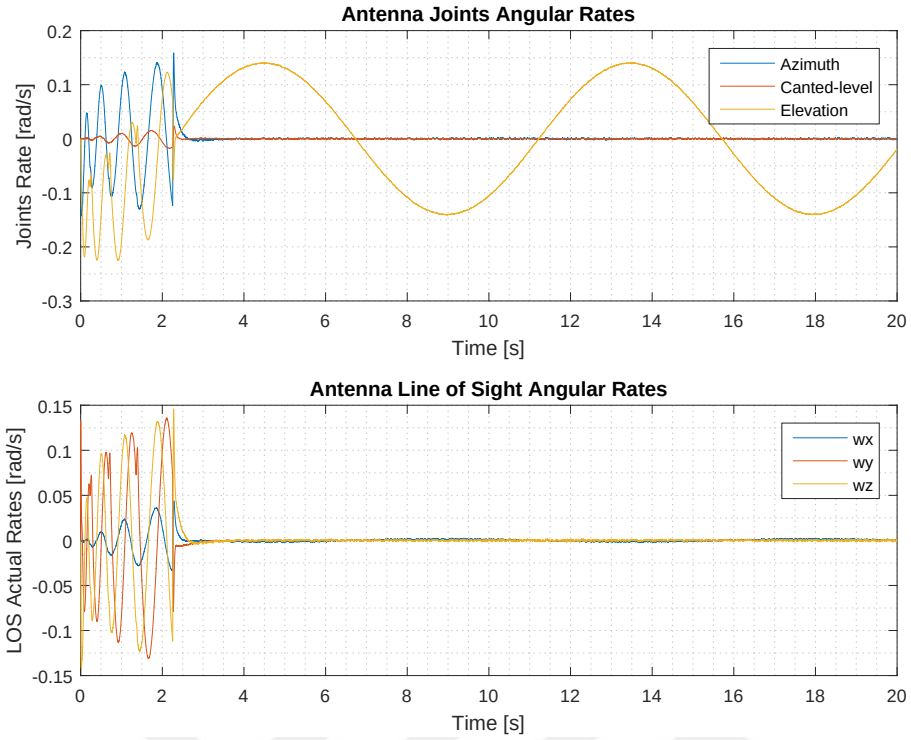

Figure 5.37 : Antenna joints angular rates during stabilization (top), LOS angular rates during stabilization (bottom) under pitch disturbance with IMU bias error.

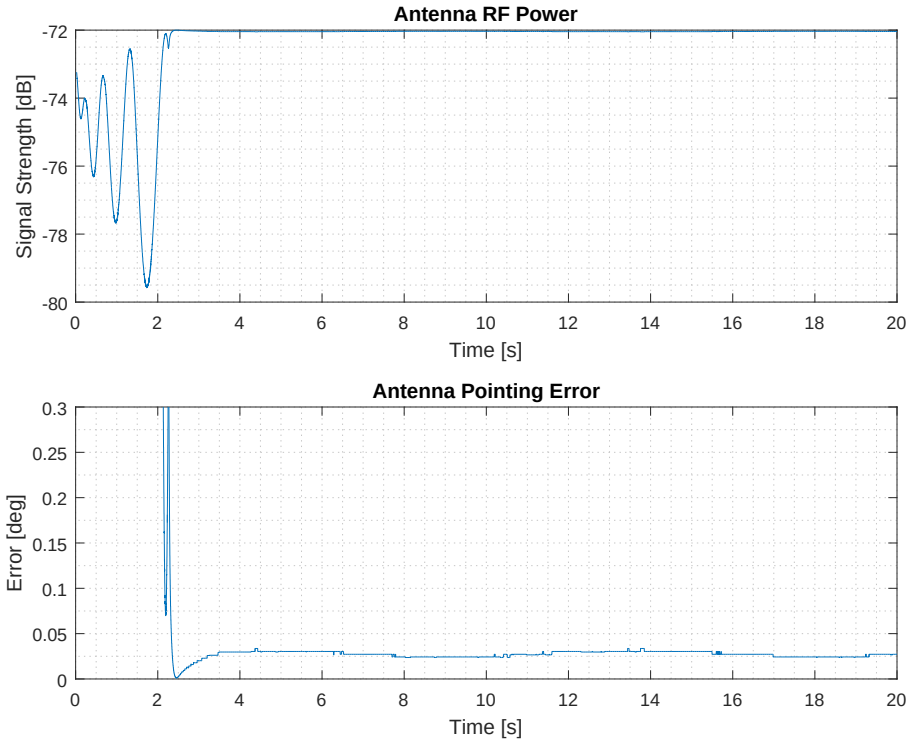

Figure 5.38 : Antenna RF signal level during scanning (top), Antenna pointing error during scanning (bottom) under pitch disturbance with IMU bias error.

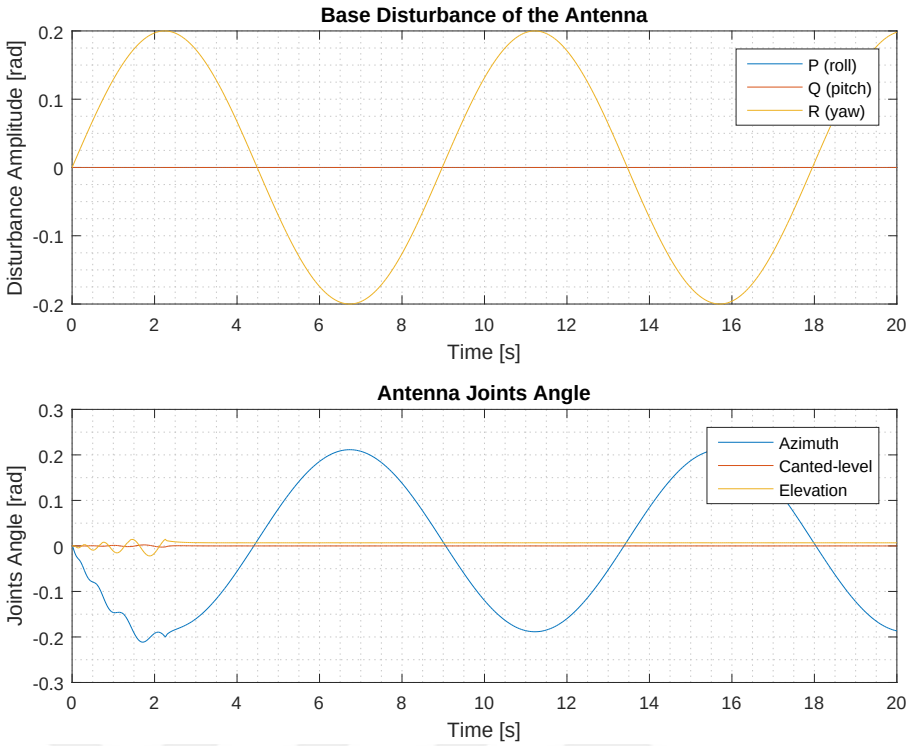

Figure 5.39 : The disturbance on the antenna (top), The actual joints angle (bottom).

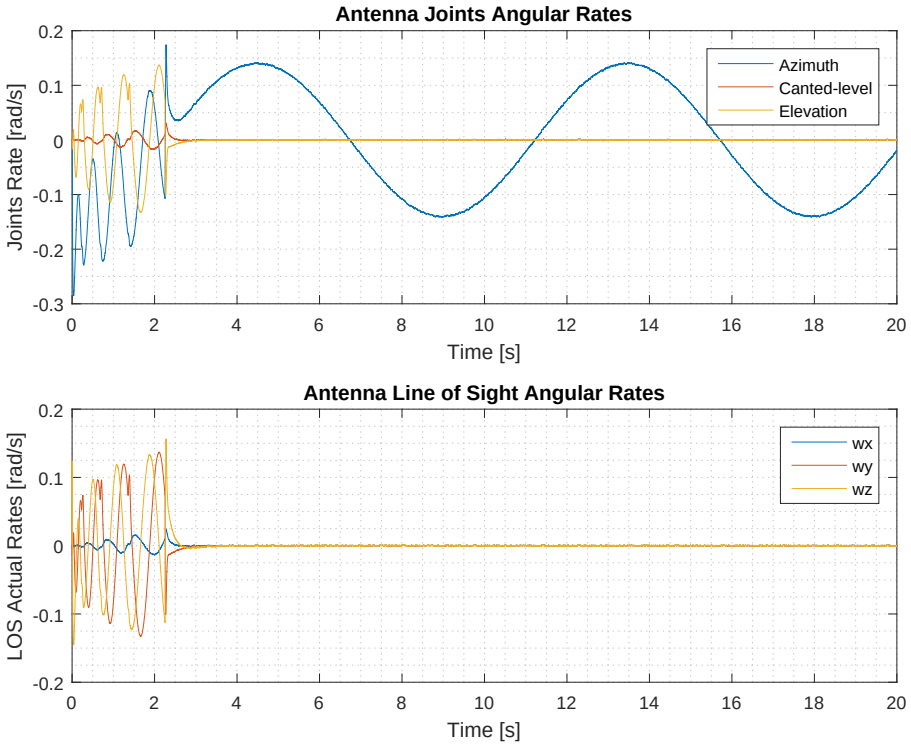

Figure 5.40 : Antenna joints angular rates during stabilization (top), LOS angular rates during stabilization (bottom) under yaw disturbance with IMU bias error.

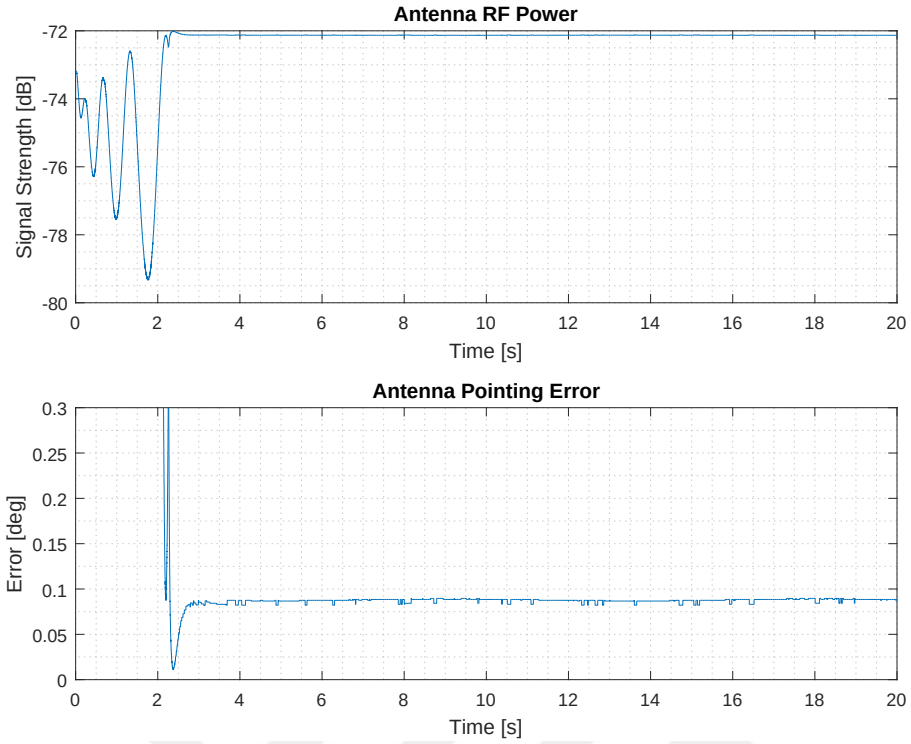

Figure 5.41 : Antenna RF signal level during scanning (top), Antenna pointing error during scanning (bottom) under yaw disturbance with IMU bias error.

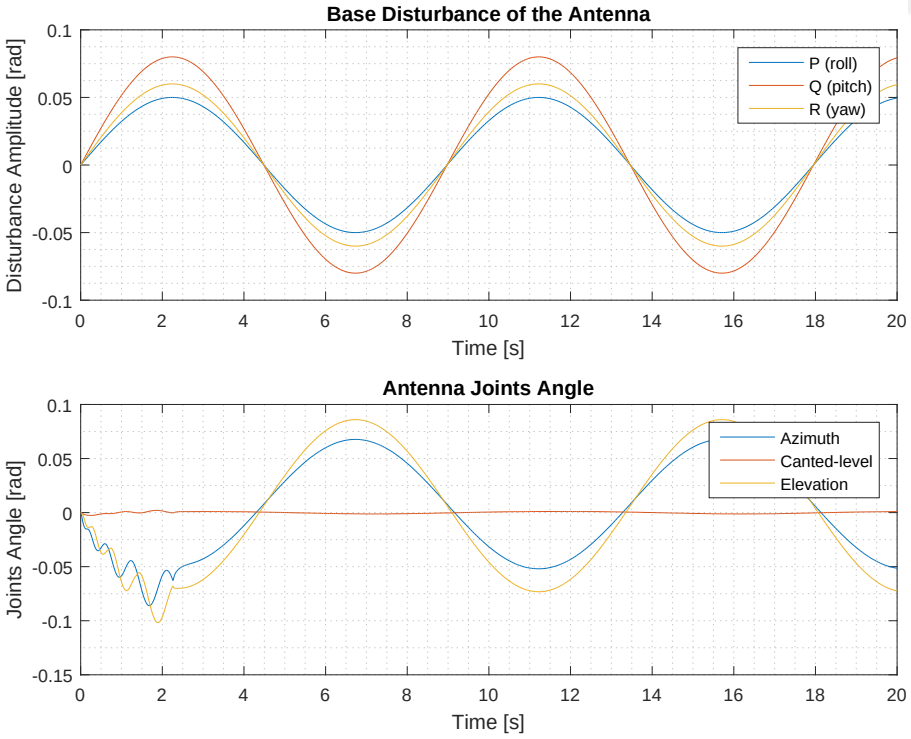

Figure 5.42 : The disturbance on the antenna (top), The actual joints angle (bottom).

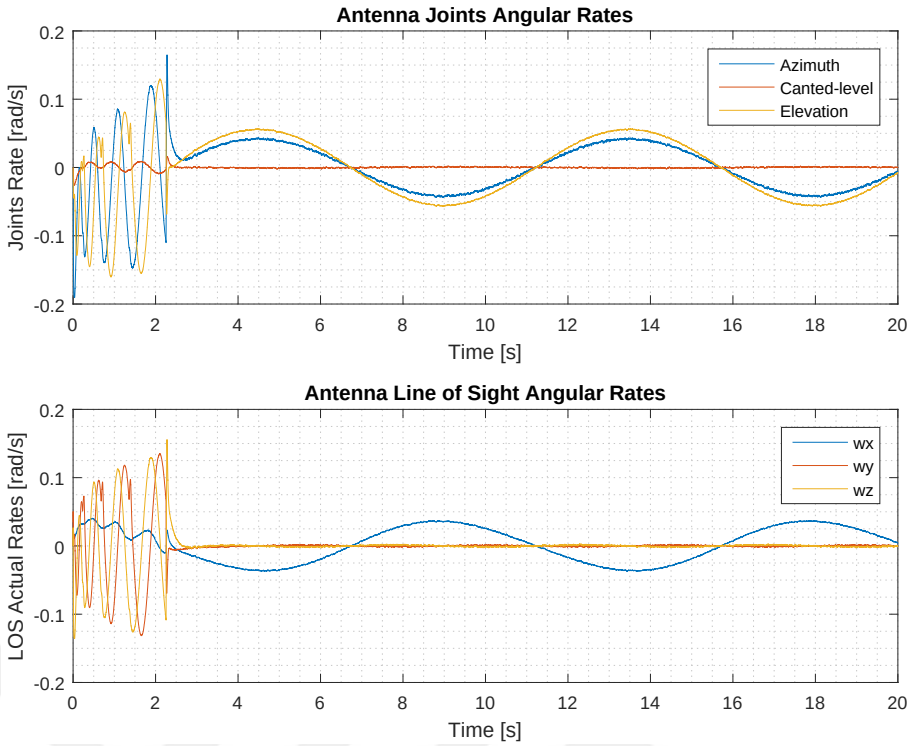

Figure 5.43 : Antenna joints angular rates during stabilization (top), LOS angular rates during stabilization (bottom) under roll, pitch and yaw disturbance with IMU bias error.

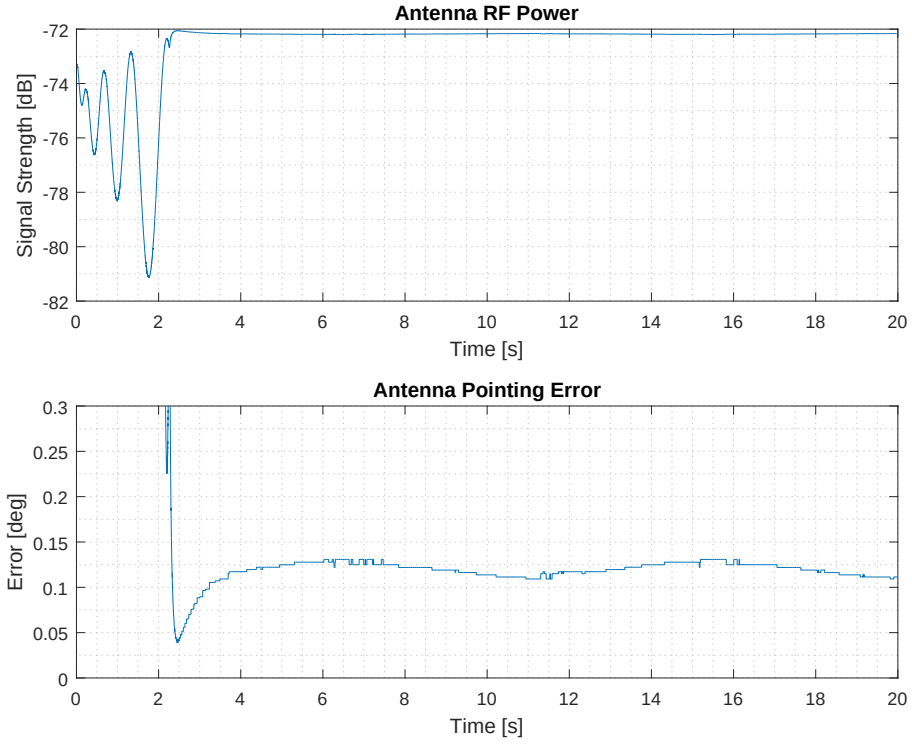

Figure 5.44 : Antenna RF signal level during scanning (top), Antenna pointing error during scanning (bottom) under roll, pitch and yaw disturbance with IMU bias error.

6. CONCLUSIONS AND RECOMMENDATIONS

6.1 Line of Sight Stabilization Simulation Results Summary

Line of sight stabilization of 2-axes pedestal was investigated to understand the behavior of the stabilization in the nominal APS. The investigated algorithm cannot be implemented directly to the and 3-axes pedestal. Therefore, the algorithm which includes the Jacobian operator has been developed to stabilize the LOS. The operator was implemented onto the feedback path due to the redundancy of the canted-level axis. The PI speed controller was designed to compensate for the axis rate to track sinusoidal reference. In order to make the model closer to the real system gyroscope, torque ripple noise was added.

The results of the proposed algorithm were presented in Figure 4.15, 4.17, 4.19, 4.21, and 4.23. Since the stabilization controller is the inner loop, to meet pointing requirement stabilization algorithm must be fast as possible. Each of the results, the angular rates of the LOS made the fast movement to settle their reference value. This situation caused by the applying cosine disturbance to the base frame. In velocity calculations, the derivative of the base disturbance was taken to calculate the angular rates of the LOS. In the results, it is clear that the stabilization algorithm keeps the angular rates of LOS between $\pm$ 0.02 rad/s (1.15 deg/s) and also compensate the error within 0.1 seconds.

6.2 Closed-loop Controller Simulation Results Summary

The closed-loop controller was constructed with the position controller and the scanning algorithm. The main concern in the SOTM antenna is that pointing error must be below than 0.2° to obtain the FCC license. The PID based position control was designed to point the satellite. Position controller was implemented as the outer loop of the stabilization controller. Just the azimuth and elevation axis were used in the pointing. The reference of the canted-level axis was set the zero. Figure 5.8, 5.11, 5.14, and 5.17 indicate that the pointing error below the FCC limitation under

various disturbance variation. However as shown in 5.20 the position controller cannot compensate the disturbance with IMU bias error. In the simulations, bias errors were taken 0.2° for roll axis, 0.1° for pitch axis, and 0.5° for yaw axis. Actually, the controller was trying to compensate for the error but due to bias error, the controller pointed the wrong reference.

To eliminate bais error scanning algorithms which are step-track and conical scan was implemented. The step-track algorithm was easier to design and implement more than the conical scan algorithm. In Figure 5.24, step-track algorithm finds the maximum RF signal level by giving step reference to the azimuth and elevation axis. When the maximum signal level was found the roll, pitch, and yaw are measured and saved. After now, saved values are decreased from the measured valued to obtain measurement without bias values. However, as shown in 5.27 the step-track algorithm couldn't find the maximum RF signal level. This may be caused by the simplification in the implementation of the usage of the axis.

Conical scan algorithm plans a sine and cosine trajectory for antenna aperture by taking into account the base disturbance. Taking into account the disturbance gives this algorithm works with the disturbance. For this reason, the conical scan is more efficient to find the maximum RF signal. Figure 5.32, 5.35, 5.38, 5.41, and 5.44 indicate that the conical scan algorithm found the maximum point of the RF signal and the worked with the position controller correctly. All results proved that the pointing error after initiation is below the FCC standards.

6.3 Suggestions for Feature Work

The Simulink model which developed in Chapter 3 includes the full kinematic model, simplified dynamic model, and antenna aperture model. The kinematic model contains whole disturbance caused by shipborne movement. But the disturbance effects in the dynamics were not implemented due to a decrease in the complexity of the simulation file. Therefore, we are not able to determine how much the disturbance effect caused by dynamics changes the pointing error. No matter the antenna has the gimbal structure and perfect balance, there are always coupling between each link. Actually, these can generate extra torque disturbance on each axis. If the torque controller or shelf driver has good performance, there may be no need to develop the dynamic model of the

antenna.

In the antenna, the noises of the gyroscope sensor, IMU sensor, and BLDC torque ripple were added in the simulation and examined to affect on the pointing error. But the RF model noises was not added in the simulation. While designing the controller and scanning algorithm, the RF aperture was assumed symmetric and there was no noise on the measurement. Especially, the asymmetric situation of the antenna may be added and examined the pointing error under this condition.

In oder to implement the scanning algorithm, it was assumed that the algorithm works just one time after initiation. In the commercial product, the scanning algorithm must plan a trajectory in a specified period. It's good way the specify the period time which depends on the rate of the disturbance. It is advised that if the disturbance rate is fast, the scanning algorithm period should be fast. Also, in the implementation of the conical scan, the algorithm couldn't find the maximum signal level under high disturbance and IMU bias error. This caused by increased amplitude of the conical scan with the IMU bias value calculates the wrong reference. This may be solved by adding varying magnitude on the conical scan algorithm.

This thesis shows a feasible simulation using LOS stabilization with the Jacobian operator and closed-loop control with the RF feedback. The recommended next step is implementing both algorithms on the actual antenna system. Firstly, the LOS stabilization should be implemented and tested under various base disturbance using a parallel simulator. Secondly, the closed-loop controller should be implemented and tested without base disturbance. Thirdly, the conical scan algorithm should be tested and verified without the base disturbance. Finally, the closed-algorithm can be tested with a base disturbance on the simulator.

REFERENCES

[1] **Shroyer, T.** (2012). Satcom-on-the-move why one size doesn't fit all, *MILCOM 2012 - 2012 IEEE Military Communications Conference*, pp.1–6.

[2] **HILKERT, J.M.** (2008). Inertially stabilized platform technology Concepts and principles, *IEEE Control Systems Magazine*, *28*(1), 26–46.

[3] **Murthy, R.** (2011). On-satellite testing of mobile communication antennas for compliance to VMES, ESV, and other pointing accuracy requirements, *2011-MILCOM 2011 Military Communications Conference*, IEEE, pp.1812–1817.

[4] **Murthy, R.** (2012). Performance criteria affecting pointing error and the impact on total cost of ownership, *MILCOM 2012 - 2012 IEEE Military Communications Conference*, pp.1–6.

[5] **DEBRUIN, J.** (2008). Control systems for mobile Satcom antennas, *IEEE Control Systems Magazine*, *28*(1), 86–101.

[6] **Bingül, Z. and Küçük, S.** (2009). *Robot Kinematiği*, Birsen.

[7] **Krishnan, R.** (2001). *Electric motor drives: modeling, analysis, and control*, volume626, Prentice Hall New Jersey.

[8] **Schmidt, G.T.** (2010). INS/GPS technology trends, **Technical Report**, Massachusetts Inst of Tech Lexington MA.

[9] **Barnes, F.N.** (1971). Stable member equations of motion for a three-axis gyro stabilized platform, *IEEE Transactions on Aerospace and Electronic Systems*, (5), 830–842.

[10] **Ekstrand, B.** (2001). Equations of motion for a two-axes gimbal system, *IEEE Transactions on Aerospace and Electronic Systems*, *37*(3), 1083–1091.

[11] **Zhao, J.**, **Gao, F.**, **Wu, Q.**, **Jin, S.**, **Wu, Y. and Jia, W.** (2018). Beam tracking for UAV mounted SatCom on-the-move with massive antenna array, *IEEE Journal on Selected Areas in Communications*, *36*(2), 363–375.

[12] **Leghmizi, S. and Sheng, L.** (2010). Kinematics modeling for satellite antenna dish stabilized platform, *2010 International Conference on Measuring Technology and Mechatronics Automation*, volume 2, IEEE, pp.558–563.

[13] **Hancioglu, O.K.**, **Celik, M. and Tumerdem, U.** (2018). Kinematics and Tracking Control of a Four Axis Antenna for Satcom on the Move, *2018 International Power Electronics Conference (IPEC-Niigata 2018-ECCE Asia)*, IEEE, pp.1680–1686.

[14] **Leghmizi, S.**, **Liu, S.**, **Fraga, R. and Boughelala, A.** (2012). Dynamics modeling for satellite antenna dish stabilized platform, *Advanced Materials Research*, volume566, Trans Tech Publ, pp.187–196.

[15] **Said, L.**, **Sheng, L.**, **Farouk, N. and Latifa, B.** (2012). Modeling design and control of a ship carried 3 dof stabilized platform, *Research Journal of Applied Sciences, Engineering and Technology*, *4*(19), 3843–3851.

[16] **Ristroph, G. and DeBruin, J.** (2010). Servo requirements for FCC VMES compliance: Servo performance levels required to meet FCC VMES pointing requirements for satcom-on-the-move antennas on ground vehicles, *2010-MILCOM 2010 MILITARY COMMUNICATIONS CONFERENCE*, IEEE, pp.1983–1987.

[17] **Stockum, L.A. and Carroll, G.R.** (1984). Precision stabilized platforms for shipboard electro-optical systems, *Optical Platforms*, volume493, International Society for Optics and Photonics, pp.414–426.

[18] **Rue, A.** (1974). Precision stabilization systems, *IEEE Transactions on Aerospace and Electronic Systems*, (1), 34–42.

[19] **Rue, A.** (1969). Stabilization of precision electrooptical pointing and tracking systems, *IEEE Transactions on Aerospace and Electronic Systems*, (5), 805–819.

[20] **Masten, M.K. and Hilkert, J.** (1987). Electromechanical system configurations for pointing, tracking, and stabilization applications, *Electromechanical system interaction with optical design*, volume779, International Society for Optics and Photonics, pp.75–88.

[21] **DeBruin, J.C.**, **Royalty, J.M.**, **Wand, M. and Allen, E.** (1996). Feedforward stabilization test bed, *Acquisition, Tracking, and Pointing X*, volume2739, International Society for Optics and Photonics, pp.204–215.

[22] **Kennedy, P.J. and Kennedy, R.L.** (2003). Direct versus indirect line of sight (LOS) stabilization, *IEEE Transactions on control systems technology*, *11*(1), 3–15.

[23] **DeBruin, J.** (2008). Shock isolation for mobile pointed satcom systems, *MILCOM 2008-2008 IEEE Military Communications Conference*, IEEE, pp.1–6.

[24] **Richharia, M.** (1986). Design considerations for an earth station step-track system, *Space Communication Broadcasting*, *4*, 215–228.

[25] **HECKERT, G.** Step-track-A simple autotracking scheme for satellite communication terminals, *3rd Communications Satellite Systems Conference*, p.416.

[26] **Pirhadi, A.**, **Hosseini, M. and HAKAK, M.** (2005). A novel implementation of geo satellite step track subsystem.

[27] **Richharia, M. and Verma, N.** (1982). Design of a Step-Track System for Low-Cost Earth Stations, *IETE Journal of Research*, *28*(10), 533–538.

[28] **Karabinis, P.**, **Egri, R. and Bennett, C.** (1988). Antenna pointing and scanning control for a two axis gimbal system in the presence of platform motion, *MILCOM 88, 21st Century Military Communications-What's Possible?'. Conference record. Military Communications Conference*, IEEE, pp.793–799.

[29] **Gosline, R.** (1973). CONSCAN Implementation at DSS 13, *The Deep Space Network Progress Report*, 87–90.

[30] **Gawronski, W. and Craparo, E.** (2001). Three scanning techniques for deep space network antennas to estimate spacecraft position, *The Interplanetary Network Progress Report*, 42–147.

[31] **Bingül, Z. and Küçük, S.** (2008). *Robot Dinamiği ve Kontrolü*, Birsen.

[32] **Najman, J.**, **Bastl, M.**, **Appel, M. and Grepl, R.** Computationally Fast Dynamical Model of a SATCOM Antenna Suitable for Extensive Optimization Tasks.

[33] **Kuo, F.G.C.** (2009). *Automatic Control Systems*, Wiley.

[34] **Url-1**, `http://en.wikizeroo.net/index.php?q=aHR0cHM6Ly9lbi53aWlpcGVkaWEub3JnL3dpa2kvV2luZF93YXZI`, date retrieved: 10.11.2018.

APPENDICES

APPENDIX A.1 : Matlab code for kinematic calculation
APPENDIX A.2 : Matlab code for RF model calculation
APPENDIX A.3 : Matlab code for Rate controller design
APPENDIX A.4 : Matlab code for Position controller design
APPENDIX A.5 : Matlab code for step-track algorithm
APPENDIX A.6 : Matlab code for conical scan algorithm

APPENDIX A.1

```
%
%
% @file Kinematic
% @author Oguz Kaan Hancioglu
% @version V1.0.0
% @date 01-May-2017
% @brief This code generates the kinematic model of the SOTM antenna
%
%
clc;clear all; close all;
% Physical Features
beta = 30;
l2 = 703;
l3 = 410.4;
l1 = 355.42;
% DH parameters
% DH link lengths
% a1 a2 a3 ... an
ai = [l1,0,0,0,0];
% DH twist angles
% alpha1 alpha2 alpha3 ... alphan
alfai = [0,(90-beta),-90,90,0];
% DH joint ofsets
% d1 d2 d3 ... dn
di = [0,-l2,-l3,0,0];
% DH joint angles
% theta1 theta2 theta3 ... thetan
% Confirmation step variable
% Set 0 to confirmate the end effector position
% Set any value which different from zero to confirmate the end effector position
confirmation_step = 1;
if confirmation_step == 0
theta1 = 0; % azimuth
theta2 = 90; % imaginary axis
theta3 = 0; % canted-level
theta4 = 0; % elevasyon
theta5 = 0; % polarizasyon
else
theta1 = 160.6; % azimuth
theta2 = 90; % imaginary axis
theta3 = 0; % canted-level
theta4 = 40.72; % elevasyon
theta5 = 165.4; % polarizasyon
end
thetai = [theta1,theta2,theta3-90,theta4+beta,theta5];
% link type: revolute is 1, prismatic is 0
```

```
link_type = [1,1,1,1,1];
% Transformation matrix
if eq(length(ai),length(alfai)) && eq(length(di),length(thetai))
T0N = eye(4);
% obtain forward kinematic model of robot
for i=1:1:length(ai)
% create DH Matrix
Ai=[cosd(thetai(i)),-sind(thetai(i))*cosd(alfai(i)),  sind(thetai(i))*sind(alfai(i))  ,
cosd(thetai(i))*ai(i);
sind(thetai(i)),cosd(thetai(i))*cosd(alfai(i))  ,  -cosd(thetai(i))*sind(alfai(i)),
sind(thetai(i))*ai(i);
0 ,sind(alfai(i)) , cosd(alfai(i)) , di(i);
0 ,0 , 0 , 1];
% display transformation matrix
fprintf('A%d\n',i);
disp(Ai);
fprintf('T0%d\n',i);
T0N = T0N * Ai;
% display forward kinematic
disp(T0N)
% obtain whole T0i matrixes in one variable
if i==1
T0Ns = T0N;
else
T0Ns = [T0Ns , T0N];
end
end
% obtain end effector matirx
T0N = T0N*[0,0,-1,0;0,1,0,0;1,0,0,0;0,0,0,1];
fprintf('End effector transformation matrix T0%d\n',6);
disp(T0N);
else
disp('Error! dimentions of variables are not mathing.')
end
% Inverse Kinematic Confirmation
inverse_elevation = atan2d(-0.8660,0.5)+atan2d(sqrt(1-T0N(3,1)^2),T0N(3,1));
inverse_elevation = inverse_elevation - beta;
aaaa = T0N(1,1)/(sind(inverse_elevation+beta)*0.5+cosd(inverse_elevation+beta)*0.8660);
bbbb = T0N(2,1)/(sind(inverse_elevation+beta)*0.5+cosd(inverse_elevation+beta)*0.8660);
inverse_azimuth = atan2d(bbbb,aaaa);
aaa = T0N(3,3)/(sind(inverse_elevation+beta)*0.5+cosd(inverse_elevation+beta)*0.8660);
bbb = T0N(3,2)/(sind(inverse_elevation+beta)*0.5+cosd(inverse_elevation+beta)*0.8660);
inverse_polarization = atan2d(bbb,aaa);
disp('Elevation Axis Angle')
disp(inverse_elevation);
disp('Azimuth Axis Angle')
disp(inverse_azimuth);
disp('Polarization Axis Angle')
```

```
disp(inverse_polarization);
```

APPENDIX A.2

```
%
%
% @file correct10dB
% @author Oguz Kaan Hancioglu
% @version V1.0.0
% @date 01-January-2018
% @brief This code generates the aperture gain model of the antenna
%
%
N = 5.0; % EL, XEL aparture degree
max = 60; % maximum RF Power dB
tendb_beamwidth = 2.8; % -10 dB beamwidth
coef_x = 0.022;
coef_y = 0.022;
x= -N:0.01:N;
y=x;
z=(max.*exp(-(coef_x * X.^2)-(coef_y * Y.^2)));
h = surf(X,Y,z);
h.FaceColor = 'interp';
xlabel('Elevation axis [Degree]');
ylabel('Azimuth axis [Degree]');
zlabel('Antenna Power [dB]');
shading interp
axis tight
```

APPENDIX A.3

```
%
%
% @file controller
% @author Oguz Kaan Hancioglu
% @version V1.0.0
% @date 01-January-2018
% @brief This code calculates and compares Rate Uncompensated and Compensated
axis.
%
%
% Azimuth axis dynamics
clc; clear all; close all;
I_az = 2.5359;
B_az = 0.2;
num_az = 1;
den_az = [I_az B_az];
```

```
tf_az = tf(num_az,den_az)
pole(tf_az)
tf_az_dis = c2d(tf_az,0.01,'zoh')
figure
subplot(2,1,1);
rlocus(tf_az);
title('Root Locus of the Uncompensated Azimuth Axis');
grid minor;
subplot(2,1,2);
step(tf_az);
title('Step Response of the Uncompensated Azimuth Axis');
grid minor;
figure
bode(tf_az,0.1,10000);
title('Bode Diagram of the Uncompensated Azimuth Axis');
grid minor;
% Controller
Kp_az = 160;
Ki_az = 10;
Kd_az = 0;
num_c_az = [Kd_az Kp_az Ki_az];
den_c_az = [1 0];
tf_c_az = tf(num_c_az,den_c_az)
% Closed loop system
tf_cl_az = feedback(tf_az*tf_c_az,1)
figure
subplot(2,1,1);
rlocus(tf_cl_az);
title('Root Locus of the Compensated Azimuth Axis');
grid minor;
subplot(2,1,2);
step(tf_cl_az);
title('Step Response of the Compensated Azimuth Axis');
grid minor;
figure
bode(tf_az,0.1,10000);
grid minor;
hold on;
bode(tf_cl_az,0.1,10000);
grid minor;
title('Bode Diagram of the Compensated and Uncompensated');
legend('Uncompensated','Compensated');
bandwith_az = bandwidth(tf_cl_az)
```

APPENDIX A.4

```
%
%
```

```
% @file poscontroller
% @author Oguz Kaan Hancioglu
% @version V1.0.0
% @date 01-January-2018
% @brief This code calculates and compares Position Uncompensated and
Compensated axis.
%
%
% Azimuth axis dynamics
clc; clear all; close all;
I_az = 2.5359;
B_az = 0.2;
num_az = 1;
den_az = [I_az B_az];
tf_az = tf(num_az,den_az)
pole(tf_az)
tf_az_dis = c2d(tf_az,0.01,'zoh')
figure
subplot(2,1,1);
rlocus(tf_az);
title('Root Locus of the Uncompensated Azimuth Axis');
grid minor;
subplot(2,1,2);
step(tf_az);
title('Step Response of the Uncompensated Azimuth Axis');
grid minor;
figure
bode(tf_az,0.1,10000);
title('Bode Diagram of the Uncompensated Azimuth Axis');
grid minor;
% Controller
Kp_az = 160;
Ki_az = 10;
Kd_az = 0;
num_c_az = [Kd_az Kp_az Ki_az];
den_c_az = [1 0];
tf_c_az = tf(num_c_az,den_c_az)
% Closed loop system
tf_cl_az = feedback(tf_az*tf_c_az,1)
figure
subplot(2,1,1);
rlocus(tf_cl_az);
title('Root Locus of the Compensated Azimuth Axis');
grid minor;
subplot(2,1,2);
step(tf_cl_az);
title('Step Response of the Compensated Azimuth Axis');
grid minor;
figure
```

```
bode(tf_az,0.1,10000);
grid minor;
hold on;
bode(tf_cl_az,0.1,10000);
grid minor;
title('Bode Diagram of the Compensated and Uncompensated');
legend('Uncompensated','Compensated');
bandwith_az = bandwidth(tf_cl_az)
% Position Controller Kp_az_pos = 14;
Ki_az_pos = 3;
Kd_az_pos = 0.5;
num_c_az_pos = [Kd_az_pos Kp_az_pos Ki_az_pos];
den_c_az_pos = [1 0];
tf_c_az_pos = tf(num_c_az_pos,den_c_az_pos)
tf_int = tf([1],[1 0])
tf_cl_az_pos = feedback(tf_c_az_pos*tf_cl_az*tf_int,1)
figure
subplot(2,1,1);
rlocus(tf_cl_az_pos);
title('Root Locus of the Compensated Azimuth Axis');
grid minor;
subplot(2,1,2);
step(tf_cl_az_pos);
title('Step Response of the Compensated Azimuth Axis');
grid minor;
print -depsc2 possetp.eps
figure
bode(tf_cl_az_pos,0.1,10000);
grid minor;
hold on;
bode(tf_cl_az_pos,0.1,10000);
grid minor;
title('Bode Diagram of the Compensated and Uncompensated');
legend('Uncompensated','Compensated');
bandwith_az = bandwidth(tf_cl_az_pos)
```

APPENDIX A.5

```
%%%%%%%%%%%%%%%%%%%%%%%%%%%%%%%%%%%%%%%%%%%%%%%%%%%%%%%%%%%%%%%%%%%%%%%%
%
% @file step-track
% @author Oguz Kaan Hancioglu
% @version V1.0.0
% @date 01-April-2018
% @brief This code is the implementation of the step track algorithm
%
%
%%%%%%%%%%%%%%%%%%%%%%%%%%%%%%%%%%%%%%%%%%%%%%%%%%%%%%%%%%%%%%%%%%%%%%%%
```

```
function [az,el,bPeak] = fcn(q,rf, Init_cnt, Init_istate, Step_Angle,Init_Az_dir,Init_El_dir, Init_Axis)
% Define the static variables using persistent keyword
persistent tracking_counter
persistent istate
persistent az_angle
persistent el_angle
persistent az_step_angle
persistent el_step_angle
persistent az_direction
persistent el_direction
persistent current_rf
persistent peak_max
persistent az_max
persistent el_max
persistent rf_max
persistent counter
persistent selected_axis; % 1 for azimuth, 0 for elevation
% In the first run, initialize the varibels
if isempty(counter)
counter = 0;
end
if isempty(tracking_counter)
tracking_counter = Init_cnt;
end
if isempty(istate)
istate = Init_istate;
end
if isempty(el_step_angle)
el_step_angle = Step_Angle;
end
if isempty(az_step_angle)
az_step_angle = Step_Angle;
end
if isempty(az_direction)
az_direction = Init_Az_dir;
end
if isempty(el_direction)
el_direction = Init_El_dir;
end
if isempty(selected_axis)
selected_axis = Init_Axis;
end
if isempty(peak_max)
peak_max = 0;
end
if isempty(current_rf)
current_rf = 0;
end
```

```
if isempty(az_angle)
az_angle = q(1);
end
if isempty(el_angle)
el_angle = q(3);
end
if isempty(az_max)
az_max = 0;
end
if isempty(el_max)
el_max = 0;
end
if isempty(rf_max)
rf_max = 0;
end
% Assign the output values for reducing Matlab error
az = az_angle;
el = el_angle;
bPeak = peak_max;
% state machine of the Step Track Algorithm
switch istate
case 0
% Idle case
tracking_counter = 0;
istate = 10;
case 10
% Move the seleceted axis (1 for azimuth, 0 for elevation) with initial
% direction.
current_rf = rf; % save the rf signal
if (selected_axis == 1) % azimuth axis selected
% Move azimuth axis with the step angle
az_angle = q(1) + (az_direction * az_step_angle);
% Update the output
az = az_angle;
% No movement in elevation axis
el_angle = q(3);
% Update the output
el = el_angle;
else % elevasyon axis selected
% No movement in azimuth axis
az_angle = q(1);
% Update the output
az = az_angle;
% Move elevation axis with the step angle
el_angle = q(3) + (el_direction * el_step_angle);
% Update the output
el = el_angle;
end
% Save the maximum RF value and correspond angle
```

```
if (rf_max < current_rf)
rf_max = current_rf;
az_max = az_angle;
el_max = el_angle;
end
% change the state
istate = 20;
case 20
% if selected axis or moving axis is azimuth
if (selected_axis == 1)
% wait until the selected axis settled
%if (abs(q(1)-az_angle) < 0.00025)
% istate = 25;
%end
counter = counter + 1;
if counter == 1000
counter = 0;
istate = 25;
end
else % if selected axis or moving axis is elevation
% wait until the selected axis settled
%if (abs(q(3)-el_angle) < 0.00025)
% istate = 25;
%end
counter = counter + 1;
if counter == 1000
counter = 0;
istate = 25;
end
end
case 25
if (rf > current_rf) % Which rf signal is higher after movement.
% if RF signal is higer continue to the movement without change
istate = 10;
else
% if RF signal is lower
% İncrement the trackking number
tracking_counter = tracking_counter + 1;
% Do total 8 iteration
if (tracking_counter < 8)
% Change the selected axis direction
if (selected_axis == 1)
% if the axis is azimuth
if (az_direction == 1)
% azimuth direction is negative
az_direction = -1;
else
% azimuth direction is positive
az_direction = 1;
```

```
end
else % if the axis is elevation
if (el_direction == 1)
% elevation direction is negative
el_direction = -1;
else
% elevation direction is positive
el_direction = 1;
end
end % end of the selected_axis if else
% Change the selected axis
if (selected_axis == 1)
% selecred axis is elevation
selected_axis = 0;
else
% selecred axis is elevation
selected_axis = 1;
end % end of the selected_axis if else
% now continue to the movement with modifed settings
istate = 10;
else
% 8 iteration is done
istate = 30; % stop the movement
end % end of the tracking if else
end % end of the rf if else loop

case 30
% digital value to represent the iteration is done.
peak_max = 1;
bPeak = peak_max;
% point the maximum position
az = az_max;
el = el_max;
%otherwise
end
if peak_max == 1
az = az_max;
el = el_max;
else
az = az_angle;
el = el_angle;
end
```

APPENDIX A.6

```
%%%%%%%%%%%%%%%%%%%%%%%%%%%%%%%%%%%%%%%%%%%%%%%%%%%%
%
% @file conscan
```

```
% @author Oguz Kaan Hancioglu
% @version V1.0.0
% @date 15-April-2018
% @brief This code is the implementation of the conical scan algorithm
%
%
%%%%%%%%%%%%%%%%%%%%%%%%%%%%%%%%%%%%%%%%%%%%%%%%%%%%%%%%%%%%%%%%%%%%%%%%%%%%%%%%
function [az,el, ell, xell, azm, elm, bend] = fcn(delta_t, teta_init, wn_init, el_sat,
az_sat, roll, pitch, yaw , rf , q, tin)
persistent n
persistent wn
persistent t
persistent teta
persistent istate
persistent az_max
persistent el_max
persistent rf_max
if isempty(wn)
wn = wn_init;
end
if isempty(n)
n = 1;
end
if isempty(t)
t = -delta_t;
end
if isempty(istate)
istate = 10;
end
if isempty(teta)
teta = 0;
end
if isempty(az_max)
az_max = 0;
end
if isempty(el_max)
el_max = 0;
end
if isempty(rf_max)
rf_max = 0;
end
bend = 0;
% State machine of the algoritm
switch istate
case 10 % initial state
wn = wn_init / n; % cosine and sine scanning frequency
t = -delta_t; % initail time
istate = 20;
case 20
```

```
t = t + delta_t; % increment time with delta_t
istate = 30;
case 30
if (t <= 1/wn_init)
% the movement in the different circles
teta = n * teta_init + teta_init*(wn_init*t -1);
else
% the movement in the same circle
teta = n * teta_init;
end
istate = 40;
case 40
if (wn*(t+delta_t) <= 2*pi)
istate = 20;
else
if (n < 4) % if scan is not completed
n = n + 1; % increment n
istate = 10; % goto begining
else
istate = 50; % end the simulation
end
end
case 50
bend = 1; % the end
otherwise
end
% xl, yl ,zl circle in local earth line of site coordinate system
xl = sin(teta)*sin(wn*t);
yl = sin(teta)*cos(wn*t);
ell = xl;
xell = yl;
zl = cos(teta);
% Transformation to the circle in local earth coordinate system
x_ll = xl;
y_ll = yl * sin(el_sat) + zl * cos(el_sat);
z_ll = -yl * cos(el_sat) + zl * sin(el_sat);
xe = y_ll * cos(az_sat) + x_ll * sin(az_sat);
ye = y_ll * sin(az_sat) - x_ll * cos(az_sat);
ze = z_ll;
% Disturbance transformation
xh = xe * cos(yaw) + ye * sin(yaw);
yh = -xe * sin(yaw) + ye * cos(yaw);
zh = ze;
xp = xh * cos(pitch) - zh * sin(pitch);
yp = yh;
zp = xh * sin(pitch) + zh * cos(pitch);
xa = xp;
ya = yp * cos(roll) - zp * sin(roll);
za = yp * sin(roll) - zp * cos(roll);
```

```
el = asin(za);
az = atan(ya/xa);
% Save the azimuth elevation and rf signal.
if (rf_max < rf)
rf_max = rf;
az_max = q(1);
el_max = q(3);
end
% assign this in order to eliminate error
azm = az_max;
elm = el_max;
if (tin > 20)
istate = 10;
n = 1;
t = -delta_t;
wn = wn_init;
teta = 0;
end
```

CURRICULUM VITAE

Name Surname: Oğuz Kaan HANCIOĞLU

Place and Date of Birth: ANKARA, 13/05/1991

E-Mail: oguzkaanhancioglu@hotmail.com

EDUCATION:

- **B.Sc.:** 2015, Kocaeli University, Faculty Of Engineering, Mechatronics Engineering

PROFESSIONAL EXPERIENCE AND REWARDS:

- 2019-... Turkish Aerospace
- 2016-2019 Profen Communications Technologies & Services, Inc.

PUBLICATIONS, PRESENTATIONS AND PATENTS ON THE THESIS:

- Hancioglu, O.K., Celik, M. and Tumerdem, U. (2018). Kinematics and Tracking Control of a Four Axis Antenna for Satcom on the Move, *International Power Electronics Conference (IPEC-Niigata 2018-ECCE Asia),* 1680–1686.